UNDERSTANDING AND IMPROVING THE DYNAMIC PERFORMANCE OF THE STRONGBACK STRUCTURAL SYSTEM

A Dissertation Presented for the

Doctor of Philosophy

Degree

The University of Tennessee, Knoxville

Sima Abolghasemi

August 2025

Copyright © 2025 by Sima Abolghasemi.

All rights reserved.

ACKNOWLEDGEMENTS

I would first like to express my deep gratitude to my advisor, Dr. Nicholas Wierschem. He's been an incredible mentor—supportive, wise, approachable, and always willing to help. I've truly appreciated his guidance, encouragement, and the trust he placed in me throughout this journey; I feel lucky to have had him as my mentor. I also want to thank my committee members, Dr. Mark Denavit, Dr. Timothy Truster, and Dr. Fernando Moreu, for their time, guidance, and helpful feedback throughout this process. A special thanks goes to Dr. Denavit, who has played an especially important role as a second advisor. I've learned so much from him and truly appreciated his advice and support.

I also want to sincerely thank the organizations that made this work possible. The research was supported by two National Science Foundation grants, Nos. 1940197 and 1944513, awarded to Dr. Wierschem, and I'm grateful for that funding. I'd also like to thank NASA for the chance to contribute to a small part of a project they funded under grant No. 80NSSC20M0185. And I truly appreciate the Department of Civil Engineering at the University of Tennessee for supporting me throughout my PhD journey.

The unwavering support and love from my parents, Jahan and Hossein, have been the foundation of my strength throughout this journey. Their encouragement helped me push through every challenge. My siblings and my nephew—Sareh, Sahar, Soheil, and Soshiant—have also been a constant source of motivation and care. I'm especially grateful to my parents-in-law, Najmeh and Reza, for their kindness, support, and encouragement over these years.

Gratitude also goes to my friends in JDT 324: Javad Esmaeelpour, Ibrahim Adediran, Anika Sarkar, Amir Behnam, and Peter Talley, who brought energy, support, and humor to my PhD experience. I'm equally thankful to those who offered help and guidance along the way, including Jonathan Shell, Paxton Lifsey, and Griffin Barley. And to my dear friends Shima, Mahsa, Mohaddesseh, Sahar, Hossein, and Mohammad—thank you for your friendship, encouragement, and presence in my life.

A very special thank you goes to my husband, Ashkan, for his unconditional love, support, and belief in me. He has been my constant companion through every step of this journey. His patience, encouragement, and countless sacrifices made this achievement possible, and I couldn't

have done it without him. I'm incredibly lucky to have you by my side and so excited to begin the next chapter of our lives together. And to my sweet dog, Pillow—thank you for being a daily source of love, comfort, and stress relief. You made even the hardest days feel a little lighter.

ABSTRACT

This dissertation investigates the dynamic behavior and performance enhancement of structural systems equipped with strongback mechanisms under seismic loading. Strongback systems are designed to mitigate soft-story collapse by promoting a uniform story drift profile. While these systems offer promising improvements to seismic resilience, important questions remain regarding their robustness and effectiveness under varying structural and seismic conditions. To address these gaps, a comprehensive investigation is conducted using both experimental and numerical approaches. This study first examines whether strongbacks can maintain their effectiveness in the presence of vertical stiffness irregularities and evaluates the impact of damper arrangement—distributed versus concentrated—on structural performance. This dissertation then explores the behavior of segmental strongbacks, in which the spine is divided by a mid-height joint to reduce internal force demands and floor accelerations in taller buildings, with particular focus on the role of joint stiffness. Finally, the research investigates the integration of inerters—devices that generate force proportional to relative acceleration—both as standalone systems and in combination with strongbacks, to assess their potential in enhancing seismic performance or serving as alternative control strategies. Through a combination of shake table testing and numerical simulations, this dissertation aims to clarify the mechanics, effectiveness, and design implications of various strongback configurations. By characterizing the interaction between system components, modal deformation patterns, and seismic input, the study helps to develop additional understanding and improvement of strongback-based systems. Ultimately, the findings contribute to advancing earthquake-resistant design by equipping structural engineers with deeper insight and greater flexibility in applying strongback solutions to mitigate seismic risks in buildings.

TABLE OF CONTENTS

Chapter 1 : INTRODUCTION 1

1.1 BACKGROUND 2

1.2 PROBLEM STATEMENT 3

1.3 DISSERTATION OVERVIEW 4

Chapter 2 : LITERATURE REVIEW 7

2.1 STRONGBACK SYSTEMS 8

2.2 SEGMENTAL STRONGBACK SYSTEMS 14

2.3 INERTER 15

2.4 SUMMARY 17

Chapter 3 : EXPERIMENTAL AND NUMERICAL MODEL 18

3.1 EXPERIMENTAL MODEL 19

3.1.1 Physical Model 19

3.1.2 Ground Motion for Experimental Investigation 21

3.1.3 Instrumentation, Data Acquisition, and Data Processing 22

3.2 NUMERICAL MODEL AND METHODOLOGY 23

3.2.1 Building Model 24

3.2.2 Structure Stiffness Matrix 24

3.2.3 Strongback Stiffness Matrix 28

3.2.4 Static Condensation Method 30

3.2.5 Equation of Motion 31

3.2.6 Ground Motion for Numerical Analysis 32

Chapter 4 : ASSESSMENT OF STIFFNESS IRREGULARITY AND DAMPER ARRANGEMENT ON STRONGBACK BEHAVIOR 33

4.1 INTRODUCTION 35

4.2 PHYSICAL MODEL 38

4.3 DESCRIPTION OF EXPERIMENTAL TESTS 43

4.3.1 Structure Configurations 43

4.3.2 Ground Motions 45

4.3.3 Instrumentation and Data Acquisition 46

4.4 RESULTS AND DISCUSSION 48

4.4.1 Stiffness Irregularity 48

4.4.2 Damper Arrangement 54

4.5 CONCLUSIONS 60

Chapter 5 : IMPACT OF A TUNED JOINT ON THE BEHAVIOR OF A SEGMENTAL STRONGBACK 62

5.1 EXPLORING THE ROLE OF A NONLINEAR ROTATIONAL INERTIAL MECHANISM AT THE JOINT OF A SEGMENTED STRONGBACK STRUCTURAL SYSTEM 64

5.1.1 Introduction 64

5.1.2 Model and Properties 66

5.1.3 Test Setup 69

5.1.4 Analysis 70

5.1.5 Conclusion 74

5.2 SEGMENTAL STRONGBACK WITH LINEAR JOINT STIFFNESS 75

5.2.1 Experimental Investigations 76

5.2.2 Numerical Investigations 81

Chapter 6 : INERTIAL STRONGBACK: COMPARING THE BEHAVIOR AND PERFORMANCE OF DISTRIBUTED INERTERS AND A TRADITIONAL STRONGBACK 94

6.1 EXPERIMENTAL STUDY ON THE IMPACT OF AN ELASTIC SPINE IN A STRUCTURE WITH INERTER-BASED DEVICES 96

6.1.1 Introduction 96

6.1.2 Physical Model 98

6.1.3 Description of Experimental Tests 101

6.1.4 Results and Discussion 107

6.1.5 Conclusion 112

6.2 NUMERICAL STUDY OF HYBRID SEISMIC CONTROL USING SEGMENTAL ELASTIC SPINE AND DISTRIBUTED INERTERS 113

6.2.1 Introduction 113

6.2.2 Numerical Model 118

6.2.3 Analysis Plan 123

6.2.4 Results and Discussion 128

6.2.5 Conclusion 142

Chapter 7 : CONCLUSION AND FUTURE WORKS 145

7.1 SUMMARY AND CONCLUSIONS 146

7.2 FUTURE WORKS 149

REFERENCES 152

VITA 163

LIST OF TABLES

Table 3-1: Identifying information and properties of ground motions used for shake table tests 22

Table 3-2 : Approximate values of parameters of fundamental period of a structure according to Table 12.8-2 of ASCE 7-16 (Charney et al., 2020) 27

Table 4-1: System configurations for stiffness irregularity and damper arrangement tests 44

Table 4-2: Identifying information and properties of ground motions used for shake table tests 45

Table 5-1: Test system configurations and associate properties 78

Table 6-1: System configurations for experimental tests 103

Table 6-2: Information on ground motions used for shake table tests 105

Table 6-3: Default EI values used for unit and segmental ES; segmental EI is one-third of unit EI. 127

LIST OF FIGURES

Figure 2-1: Soft-story failure of Olive View Medical Center during the 1971 San Fernando earthquake (Mahin et al., 1976) 9

Figure 2-2: Story drift in a brace frame structure a) without the strongback b) with the strongback (Lai and Mahin, 2015) 9

Figure 2-3:Examples of rocking frame system configurations as proposed by Eatherton et al. (2014), including (a) single-frame, (b) dual-frame, (c) alternate fuse type, and (d) alternate component locations. 11

Figure 2-4: Schematic representation and constructed test specimen of the strongback structure (Simpson and Mahin, 2018) 12

Figure 2-5: Cross section view of two common inerter mechanism a) ball screw b) rack and pinion (Javidialesaadi and Wierschem, 2019a) 17

Figure 3-1: Isometric view of the physical model of the primary structure with the spine. Left) 4-story structure with unit spine. Right) 5-story structure with segmental strongback. 20

Figure 3-2: model Simplified of five-story structure with elastic spine. 25

Figure 4-1: Isometric view of the physical model of the primary structure with the strongback– units are mm 39

Figure 4-2: Dimensioned elevation view of the primary structure with the strongback – units are mm, CL = centerline 40

Figure 4-3: Dampers connected in a story of the structure. Left- Concentrated arrangement in the first story, Right- Distributed arrangement showing first story only. 42

Figure 4-4: Primary structure with the strongback on the shake table with annotations highlighting the instrumentation 47

Figure 4-5: Estimated first mode frequency of the structure with and without the strongback given the structural configurations used for the stiffness irregularity study 49

Figure 4-6: Maximum story drift from tests in the stiffness irregularity study. 49

Figure 4-7: Normalized maximum story drift from tests in the stiffness irregularity study. Normalization of results from each record are performed with respect to the NSI configuration story drift results for systems without the strongback and with respect to the NSI-SB configuration story drift results for systems with the strongback 50

Figure 4-8: Normalized maximum roof drift from tests in the stiffness irregularity study. Normalization of results from each record are performed with respect to the NSI configuration roof drift results for systems without the strongback and with respect to the NSI-SB configuration roof drift results for systems with the strongback 52

Figure 4-9: Story drifts with and without strongback for all configurations in the stiffness irregularity study and for all seismic records 53

Figure 4-10: Estimated first mode frequency of the structure with and without the strongback given the structural configurations used for the damper arrangement study 54

Figure 4-11: Estimated damping ratio of the structure with and without the strongback given the structural configurations used for the damper arrangement study 56

Figure 4-12: Maximum story drift from tests in the damper arrangement study 56

Figure 4-13: Normalized maximum story drift from tests in the damper arrangement study. Normalization of results from each record are performed with respect to the DDA configuration story drift results for systems without the strongback and with respect to the DDA-SB configuration story drift results for systems with the strongback 57

Figure 4-14: Normalized maximum roof drift from tests in the damper arrangement study. Normalization of results from each record are performed with respect to the DDA configuration roof drift results for systems without the strongback and with respect to the DDA-SB configuration roof drift results for systems with the strongback 58

Figure 4-15: Story drifts of structure with and without strongback for all damper arrangement configurations and for all seismic records 59

Figure 5-1: Five-story structure with segmented strongback (Left) overall view (Right) close up view of segmented strongback joint and rotational inertial mechanism installed across the joint 67

Figure 5-2: Ball-screw-based nonlinear rotational inertial mechanism (a) assembled device (b) disassembled device (c) close up view of outer nut for the ball-screw and its fixed ball bearings (d) close up view of the inner nut 68

Figure 5-3: 3D models of different shafts used in the ball-screw-based rotational inertial mechanism with approximate at rest position of the fixed ball bearings of the outer shaft shown (a) Low Inertance (b) High Inertance (c) Low to High Inertance (d) High to Low Inertance 69

Figure 5-4: Frequency response functions from ground acceleration to fifth-floor acceleration of all configurations for all amplitudes. 71

Figure 5-5: Normalized maximum story drift of all configurations with respect to the No Inerter case for all amplitudes 73

Figure 5-6: Story drifts of all configurations for all amplitudes 73

Figure 5-7: Normalized maximum story acceleration of all configurations with respect to the No Inerter case for all amplitudes 73

Figure 5-8: Normalized maximum link force of all configurations with respect to the No Inerter case for each load amplitude 74

Figure 5-9: Relative rotation changes respect to a range of rotational stiffness diagram 77

Figure 5-10: Linear beam design for joint stiffness between two segments of the segmented strongback model 77

Figure 5-11: Frequency response functions from ground acceleration to fifth-floor acceleration for all system configurations 79

Figure 5-12: Normalized maximum acceleration. Normalization of results from each record are performed with respect to the SSL0 configuration results. 79

Figure 5-13: Normalized maximum force. Normalization of results from each record are performed with respect to the SSL0 configuration results. 79

Figure 5-14: Normalized maximum story drift. Normalization of results from each record are performed with respect to the SSL0 configuration results. 80

Figure 5-15: Maximum absolute floor acceleration (g) for a 5-story structure with a segmental strongback pinned at the second floor, across a range of linear joint stiffness values (kN·m/rad). Each gray line represents results from one ground motion record; the red line shows the median response across all records. Acceleration values were computed by identifying the maximum floor acceleration for each joint stiffness value per record. 85

Figure 5-16: Normalized RMS of maximum floor acceleration for a 5-story structure with a segmental strongback pinned at the second floor, across a range of linear joint stiffness values (kN·m/rad). For each record, the time history of the maximum floor acceleration at each time step was computed, and its RMS was calculated for each joint stiffness. Gray lines represent individual records, while the red line shows the median normalized RMS across all ground motions, with normalization relative to the zero joint stiffness case. 86

Figure 5-17: Maximum moment demand (KN.m) in the spine for a 5-story structure with a segmental strongback pinned at the second floor, across a range of linear joint stiffness values (kN·m/rad). For each ground motion, the maximum moment in the spine was identified for each joint stiffness value. Gray lines represent results from individual records, and the red line shows the median of maximum moments across all ground motions. 88

Figure 5-18: Normalized RMS moment in the spine for a 5-story structure with a segmental strongback pinned at the second floor, across a range of linear joint stiffness values (kN·m/rad). For each ground motion, the maximum spine moment at each time step was tracked to construct a time history of maximum moment, from which the RMS was computed. Results are normalized relative to the zero joint stiffness case across all joint stiffnesses for each record; the red line represents the median across all records..... 89

Figure 5-19: Maximum interstory drift (mm) for a 5-story structure with a segmental strongback pinned at the second floor, evaluated across a range of linear joint stiffness values (kN·m/rad). For each ground motion, the maximum interstory drift was extracted for every

joint stiffness value. Gray lines represent individual ground motions, while the red line indicates the median drift across all records. 90

Figure 5-20: Normalized RMS of maximum interstory drift for a 5-story structure with a segmental strongback pinned at the second floor, across a range of linear joint stiffness values (kN·m/rad). For each ground motion, the time history of the maximum interstory drift across all stories was extracted, and its RMS was computed for each joint stiffness value. Gray lines indicate individual records, and the red line represents the median normalized RMS, with normalization performed relative to the zero joint stiffness case. ... 91

Figure 5-21: Median normalized RMS values of maximum floor acceleration, interstory drift, and moment for a 5-story structure with a segmental strongback pinned at the second floor, across a range of linear joint stiffness values (kN·m/rad). Each response measure was normalized with respect to the zero joint stiffness case, and the median was computed across all ground motions. The combined plot highlights the trade-offs between acceleration, drift, and moment responses as joint stiffness varies. 92

Figure 6-1: (a) Isometric view of the physical model of the primary structure with the spine – units are mm, (b) inerter used in this study with annotations identifying its components 99

Figure 6-2: (a) Primary structure with distributed inerter arrangement, (b) Primary structure with concentrated inerter arrangement 102

Figure 6-3: Physical model with instrumentation: accelerometers and infrared markers 106

Figure 6-4: Frequency response functions from ground acceleration to fourth-floor acceleration for all system configurations 108

Figure 6-5: First mode frequency estimated by system identification for structure with and without spine and for all inerter configurations..... 108

Figure 6-6: First mode damping ratio estimated by system identification for structure with and without spine and for all inerter configurations..... 109

Figure 6-7: Maximum story drift and normalized maximum story drift results. Results were normalized with reference to the maximum story drift of the INFD configuration (for systems without a spine) and the INFD-S configuration (for systems with a spine) 111

Figure 6-8: Maximum absolute acceleration results 111

Figure 6-9: Maximum drifts for each story of the structure with and without spine for all inerter configurations 112

Figure 6-10: Simplified model of five-story structure with elastic spine. 119

Figure 6-11: System natural frequencies over a range of inertance values, b, in the hybrid system with a unit ES and distributed inerters with equal inertance. 125

Figure 6-12: Natural mode shapes of the 5-story structure without ES and inerter 129

Figure 6-13: Median of maximum inter-story drift in mm for 5-story structure with unit and the segmental ES pinned at the second floor across a range of spine stiffness values (EI). Each point represents the median of suite of ground motions' maximum inter-story drift for a specific EI. Configurations include b0 (no inerter), bEq (equal distribution), and bOpt (optimized distribution) in both unit and segmental ES systems. 130

Figure 6-14: Median of maximum inter-story drift in mm for 5-story structure with unit and the segmental ES pinned at the third floor across a range of spine stiffness values (EI). Each point represents the median of suite of ground motions' maximum inter-story drift for a specific EI. Configurations include b0 (no inerter), bEq (equal distribution), and bOpt (optimized distribution) in both unit and segmental ES systems. 132

Figure 6-15: Median of maximum moment demand (KN.m) in the ES for 5-story structure with unit and the segmental ES pinned at the second floor across a range of spine stiffness values (EI). Each point represents the median of suite of ground motions' maximum moment for a specific spine stiffness. Configurations include b0 (no inerter), bEq (equal distribution), and bOpt (optimized distribution) in both unit and segmental ES systems. 133

Figure 6-16: Median of maximum moment demand (KN.m) in the ES for 5-story structure with unit and the segmental ES pinned at the third floor across a range of spine stiffness values

(EI). Each point represents the median of suite of ground motions' maximum moment for a specific spine stiffness. Configurations include b0 (no inerter), bEq (equal distribution), and bOpt (optimized distribution) in both unit and segmental ES systems. 135

Figure 6-17: Median of maximum absolute floor acceleration (g) for the 5-story structure with unit and segmental ES pinned at the second floor, evaluated over a range of spine stiffness values (EI). Each point reflects the median of maximum floor accelerations recorded across a suite of ground motions for a given EI. Configurations include b0 (no inerter), bEq (equal distribution), and bOpt (optimized distribution) applied to both unit and segmental ES systems..... 137

Figure 6-18: Median of maximum absolute floor acceleration (g) for the 5-story structure with unit and segmental ES pinned at the third floor, evaluated over a range of spine stiffness values (EI). Each point reflects the median of maximum floor accelerations recorded across a suite of ground motions for a given EI. Configurations include b0 (no inerter), bEq (equal distribution), and bOpt (optimized distribution) applied to both unit and segmental ES systems..... 138

Figure 6-19: Normalized median of maximum interstory drift for various configurations with and without unit or segmental ES, considering different pin locations and distributed inerters in a 4-,5-, and 6-story structure. Values are normalized with respect to no ES and no distributed inerter. Each bar represents the median of maximum interstory drift responses across suite of ground motion records. 140

Figure 6-20: Normalized median of maximum absolute floor acceleration for various configurations with and without unit or segmental ES, considering different pin locations and distributed inerters in a 4-,5-, and 6-story structure. Values are normalized with respect to no ES and no distributed inerter. Each bar represents the median of maximum absolute floor acceleration responses across suite of ground motion records. 140

Figure 6-21: Median of the maximum moment demand (kN·m) in the spine for systems with and without unit or segmental ES, considering different pin locations and distributed inerter configurations in a 4-,5-, and 6-story structures. Each bar represents the median of the peak

moment values across suite of ground motion records for a given structural configuration. Only configurations with a spine are shown, as moment is not generated without an ES. . 141

Chapter 1 : INTRODUCTION

1.1 BACKGROUND

Earthquakes continue to pose a significant threat to the safety, functionality, and resilience of built infrastructure. Earthquakes can induce severe damage in structures, leading to partial or complete collapse, economic loss, disruption of essential services, and, in many cases, loss of life. The devastating impacts of past seismic events have underscored the critical need for advancing our understanding of how structures respond to earthquake excitations.

As a result, extensive research efforts have focused on two broad but interconnected areas: understanding the characteristics of earthquake ground motions and developing strategies to improve the performance of structures subjected to such demands. Studies in the first area aim to characterize seismic hazards by examining parameters such as intensity, duration, frequency content, and temporal variability of ground motions (Kramer and Stewart, 2024; Shokrgozar-Yatimdar et al., 2024). This information is essential for developing accurate analytical models and for informing seismic design provisions.

Parallel to this, structural engineering research has concentrated on enhancing the static and dynamic performance of structural systems. This includes developing innovative strengthening techniques, improving the ductility and energy dissipation capacity of structural members, and introducing control devices that mitigate seismic demands. Whether applied to individual components or entire systems, these advancements aim to increase structural resilience and reduce vulnerability to seismic events.

Among various seismic protection strategies, the strongback system has emerged as a promising concept to minimize damage by preventing soft-story mechanisms or reducing their effect through the integration to the structure of a rigid vertical member or group of elements that are pinned at the structure's base. However, the effectiveness of strongback systems under varying structural configurations and ground motion scenarios, particularly when combined with control devices, remains largely underexplored.

One type of structural control device that has gained significant attention in recent years is the rotational inertia mechanism, known as an inerter (Smith, 2002a). These two-terminal mechanical devices generate a force proportional to the relative acceleration between their terminals, offering a unique mechanism for controlling structural vibrations. Due to their high

mass amplification capability, inerters have been widely explored in various vibration control applications for buildings and bridges subjected to seismic loading (Hwang et al., 2007a; Nakamura et al., 2014a; Giaralis and Petrini, 2017a; Javidialesaadi and Wierschem, 2019a; Di Egidio et al., 2021a; Ma et al., 2021a). However, their integration into strongback systems remains largely unexplored, and the potential benefits of combining these two strategies have not been fully evaluated.

1.2 PROBLEM STATEMENT

The strongback is a stiff and strong element or group of elements that is pinned at the base of a structure and runs the height of the structure. As a result, the strongback experiences rigid body motion when the structure has uniform drift but provides significant resistance to any other pattern of drifts, such as those that would be present with a soft story mechanism. By preventing premature failure due to a soft story mechanism, the strongback is intended to help structures have an overall more ductile response (Chen et al., 2017; Faramarzi and Taghikhany, 2021; Simpson and Mahin, 2018). While prior studies have examined the influence of strongback stiffness on structural behavior (Chen et al., 2017) and evaluated its role in systems with localized stiffness reductions (Simpson and Mahin, 2018), the positional variation of vertical stiffness irregularities within the primary structure (i.e., the structure into which the strongback is incorporated) has not been adequately addressed. As a result, the effectiveness of strongbacks under varying location of stiffness irregularity within the primary structure remains an open research question.

The inerter is fundamentally different than other structural control devices in that the intrinsic damping that is present in a realistic inerter is accompanied by large mass effects. Thus, the inerter's effect on a structure with a spine is unknown, as well as how various arrangements of inerters impact the performance and behavior of the structure with and without a spine. While some studies have investigated the impact of damper configurations in a strongback system, the effect of concentrating all of the structure's dampers in one story and the effect of the location of that damped story have not been widely considered or experimentally investigated. This is an important gap in knowledge as the ability to concentrate dampers at a single story can add desirable design flexibility.

Previous studies have shown that continuous strongback systems may be less effective in tall buildings due to increased force and acceleration demands associated with higher-mode effects. To address this limitation, segmenting the strongback has been proposed as a strategy to reduce these demands and improve overall performance. (Chen et al., 2012, 2019a; Tremblay et al., 2014). Research on segmental strongback systems is still limited, with most existing studies relying primarily on numerical simulations. Experimental investigations, in particular, are scarce. Among the few available studies, the joints connecting the spine segments are typically modeled as ideal pins, despite the fact that joint stiffness can significantly influence internal force distribution and drift patterns. As a result, the potential impact of joint properties or modifications on system performance remains largely unexplored.

While strongback systems and related configurations offer substantial potential to enhance structural resilience during seismic events by preventing soft-story mechanisms, key questions related to these systems still remain.

1.3 DISSERTATION OVERVIEW

Some aspects of the behavior and performance of strongbacks remain unclear, particularly concerning the impact of vertical stiffness irregularities at different positions along the structure's height and whether the strongback can allow for the concentration of energy dissipation devices in structures. Additionally, it is unclear if the behavior of strongbacks can be improved through the use of inerters or through segmentation of the strongback with or without specialized joints.

To address these gaps, this dissertation employs a combination of numerical simulations and small-scale experimental testing. The research is organized around three primary focus areas, each targeting a specific aspect of strongback system behavior.

- Focus Area 1: Assessment of Stiffness Irregularity and Damper Arrangement on Strongback Behavior.

This area investigates how vertical stiffness irregularities and damper arrangements affect the performance of strongback structures and answers key questions including: Can a strongback

effectively mitigate the adverse effects of stiffness irregularities, regardless of their location? To what extent does the arrangement of energy dissipation devices affect system properties and response in the presence of a strongback? By addressing these questions, this research aims to elucidate if strongback systems reduce structure's sensitivity to the arrangement of stiffness and damping across the height of the structure.

- Focus Area 2: Impact of a tuned joint on the behavior of a segmented strongback

This area examines how tuning the properties of the joint between segments in a segmented strongback influences the structural response. Key questions include: Can reducing joint stiffness effectively lower force demands on the strongback while maintaining control over drift? How does adjusting the stiffness at the joint affect the distribution of forces and drifts within the structure? Additionally, what role could a nonlinear rotational inertia mechanism play in enhancing system performance under different load amplitudes? By exploring these questions, this research seeks to provide insights into improving the behavior of segmented strongbacks under seismic loading.

- Focus Area 3: Inertial Strongback: comparing the behavior and performance of distributed inerters and a strongback structure.

This area seeks to investigate how distributed inerters are compared to a traditional strongback in suppressing soft story behavior and controlling higher mode displacements in structures. How do distributed inerters perform in reducing drifts and forces compared to a strongback? Can a combination of both systems provide enhanced performance by addressing higher mode effects and minimizing floor accelerations? By exploring these questions, this research aims to evaluate whether the integration of distributed inerters with a strongback can offer superior seismic performance.

These focus areas are comprehensively addressed in Chapters 4 through 6 of the dissertation. The supporting chapters are outlined as follows:

Chapter 2 presents a literature review of previous research relevant to this study. It covers both numerical and experimental investigations on traditional and segmental strongback systems, the

use of energy dissipation devices, and structural control devices—with particular emphasis on the application of these devices within strongback frameworks.

Chapter 3 describes the physical model of the primary structure and strongback, along with the configurations used in the experimental study. It includes details of the installed dampers and inerters, as well as the instrumentation setup and ground excitations. Additionally, this chapter outlines the development of numerical models representing both traditional and segmental strongback systems under various configurations.

Chapter 4 addresses Focus Area 1, which examines the influence of stiffness irregularity and damper arrangement on the behavior of strongback systems.

Chapter 5 presents Focus Area 2, focusing on the impact of a tuned joint on the performance of a segmented strongback.

Chapter 6 explores Focus Area 3, which compares the seismic performance of distributed inerters and strongback systems.

Chapter 7 presents a concise overview of the research contributions and highlights the key findings from each area of investigation. It also identifies opportunities for continued research to further improve the design and performance of strongback systems in seismic applications.

This dissertation aims to characterize and quantify the contribution of various strongback system components and configurations to the seismic performance of multi-story structures. By developing a deeper understanding of the performance and behavior of strongback systems and evaluating potential enhancements, this work seeks to provide fundamental insights that can inform the design of earthquake-resistant buildings. The findings are intended to guide engineers in selecting and optimizing strongback configurations, thereby improving structural resilience and promoting broader adoption of these systems in seismic design.

Chapter 2 : LITERATURE REVIEW

This chapter presents a comprehensive review of prior research related to strongback systems and rotational inertia devices known as inerters. The objective is to establish the current state of knowledge, identify critical gaps, and provide context for the research presented in this dissertation. The review covers both traditional and segmental strongback systems, with attention to their structural configurations, seismic performance, and integration with energy dissipation mechanisms. Additionally, the chapter examines the development and application of inerters in structural control, highlighting their unique dynamic behavior and noting the lack of studies exploring their integration with strongback systems.

2.1 STRONGBACK SYSTEMS

Seismic-force-resisting systems that are susceptible to soft story mechanisms are particularly vulnerable to earthquakes. These mechanisms result in the concentration of damage at a single vulnerable story and potentially the non-ductile premature failure of the structure. The formation of a soft story mechanism reduces the overall strength of the structure and substantially increases expenses to repair and restore a structure's functionality if it does survive a seismic event (AISC, 2018; Sabelli, 2001). The vulnerability of structures to soft-story mechanisms has been evident for decades, with several notable cases documented in past earthquakes. One recognized example is the Olive View Medical Center, which experienced severe soft-story deformation during the 1971 San Fernando earthquake (Mahin et al., 1976). Illustrating the real-world consequences of this failure mode, **Figure 2-1** shows the lower story sustained extensive damage due to lateral instability, while much less damage is observed in the higher stories.

The strongback has emerged as a promising design strategy to address the localized concentration of structural damage and to prevent soft story mechanisms from forming. Strongback systems incorporate a vertical elastic spine, typically a stiff element, or a group of elements, that is pinned at the base of the structure. This elastic spine is designed to control the lateral deformation profile of a structure under extreme demands, such as seismic loading. In a seismic event, the strongback is expected to remain elastic and help to vertically distribute seismic forces to the dissipators (**Figure 2-2**). By redistributing story drifts more uniformly along the building height, strongbacks help prevent concentration of damage in any single story, and thus suppress a soft-story mechanism.

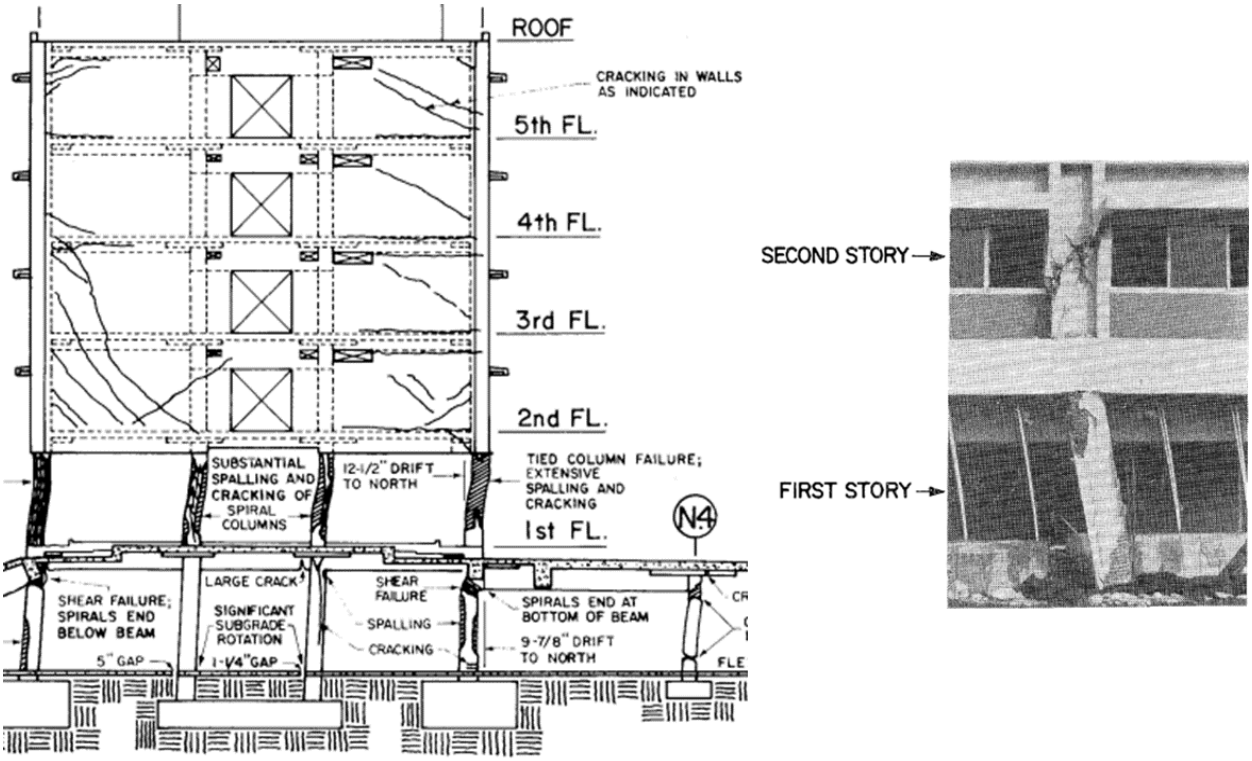


Figure 2-1: Soft-story failure of Olive View Medical Center during the 1971 San Fernando earthquake (Mahin et al., 1976)

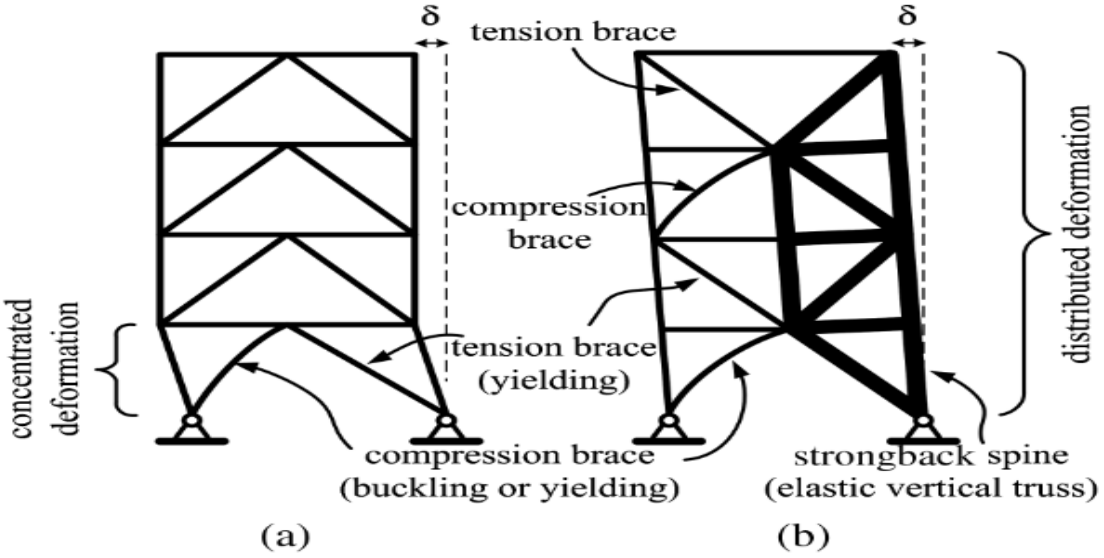


Figure 2-2: Story drift in a brace frame structure a) without the strongback b) with the strongback (Lai and Mahin, 2015)

Many numerical studies have investigated the performance of systems that behave like strongbacks, which have appeared in the literature under various names, including the hinged wall (or pin-supported wall), rocking steel shear wall, stiff rocking core, vertical rigid truss, and elastic spine frame.(Alavi and Krawinkler, 2004; Chen et al., 2017, 2018, 2022; Djojo et al., 2014; Eatherton et al., 2014; Faramarzi and Taghikhany, 2021; Hu et al., 2021; Lai and Mahin, 2015; Palermo et al., 2021a; Qu et al., 2012; Simpson and Mahin, 2018; Slovenec et al., 2017; Takeuchi et al., 2015; Talley et al., 2024). One example of a system with strongback-like behavior is the controlled rocking frame introduced by Beck and Skinner (1973) to improve the seismic performance of tall reinforced-concrete bridges. In this system, piers are allowed to "rock" or "step" and temporarily separate from their foundations during strong shaking, which limits stress levels below yielding and reduces the need for heavy reinforcement, thereby lowering construction costs. Following this, Kelly and Tsztoo (1977) extended the concept by testing a rocking frame with energy-absorbing devices, demonstrating that allowing controlled uplift combined with passive dissipation improved seismic performance compared to both fixed-base and freely rocking systems. Over the past decades, substantial progress has been made in developing this strategy for soft-story mitigation, particularly in steel braced frames, often through a combination of structural design techniques and energy dissipation devices, supported by both experimental and numerical investigations (Deierlein et al., 2011; Eatherton et al., 2012, 2014; Roke et al., 2008; Tremblay et al., 2008; Wiebe et al., 2012). **Figure 2-3** illustrates several system configurations developed by Eatherton et al. (2014), highlighting different frame arrangements and energy-dissipating components.

Experimental studies system with strongback-like behavior are limited. Simpson and Mahin (2018) studied the weak-story behavior of a nearly full-scale two-story structure with a strongback that effectively delayed or prevented soft-story formation even after the rupture of the structure's buckling-restrained-braces (**Figure 2-4**). Hu et al. (2021) studied a self-centering companion spine composed of two rigid spines and friction dampers to enhance structural response and mitigate damage during seismic events using an experimental structural model based on a length scale of 0.35. A collaborative study conducted by a combined American and Japanese team (Fahnestock et al., 2021) focused on the full-scale testing of a frame-spine system with force-limiting connections added to a moment-resistant frame.

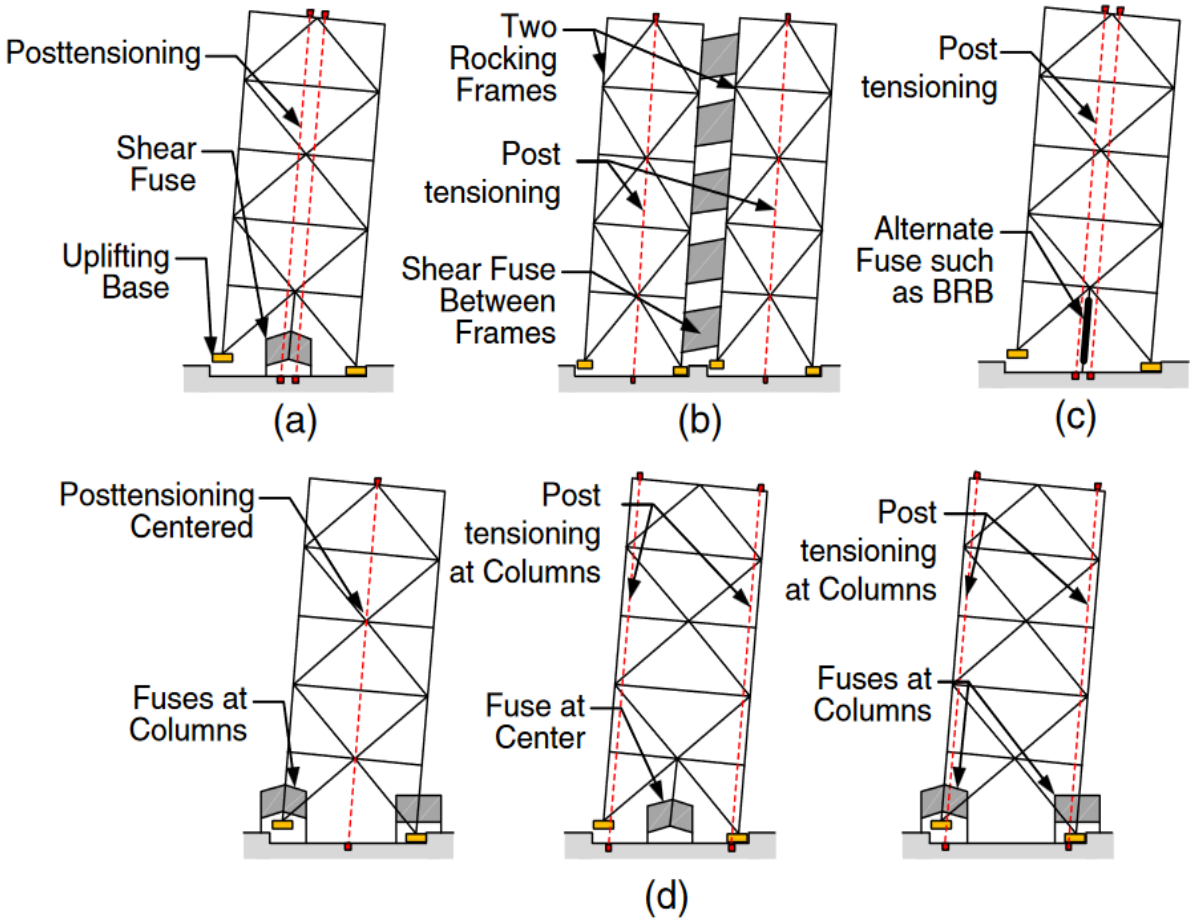


Figure 2-3:Examples of rocking frame system configurations as proposed by Eatherton et al. (2014), including (a) single-frame, (b) dual-frame, (c) alternate fuse type, and (d) alternate component locations.

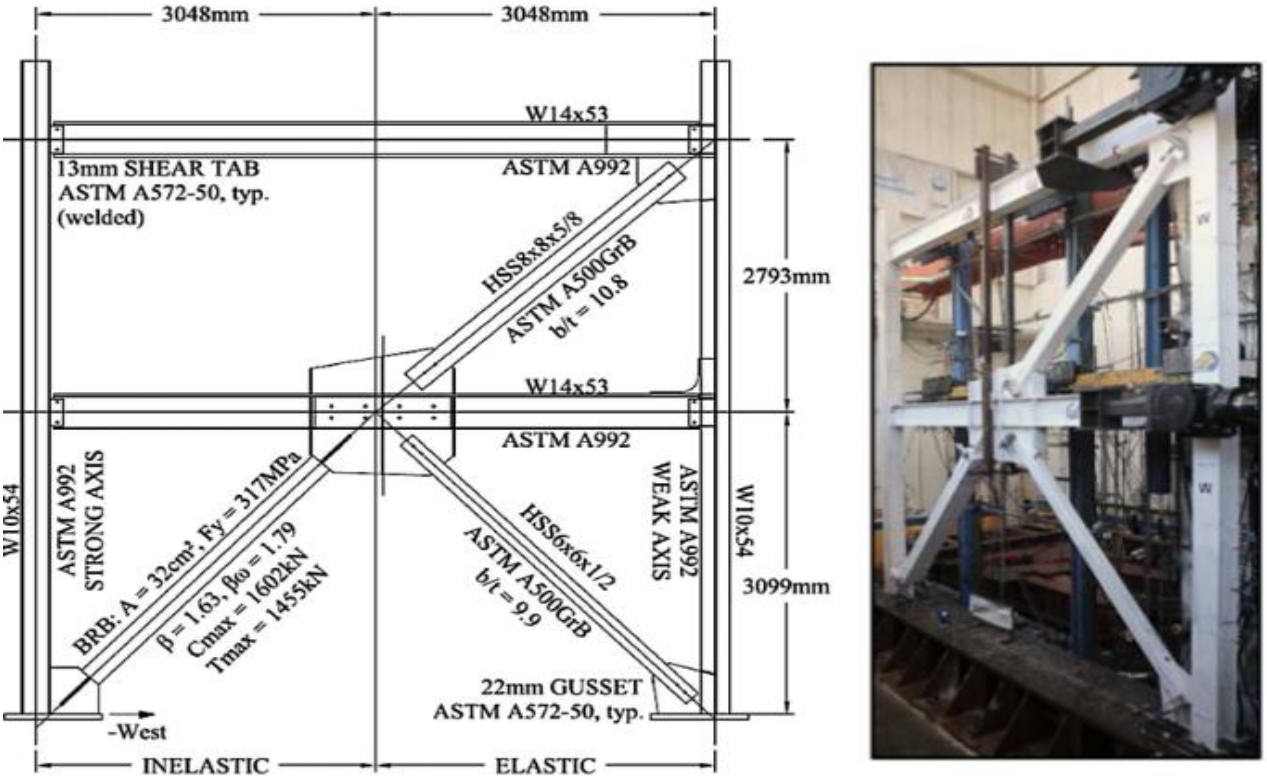


Figure 2-4: Schematic representation and constructed test specimen of the strongback structure (Simpson and Mahin, 2018)

Due to the large scales considered and other experimental complexities, the majority of the experimental works related to strongbacks have featured a small number of tests or a single test; thus, wider-ranging experimental parametric studies on structures with strongbacks have not been performed.

The stiffness of the strongback and the stiffness of the primary structure (i.e., the structure into which the strongback is incorporated) are both important and impact the behavior of the combined system. Chen et al. (2017) numerically investigated the impact of strongback stiffness and strength on the behavior of a three-story special concentrically braced frame with an attached strongback. Lin et al. (2019) conducted a numerical study on several stiffness configurations for the strongback, considering both the overall stiffness of the strongback and the distribution of stiffness in the strongback. This work also investigated the effectiveness of the strongback for different primary structure types: a three-story shear deformation-dominated structure and a nine-story flexure deformation-dominated structure. Other work explicitly considered the impact of a strongback on a structure with a story with reduced stiffness (Simpson and Mahin, 2018), but this work did not vary the position of the soft story vertical irregularity in the structure. Consequently, investigations focusing on the effectiveness of the strongback given changes to the primary structure's stiffness are limited.

The effects of including strongbacks in structures with different types of energy dissipation devices have also been considered. Qu et al. (2012) investigated the retrofit of an eleven-story steel-reinforced concrete frame using post-tensioned pin-supported walls and shear-type steel dampers distributed along the wall height. Their nonlinear dynamic analysis demonstrated that the pin-supported walls effectively improved the deformation pattern and prevented weak story failure. They also demonstrated that strategically placed dampers in this system could absorb most of the seismic energy, thereby limiting inelastic deformation and damage in the surrounding frame members. Wang et al. (2023) numerically evaluated the floor velocity and acceleration responses of pin-supported wall-frame structures with different dampers, concluding that while both hysteretic and viscoelastic dampers reduce interstory drift, viscoelastic dampers offer better protection for nonstructural components by more effectively controlling floor motion. Hu et al. (2021) proposed a self-centering companion spine system, consisting of a pair of rigid spines and distributed friction spring dampers, which provided uniform drift distribution and demonstrated

stable, recentering hysteretic behavior under repeated loading, confirming its potential as a resilient seismic-resistant system.. Palermo et al. (2021a) numerically investigated a structure with a strongback and several configurations of viscous dampers in the structure, including dampers at each story, at some select stories, and concentrated vertically at the base of the strongback. This work concluded that the strongback's presence allowed for the increase in seismic performance effectiveness of these different configurations of viscous dampers due to a more uniform potential for energy dissipation by dampers located throughout the height of the structure. While some studies have investigated the impact of damper configurations in a strongback system, the effect of concentrating all of the structure's dampers in one story and the effect of the location of that damped story have not been widely considered or experimentally investigated. This is an important gap in knowledge as the ability to concentrate dampers at a single story can add desirable design flexibility.

2.2 SEGMENTAL STRONGBACK SYSTEMS

A continuous strongback may be less effective in tall buildings due to the heightened force and acceleration demands resulting from more influential higher modes of vibration in tall structures. To address this issue, it has been proposed that dividing the strongback into two or multiple independent segments, each spanning only a portion of the building height, can reduce internal force demands and improve dynamic performance. In such segmental strongback systems, the segments are typically connected through a pin, allowing relative rotation while preserving overall vertical continuity. Related research has mainly centered on steel-braced frame structures with segmental strongbacks, identified under various terms such as modular tied-braced frame, M-TBF, (Chen et al., 2012; Tremblay et al., 2014) and segmental elastic spine (Chen et al., 2019a). Chen et al. (2012) found that seismic forces in tie members are significantly reduced when using the M-TBF system compared to the conventional TBF configuration. However, this reduction comes with a slight increase in story drifts and link plastic rotations.

Balazadeh-Minouei et al. (2018) indicated that segmenting a strongback improves retrofit cost-efficiency. Chen et al. (2019b) demonstrated that the M-TBF configuration was the most cost-effective solution when designed with four elastic vertical truss segments. Their study has also shown that M-TBF reduces story shear forces and column axial loads. To prevent concentrated

story drift in any single module, a minimum number of stories per module is required. Both M-TBF and tied-braced frame systems demonstrated enhanced collapse safety and increased global ductility.

In segmented strongback structures, Tremblay et al. (2014) found that placing energy dissipation devices at the connection between segments enhanced story drift responses of above and below placement of these devices. They also noted that the effectiveness of the energy dissipation devices increases as the number of modules grows. In the context of M-TBF systems, introducing energy dissipation devices does not alter the force demands on tie members.

Chen et al. (2018) extended the investigation of segmental strongback systems to high-rise buildings by applying the concept to controlled spine frames and introducing a segmented-spine configuration aimed at reducing base shear and achieving a uniform distribution of story drift. Through parametric studies and modal analyses, they demonstrated that a two-segment spine system can deliver seismic performance comparable to that of a continuous spine for buildings up to 30 stories tall, provided that appropriate damper-to-frame and spine-to-frame stiffness ratios are maintained.

Most previous work on segmental spines has been numerical, with limited experimental validation, particularly for systems with elastic segmental spines. In these studies, the joints between segments are typically modeled as ideal pins, overlooking the potential influence of joint stiffness or alternative joint configurations on overall structural performance. Furthermore, while prior research has primarily focused on drift control, force distribution, and moment demand, the impact of segmental strongback configurations on floor acceleration, an important consideration for nonstructural performance, remains largely unexplored. This represents a key gap in understanding the full dynamic behavior of such systems.

2.3 INERTER

One type of structural control device considered in other structural systems is the inerter. Inerters are two-terminal mechanical devices that produce resistive force proportional to the relative acceleration between their terminals. The proportionality constant of inerters has the same units as mass, referred to as inertance. Physical mechanisms, including ball-screws and rack and

pinion assemblies (**Figure 2-5**), can be used to realize inerters by converting translational motion into the rotational motion of a flywheel (Smith, 2002a; Smith et al., 2012; Swift et al., 2013a). This conversion allows inerters to produce large mass effects even though they may have a relatively small physical mass (Sugimura et al., 2012b).

The restoring force provided by an ideal inerter is expressed as below:

$$F = b\left(\ddot{u}_2 - \ddot{u}_1\right) \tag{2-1}$$

where the inerter is subjected to equal and opposite forces F at terminals 1 and 2 with accelerations $\ddot{u}_1$ and $\ddot{u}_2$.

Furthermore, a nonlinear rotational inertial mechanism is a type of nonlinear inerter that can produce variable mass effects that can be used to disrupt the formation of resonant conditions (Sarkar and Wierschem, 2024a). This nonlinearity can be due to geometric nonlinearity (Faraj et al., 2019; Moraes et al., 2018; Yang et al., 2020), like changes in lead-screw properties that can vary the inertance along the lead, as well as from adjustments in the properties of the device's flywheel (Kushwaha et al., 2020; Mahato et al., 2019).

Due to the inerter's significant mass amplification capacity, they have been suggested for incorporation into a variety of vibration control systems to help mitigate the response of structures to earthquakes (Hwang et al., 2007a; Nakamura et al., 2014a; Giaralis and Petrini, 2017a; Javidialesaadi and Wierschem, 2019a; Di Egidio et al., 2021a; Ma et al., 2021a). Inerters can serve different purposes depending on the structural control objectives. In some applications, the primary goal is to adjust the natural frequencies of the system, effectively shifting the dynamic characteristics to avoid resonance or to better align with desired performance targets (Beeby et al., 2006; Yu et al., 2001). In other cases, inerters are employed to achieve structural mode control (Zhang et al., 2021), promoting more favorable deformation patterns or reducing localized demands. However, these devices have not been studied for use in structures with strongbacks. The inerter is fundamentally different from other structural control devices in that the intrinsic damping present in a realistic inerter is accompanied by large mass effects.

2.4 SUMMARY

In summary, the existing body of research has established the effectiveness of strongback systems in mitigating undesirable drift patterns and enhancing the seismic performance of multi-story structures. While traditional and segmental configurations have been studied numerically and, to a lesser extent, experimentally, several important aspects—such as the influence of joint stiffness, stiffness irregularity, and damper arrangement—remain underexplored. In parallel, inerters have demonstrated strong potential as structural control devices due to their unique acceleration-dependent behavior and mass-amplification feature. While the effectiveness of different energy dissipation and passive control devices in structures with strongbacks has been investigated previously, the combination of inerters and a strongback has not been previously considered. Thus, the inerter's impact on a structure with a strongback is unknown, as well as how various arrangements of inerters impact the performance and behavior of the structure with and without an elastic spine system. These gaps in the literature form the basis for the research presented in the subsequent chapters, which aim to address these limitations through a combination of numerical modeling, experimental validation, and performance evaluation.

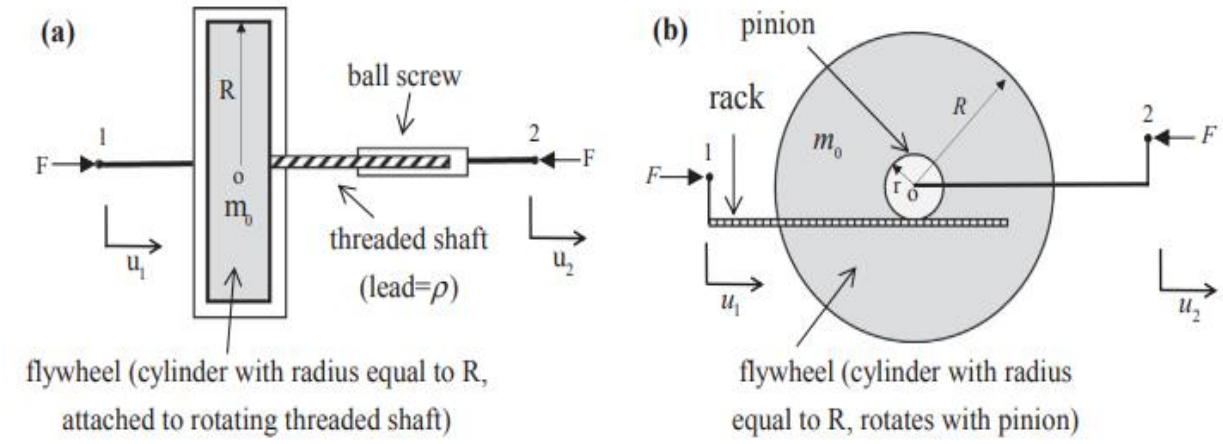


Figure 2-5: Cross section view of two common inerter mechanism a) ball screw b) rack and pinion (Javidialesaadi and Wierschem, 2019a)

Chapter 3 : EXPERIMENTAL AND NUMERICAL MODEL

This chapter presents the experimental and numerical models developed to investigate the seismic performance of strongback systems under various configurations. The first part of the chapter describes the physical model used in shake table testing, including structural design and properties, instrumentation, and input ground motions. The second part introduces the numerical modeling approach used to simulate the structural response of systems incorporating both traditional and segmental strongback configurations under seismic excitation.

3.1 EXPERIMENTAL MODEL

As a part of the investigation of the focus areas of this work, experiments were conducted using small-scale models of a four- and five-story structure with strongbacks subjected to various ground motions. This section describes the experimental model shared by these focus areas and used to investigate the performance of strongback systems in structures under seismic loading. Additionally, this section describes the selection of ground motion properties and the equipment used for data collection during these tests.

3.1.1 Physical Model

Two primary structures were used for the experimental testing in this project: a four-story structure with a unit strongback and a five-story structure with a segmented strongback, as shown in **Figure 3-1**.

3.1.1.1 4-Story Structure Used in Chapter 4 and 6 Studies

Each of the floors and the base of the structure is an 18 in. × 18 in. × 0.5 in. 6061-T6511 aluminum plate. Grade 1095 spring steel columns were located in the corners of the structure and bolted to the sides of the plate, forming a moment-resisting connection. The columns were 2 in. wide and had a thickness of either 0.062 in. (original thickness) or 0.042 in. (reduced thickness). The columns were oriented in the same direction such that the overall structure was flexible in one lateral direction and stiff in the orthogonal lateral direction, and the connections were such that the bending span of the columns was the clear story height. The center-to-center height of each story was 9.625 in. and the clear story height was 9.125 in. The flexural rigidity, EI, of the

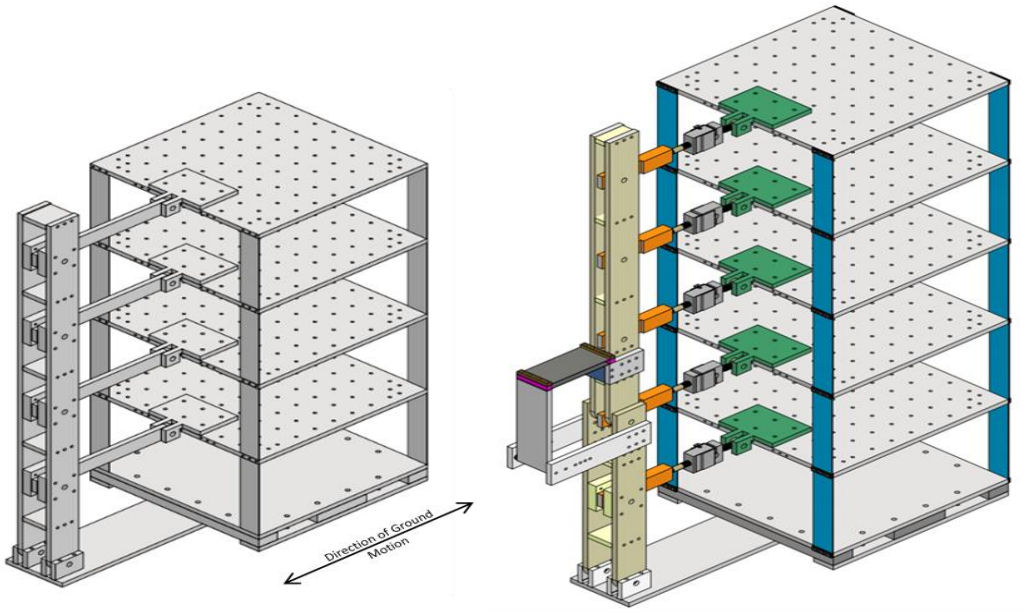


Figure 3-1: Isometric view of the physical model of the primary structure with the spine. Left) 4-story structure with unit spine. Right) 5-story structure with segmental strongback.

spring steel columns, was determined through a three-point bending test as EI = 28.4 lb-in2 and 9.28 lb-in2 for the original and reduced thickness columns, respectively.

The strongback was constructed from two 3 in. wide and 0.5 in. thick aluminum plates. The plates were joined together by several connector pieces. The strongback was pinned at the base using a partially threaded bolt. The centerline of the strongback pin was at the same elevation as the centerline of the base plate. The strongback was attached to the primary structure on each floor with aluminum link arms with cross-sectional dimensions of 1.5 in. width and 0.5 in. thickness that were pinned at the strongback (left arm pin) and brackets (right arm pin). The brackets were rigidly connected to the floor plates. The centerline of the right arm pins was at the same elevation as the centerline of the floor plates. Due to a design error, the center-to-center spacing of the left arm pins was 9.5 in., less than the story height of the primary structure, resulting in the arms being slightly tilted when the structure is in its undeformed position. The strongback was oriented such that it rotated about its base pin with motion in the flexible direction of the primary structure.

The mass of each floor, including associated hardware (e.g., the bracket, but not the link arm), was 17.82 lb. The mass of each of the original thickness columns was 0.34 lb. The mass of each of the reduced thickness columns was 0.25 lb. The mass of each link arm was 1.27 lb. The mass of the strongback, including associated hardware, was 22.4 lb. The center of gravity of the strongback was 22.37 in. above the center of the strongback pin. In cases when the strongback is not present, the strongback, link arms, and associated hardware were removed, but the brackets connected to the floor plates remained.

3.1.1.2 5-Story Structure Used in Chapter 5 Study

The main structure without the strongback has the same properties as the four-story version, with the addition of one extra floor and a uniform column thickness of 0.062 in. throughout. Another difference is the link arms, which are now shorter and equipped with load cells, attached via a threaded rod connector and a rod-end bolt, resulting in a combined weight of 2.2 lb.

The segmented strongback consists of two segments, each made up of two plates measuring 3 in. wide and 0.5 in. thick. The smaller segment is pinned to the bigger segment at the level of the second floor. The mass of the whole segmented strongback is 21 lb.

3.1.2 Ground Motion for Experimental Investigation

Six seismic ground motions were used to assess the differences in seismic response with different structures and strongback configurations (**Table 3-1**). The six records chosen were recorded from historic events and were obtained from the Pacific Earthquake Engineering Research Center (PEER) ground motion database (Ancheta et al., 2014). In all cases, only Component A of the recorded ground motions, as designated in the PEER database, was used. These motions were applied as unidirectional horizontal excitations by the shake table, oriented along the flexible direction of the test structures. The characteristics of the six selected recorded historical ground motions used in this study are summarized in **Table 3-1.**

In addition to the recorded seismic ground motions, a shaped white noise loading was employed to produce experimentally estimated system frequency response functions and examine the dynamic properties of the model structure, especially its first natural frequency and first mode

Table 3-1: Identifying information and properties of ground motions used for shake table tests

No.	Earthquake name	Station	Year	Mag.	Unscaled PGA max (g)
1	Northridge	Beverly Hills-Mulhol	1994	6.7	0.52
2	Kobe, Japan	Shin-Osaka	1995	6.9	0.24
3	Imperial Valley	El Centro Array #11	1979	6.5	0.38
4	Manjil, Iran	Abbar	1990	7.4	0.51
5	Chi-Chi, Taiwan	CHY101	1999	7.6	0.44
6	Landers	Coolwater	1992	7.3	0.42

damping ratio. The white noise loading was generated from a 300-second random acceleration that was subjected to a lowpass filter with a cutoff frequency of 200 Hz.

3.1.3 Instrumentation, Data Acquisition, and Data Processing

Response measures for this experimental study will be calculated using data collected from the following instrumentation.

3.1.3.1 Accelerometers:

PCB model 352C33SN accelerometers connected to a data acquisition system with sampling rates of 10,240 Hz, 5,120 Hz, or 2,560 Hz were used to capture the acceleration of the ground (shake table) and the acceleration of each floor of the structure. The accelerometers were mounted to the middle of the side of each floor plate and the base plate. These accelerometers measured the acceleration in the structure's flexible direction, which was the primary direction of motion. The maximum absolute acceleration of the structure and each floor was calculated using lowpass filtered versions of these measured signals when the structure was excited by the selected ground motions.

Additionally, acceleration measurements were primarily used to estimate the natural frequency and damping of the structures. The system's response to white noise provided estimates for the first-mode natural frequency and damping ratio across each configuration. Frequency response functions were estimated between the roof and base absolute accelerations using the *tfestimate*

function in MATLAB (The MathWorks Inc, 2020a). Curve fitting was applied to match a simplified analytical dynamic model to the experimentally estimated frequency response functions, utilizing the system identification toolbox in MATLAB (The MathWorks Inc, 2020a). Final estimates for the system's first-mode damping and natural frequency were extracted from the fitted analytical model.

3.1.3.2 Optotrak:

The displacement response of each floor plate, the base plate, and the strongback were captured using an Optotrak, an optical measurement system that tracks emitted infrared light from markers placed on these components. This system used a sampling rate of 50 Hz. The absolute position of each marker was measured in three dimensions with a separate data acquisition system and synchronized with the acceleration measurements in post-processing. The motion of the structure in its flexible direction was extracted from the three-dimensional marker position data. These displacement measurements were primarily used to calculate the resulting story and roof drifts.

3.1.3.3 Load Cells:

In Chapter 5, five Interface S-type load cells were utilized at each floor level, attached to the structural link between the floors and the strongback. These load cells were used to measure the lateral forces transferred between the strongback and the structure. This force data was collected at sampling rates of 5120 Hz and 2560 Hz using the same data acquisition system as the acceleration measurements. Note that load cells were not used in the link arms for the testing in studies of Chapter 4 and 6.

3.2 NUMERICAL MODEL AND METHODOLOGY

This section presents the numerical model developed to investigate the performance and efficiency of various strongback configurations, referred to here as elastic spines (ES). The model is used in Chapter **5** and Chapter **6** to simulate and compare different ES configurations under seismic loading conditions. Numerical simulations are used in these Chapters in order to consider a large number of seismic ground motions and system configurations in the investigations. This numerical model combines a shear structure model for the main structure

with a beam model of the strongback. **Figure 3-2** shows the desired simplified model for the numerical analysis. The MATLAB model of this simplified model can be modified to have inerters as well as become a segmented strongback with adjustable joint stiffness. A five-story structure is used as an example for the numerical demonstration in the following sections.

3.2.1 Building Model

The three building configurations considered for this study (4, 5, and 6 stories), are assumed to represent office buildings with Seismic Design Category (SDC) D and with identical floor plans. Each story has a height of 4.5 meters. The mass of a typical floor is taken as 500,000 kg, while the roof mass is assumed to be 400,000 kg, representing 80% of the typical floor mass.

Considering a 5-story structure as an example, the general parametric mass matrix is as follows, considering the system DOF as displacement relative to the base.

$$Ms = \begin{bmatrix} m & 0 & 0 & 0 & 0 \\ 0 & m & 0 & 0 & 0 \\ 0 & 0 & m & 0 & 0 \\ 0 & 0 & 0 & m & 0 \\ 0 & 0 & 0 & 0 & 0.8m \end{bmatrix} \tag{3-1}$$

In most designs, the inclusion of the elastic spine primarily modifies the stiffness of a structure without significantly increasing the overall mass. As a result, the mass of the ES is excluded from the equations of motion (EOM); only the contribution to the stiffness matrix will be considered. This will allow this study to focus on the stiffness contribution of the ES.

3.2.2 Structure Stiffness Matrix

A linearly decreasing stiffness distribution is applied to the main structure, where the first story has stiffness k, and the stiffness of each subsequent story decreases by a fixed amount of 0.1k. For a structure with n stories (n = 4, 5, or 6), the story stiffnesses, k_i, replace with k, 0.9k, 0.8k, and so on, down to $(1 - 0.1 \times (n - 1))$ k at the top story. This linear reduction reflects a vertical stiffness nonuniformity commonly observed in real structural systems.

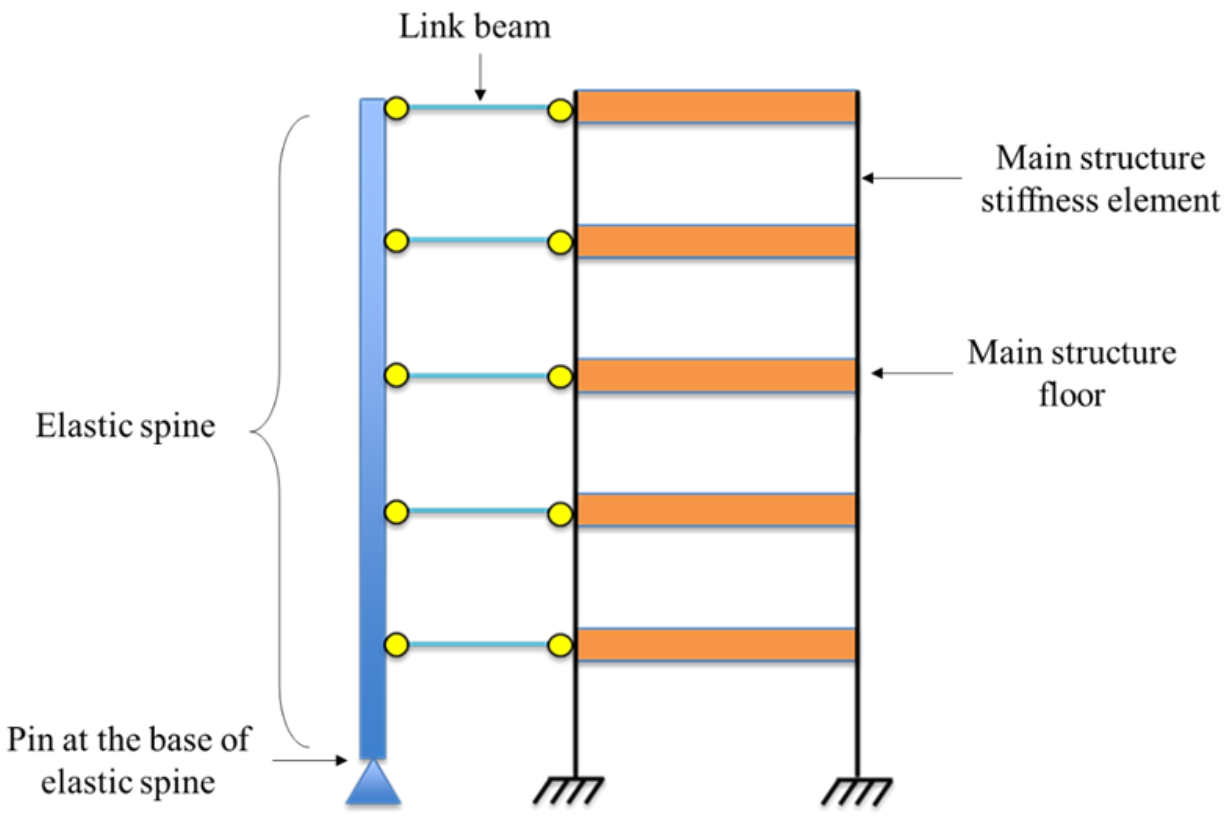


Figure 3-2: model Simplified of five-story structure with elastic spine.

The structure stiffness matrix for a 5-story structure is:

$$Ks = \begin{bmatrix} k_1 + k_2 & -k_2 & 0 & 0 & 0 \\ -k_2 & k_2 + k_3 & -k_3 & 0 & 0 \\ 0 & -k_3 & k_3 + k_4 & -k_4 & 0 \\ 0 & 0 & -k_4 & k_4 + k_5 & -k_5 \\ 0 & 0 & 0 & -k_5 & k_5 \end{bmatrix} \tag{3-2}$$

$$Ks = \begin{bmatrix} k_1 + 0.9k_1 & -0.9k_1 & 0 & 0 & 0 \\ -0.9k_1 & 0.9k_1 + 0.8k_1 & -0.8k_1 & 0 & 0 \\ 0 & -0.8k_1 & 0.8k_1 + 0.7k_1 & -0.7k_1 & 0 \\ 0 & 0 & -0.7k_1 & 0.7k_1 + 0.6k_1 & -0.6k_1 \\ 0 & 0 & 0 & -0.6k_1 & 0.6k_1 \end{bmatrix} \tag{3-3}$$

$$Ks = \begin{bmatrix} 1.9k & -0.9k & 0 & 0 & 0 \\ -0.9k & 1.7k & -0.8k & 0 & 0 \\ 0 & -0.8k & 1.5k & -0.7k & 0 \\ 0 & 0 & -0.7k & 1.3k & -0.6k \\ 0 & 0 & 0 & -0.6k & 0.6k \end{bmatrix} \tag{3-4}$$

According to ASCE 7-16 (Charney et al., 2020), the approximate fundamental period of a structure, T_a, can be calculated using the following formula:

$$T_a = C_t \times (L)^x \tag{3-5}$$

Here, Ct is a coefficient that depends on the type of lateral load-resisting system. According to **Table 3-2**, Ct is equal to 0.0731 for the system considered in this study, assuming to be representative of a braced frame, with units in meters. L is the height of the building (4.5 m (height of each story) * 5 = 22.5 m). x is an exponent that varies based on the construction type, which is 0.75 here.

Table 3-2 : Approximate values of parameters of fundamental period of a structure according to Table 12.8-2 of ASCE 7-16 (Charney et al., 2020)

Structure Type	**Ct**	**X**
Moment-resisting frame systems in which the frames resist 100% of the required seismic force and are not enclosed or adjoined by components that are more rigid and will prevent the frames from deflecting where subjected to seismic forces:		
Steel moment-resisting frames	0.028 (0.0724)[a]	0.8
Concrete moment-resisting frames	0.016 (0.0466)[a]	0.9
Steel eccentrically braced frames in accordance with Table 12.2-1 lines B1 or D1	0.03 (0.0731)[a]	0.75
Steel bucking-restrained braced frames	0.03 (0.0731)[a]	0.75
All other structural systems	0.02 (0.0488)[a]	0.75
[a]Metric equivalents are shown in parentheses		

So, based on this, the stiffness will be determined to achieve this natural frequency (1/Ta).

$$T_a = 0.0731 \times (22.5)^{0.75} = 0.7552\ s \tag{3-6}$$

$$f = \frac{1}{T_a} = 1.324\ Hz \tag{3-7}$$

To determine appropriate stiffness values, modal natural frequencies are tracked over a range of stiffness values ($0 < k < 5x10^6$ KN/m) using the eigenvalue equation:

$$\left| Ks - \omega^2 M \right| = 0 \tag{3-8}$$

The stiffness value that results in a first-mode natural frequency of 1.324 Hz for the 5-story structure is selected as the base stiffness (k). This value is used in **Equation (3-4)**, to construct the structural stiffness matrix (Ks) for the system.

A 5% damping ratio is considered for all modes of the structure, and the damping matrix is calculated accordingly, with modal damping coefficient and modal shapes.

3.2.3 Strongback Stiffness Matrix

A numerical model of the strongback based on Euler-Bernoulli beam stiffness was developed for this work. By using the Euler-Bernoulli beam as a basis, shear deformations are neglected when calculating the stiffness contribution of the strongback. The stiffness matrix of a single element of a two-node Euler-Bernoulli beam, K, is

$$K = \frac{12EI}{L^3} \begin{bmatrix} 12 & 6L & -12 & 6L \\ 6L & 4L^2 & -6L & 2L^2 \\ -12 & -6L & 12 & -6L \\ 6L & 2L^2 & -6L & 4L^2 \end{bmatrix} \tag{3-9}$$

where, E is the modulus of elasticity, I is the moment of inertia, and L is the length of the beam. Each end of the beam has two DOF: one for displacement and one for rotation. In **Equation**

(3-9), the first and third rows correspond to displacement (u), while the second and fourth rows correspond to rotation (θ). For a beam with two elements, three nodes, and six DOF, the stiffness matrix is:

$$K = \frac{12EI}{L^3}\begin{bmatrix} 12 & 6L & -12 & 6L & 0 & 0 \\ 6L & 4L^2 & -6L & 2L^2 & 0 & 0 \\ -12 & -6L & 12+12 & -6L+6L & -12 & 6L \\ 6L & 2L^2 & -6L+6L & 4L^2+4L^2 & -6L & 2L^2 \\ 0 & 0 & -12 & -6L & 12 & -6L \\ 0 & 0 & 6L & 2L^2 & -6L & 4L^2 \end{bmatrix}$$

$$= \frac{12EI}{L^3}\begin{bmatrix} 12 & 6L & -12 & 6L & 0 & 0 \\ 6L & 4L^2 & -6L & 2L^2 & 0 & 0 \\ -12 & -6L & 24 & 0 & -12 & 6L \\ 6L & 2L^2 & 0 & 8L^2 & -6L & 2L^2 \\ 0 & 0 & -12 & -6L & 12 & -6L \\ 0 & 0 & 6L & 2L^2 & -6L & 4L^2 \end{bmatrix} \quad (3\text{-}10)$$

This matrix can be expanded for the 5-story model structure in this study considering five elements, six nodes, and twelve DOF:

$$K = \frac{12EI}{L^3}\begin{bmatrix} 12 & 6L & -12 & 6L & 0 & 0 & 0 & 0 & 0 & 0 & 0 & 0 \\ 6L & 4L^2 & -6L & 2L^2 & 0 & 0 & 0 & 0 & 0 & 0 & 0 & 0 \\ -12 & -6L & 24 & 0 & -12 & 6L & 0 & 0 & 0 & 0 & 0 & 0 \\ 6L & 2L^2 & 0 & 8L^2 & -6L & 2L^2 & 0 & 0 & 0 & 0 & 0 & 0 \\ 0 & 0 & -12 & -6L & 24 & 0 & -12 & 6L & 0 & 0 & 0 & 0 \\ 0 & 0 & 6L & 2L^2 & 0 & 8L^2 & -6L & 2L^2 & 0 & 0 & 0 & 0 \\ 0 & 0 & 0 & 0 & -12 & -6L & 24 & 0 & -12 & 6L & 0 & 0 \\ 0 & 0 & 0 & 0 & 6L & 2L^2 & 0 & 8L^2 & -6L & 2L^2 & 0 & 0 \\ 0 & 0 & 0 & 0 & 0 & 0 & -12 & -6L & 24 & 0 & -12 & 6L \\ 0 & 0 & 0 & 0 & 0 & 0 & 6L & 2L^2 & 0 & 8L^2 & -6L & 2L^2 \\ 0 & 0 & 0 & 0 & 0 & 0 & 0 & 0 & -12 & -6L & 12 & -6L \\ 0 & 0 & 0 & 0 & 0 & 0 & 0 & 0 & 6L & 2L^2 & -6L & 4L^2 \end{bmatrix} \quad (3\text{-}11)$$

Odd rows are associated with displacement $u1, u2, u3, u4, u5, u6$ and even rows are associated with rotation $\theta1, \theta2, \theta3, \theta4, \theta5, \theta6$ of nodes one to six.

3.2.4 Static Condensation Method

To be incorporated into the numerical model used in this project, the stiffness matrix for the strongback is reduced to a nxn matrix, in which n refers to the number of stories in the structure. To reduce this matrix, the Guyan Reduction (GUYAN, 1965) method can be used; this method is also known as static condensation. This approach reformulates the stiffness matrix based on primary DOFs and effectively reduces the size of the model while retaining the essential characteristics of the underlying structure. This method starts with the static equilibrium equation:

$$K*U = F \tag{3-12}$$

where K is the stiffness matrix, U is a vector of displacements and rotations, and F is the vector of forces and moments. By reordering the stiffness matrix and prioritizing DOF according to the desired ones, which is displacement in our case, **Equation (3-12)** can be expressed as:

$$\begin{bmatrix} K_{mm} & K_{ms} \\ K_{sm} & K_{ss} \end{bmatrix} \begin{Bmatrix} u_m \\ u_s \end{Bmatrix} = \begin{Bmatrix} f_m \\ f_s \end{Bmatrix} \tag{3-13}$$

This equation is partitioned into independent (master) and dependent (slave) DOF, denoted by m and s, respectively. The lower portions of these equilibrium equations can be written as

$$K_{sm}u_m + K_{ss}u_s = f_s \tag{3-14}$$

From this, the slave DOF can be solved for

$$u_s = K_{ss}^{-1} f_s - K_{ss}^{-1} K_{sm} u_m \tag{3-15}$$

This expression can then be substituted into **Equation (3-12)**.

$$\left[K_{mm} - K_{ms} K_{ss}^{-1} K_{sm} \right] u_m = f_m - K_{ms} K_{ss}^{-1} f_s \tag{3-16}$$

The resulting reduced equilibrium equation is

$$K_{reduced} u_m = f_{reduced} \tag{3-17}$$

where $K_{reduced} = \left[K_{mm} - K_{ms} K_{ss}^{-1} K_{sm} \right]$ and $f_{reduced} = f_m - K_{ms} K_{ss}^{-1} f_s$. **Equation (3-17)** represents a linear equation that simplifies the original system by reducing the DOF.

In this study, rotational DOF at each node is treated as slave DOF and the node displacements are the master DOF. The stiffness matrix for the ES, as shown in **Equation (3-11)**, can be rearranged based on the DOF associated with displacements and then, rotations. By using the static condensation method and following the steps outlined in **Equations (3-13)** through **(3-16)**, $K_{reduced}$ can be formed. Note that the ES in this study does not have any moments applied to it from boundary conditions or loads; thus, $f_{reduced} = f_m$. After applying the boundary conditions of the support, which is a pin at the base, the original 12x12 matrix is effectively reduced to a 5x5 matrix and can be added to the structure stiffness matrix, Ks.

$$K = K_{reduced} + Ks \tag{3-18}$$

3.2.5 Equation of Motion

The equation of motion (EOM) for a structure with a strongback is:

$$M\ddot{U} + C\dot{U} + KU = F(t) \tag{3-19}$$

where M is a mass matrix, C is a damping matrix, K is the combined structure and strongback stiffness matrix, and $F(t)$ is the vector of applied forces on each story. The separate mass of strongback is neglected; thus, the mass matrix of the EOM is a diagonal matrix of the mass of each floor for the 5-story structure model. This mass matrix will be modified with the inclusion of inerters and will become nondiagonal. The main structure is assumed to be a shear structure and its stiffness matrix, Ks, can be presented as

$$Ks = \begin{bmatrix} k_1 + k_2 & -k_2 & 0 & 0 & 0 \\ -k_2 & k_2 + k_3 & -k_3 & 0 & 0 \\ 0 & -k_3 & k_3 + k_4 & -k_4 & 0 \\ 0 & 0 & -k_4 & k_4 + k_5 & -k_5 \\ 0 & 0 & 0 & -k_5 & k_5 \end{bmatrix} \quad (3\text{-}20)$$

where $k1$ to $k5$ are the stiffnesses of the first to fifth story. Displacement, u_i, is the associated DOF for this stiffness matrix. Since the entire strongback system will undergo numerical analysis, the reduced stiffness matrix from **Equation (3-16)** must be added to the structure stiffness, Ks:

$$K = K_{reduced} + Ks \quad (3\text{-}21)$$

3.2.6 Ground Motion for Numerical Analysis

A total of 22 far-field ground motions, each recorded in two horizontal directions (44 records in total), were selected from the FEMA P695 (FEMA P695, 2009) ground motion set to serve as seismic input for this study. Each ground motion was first scaled using a normalization factor (NF) from Table A-4D of FEMA P695 to adjust its peak ground velocity (PGV) to match the median PGV of the full record set. In addition, the motions were scaled using the Seismic Design Category D scaling factor (SDC_D) from Table A-3 of FEMA P695 to anchor the normalized record set to the Maximum Considered Earthquake (MCE) spectral demand.

This two-step scaling ensures a consistent intensity level across all simulations and reflects design-level seismic hazard for structures in SDC D. The final scaled ground motion used in the analyses is computed as:

$$\ddot{U}_{g,scaled}(t) = SDC_D \times NF \times \ddot{U}_{g,recorded}(t) \quad (3\text{-}22)$$

The value of SDC_D is based on linear interpolation at the 5-story structure fundamental period of 0.7552 seconds. All ground motion records were resampled to a uniform sampling rate of 400 Hz to ensure consistency in numerical integration.

Chapter 4 : ASSESSMENT OF STIFFNESS IRREGULARITY AND DAMPER ARRANGEMENT ON STRONGBACK BEHAVIOR

This chapter includes a manuscript which focuses on the impact of strongback on structure with varying damper and stiffness irregularity arrangements. The main focus of this chapter is to explore the impacts of damper arrangement and the location of soft story vertical stiffness irregularities on the dynamic behavior and properties of a structure with a strongback.

The investigation along with its findings, has been published in the Journal of Constructional Steel Research (Abolghasemi et al. 2024). The paper provides a detailed account of the experimental setup, methodology, and the key results related to the impact of stiffness irregularities and damper arrangement on strongback behavior.

Abolghasemi, S., Wierschem, N.E., Denavit, M.D., 2024. Impact of strongback on structure with varying damper and stiffness irregularity arrangements. Journal of Constructional Steel Research 213, 108333. https://doi.org/10.1016/j.jcsr.2023.108333

4.1 INTRODUCTION

Structures susceptible to soft story mechanisms are particularly vulnerable to earthquakes as these mechanisms result in localized damage concentration and the non-ductile premature failure of the structure. Connecting a vertical elastic spine, also known as a strongback, to a primary structural system is one proposed method to prevent the formation of soft story mechanisms. Elastic spines have also been proposed to help address vertical structural irregularities in design.

The strongback is a stiff and strong element or group of elements that is pinned at the base of a structure and runs the height of the structure. As a result, the strongback experiences rigid body motion when the structure has uniform drift, but provides significant resistance to any other pattern of drifts, such as those that would be present with a soft story mechanism. By preventing premature failure due to a soft story mechanism, the strongback is intended to help structures have an overall more ductile response (Faramarzi and Taghikhany, 2021; Simpson and Mahin, 2018).

The fundamental concept behind the strongback, imposing a displacement pattern to reduce or prevent the concentration of damage, has been studied under different names as well, including the hinged wall (Alavi and Krawinkler, 2004), rocking steel shear wall (Djojo et al., 2014; Eatherton et al., 2014), spine frame (Chen et al., 2022; Hu et al., 2021; Takeuchi et al., 2015), stiff rocking core (Slovenec et al., 2017), and vertical rigid truss (Palermo et al., 2021a; Simpson and Mahin, 2018). Furthermore, some basic structural elements, including continuous columns (MacRae et al., 2004), have been identified as possessing similar capabilities as the strongback, imposing a displacement pattern, if designed with sufficient stiffness and strength.

The efficient design of strongbacks and other types of elastic spines is an area of current research. Design by nonlinear response history analysis is an option but is difficult to implement in practice. Simplified modal pushover analysis (Simpson and Rivera Torres, 2021) and

generalized modified modal superposition (Martin and Deierlein, 2021) are among the simpler methods that have been proposed specifically for the design of strongback systems. Both methods consider the higher mode effects and partial yield mechanisms that can complicate strongback design. With the formation of a global plastic mechanism being a primary goal of strongback systems, the theory of plastic mechanism control (Montuori et al., 2022) may also be well-suited for their design. However, none of these simpler methods have been included in design standards yet.

Many numerical studies have investigated the performance of systems that behave like strongbacks (Chen et al., 2017, 2018; Faramarzi and Taghikhany, 2021; Palermo et al., 2021a), but experimental studies on these systems are limited. Simpson and Mahin (2018) studied the weak-story behavior of a nearly full-scale two-story structure with a strongback that effectively delayed or prevented soft-story formation even after the rupture of the structure's buckling-restrained braces. Hu et al. (2021) studied a self-centering companion spine composed of two rigid spines and friction dampers to enhance structural response and mitigate damage during seismic events using an experimental structural model based on a length scale of 0.35. A collaborative study conducted by a U.S.-Japan team (Fahnestock et al., 2021) focused on the full-scale testing of a frame-spine system with force-limiting connections added to a moment-resistant frame. Due to the large scales considered and other experimental complexities, the majority of the experimental works related to strongbacks have featured a small number of tests or a single test; thus, wider-ranging experimental parametric studies on structures with strongbacks have not been performed.

The stiffness of the strongback and the stiffness of the primary structure (i.e., the structure into which the strongback is incorporated) are both important and impact the behavior of the combined system. Chen et al. (2017) numerically investigated the impact of strongback stiffness and strength on the behavior of a three-story special concentrically braced frame with an attached strongback. Lin et al. (2019) conducted a numerical study on several stiffness configurations for the strongback, considering both the overall stiffness of the strongback and the distribution of stiffness in the strongback. This work also investigated the effectiveness of the strongback for different primary structure types: a three-story shear deformation-dominated structure and a nine-story flexure deformation-dominated structure. Other work explicitly considered the impact

of a strongback on a structure with a story with reduced stiffness (Simpson and Mahin, 2018), but this work did not vary the position of the soft story vertical irregularity in the structure. Consequently, investigations focusing on the effectiveness of the strongback given changes to the primary structure's stiffness are limited.

There have been many investigations on improving structural behavior and mitigating soft-story mechanisms through the use of energy dissipation devices (Swain and Patro, 2015; Siar Mahmood Shah and Moradi, 2020) and buckling restrained braces (Panian et al., 2015; Mashhadiali et al., 2021). The effects of including different types of energy dissipation devices in structures with strongbacks have also been considered. Qu et al. (2012) investigated the effectiveness of shear-type steel dampers that were distributed throughout the height of an eleven-story steel-reinforced concrete frame with pin-supported walls. Wang et al. (2023) also investigated a pin-supported wall frame structure and considered hysteretic and viscoelastic dampers in this structure. Hu et al. (2021) proposed the use of friction spring dampers with recentering properties that were distributed along the height of a steel structure that featured a pair of rigid spines. Palermo et al. (2021a) numerically investigated a structure with a strongback and several configurations of viscous dampers in the structure, including dampers at each story, at some select stories, and concentrated vertically at the base of the strongback. This work concluded that the strongback's presence allowed for the increase in seismic performance effectiveness of these different configurations of viscous dampers due to a more uniform potential for energy dissipation by dampers located throughout the height of the structure. While some studies have investigated the impact of damper configurations in a strongback system, the effect of concentrating all of the structure's dampers in one story and the effect of the location of that damped story, have not been widely considered or experimentally investigated. This is an important gap in knowledge as the ability to concentrate dampers at a single story can add desirable design flexibility.

The objective of this work is to determine the effect of the position of stiffness irregularities in a primary structure and the arrangement of dampers in the structure on the dynamic performance and properties of a structure with a strongback. This experimental investigation was performed with a small-scale four-story model structure with and without an attached strongback subjected to shake table-produced ground motion. This investigation is composed of an experimental

parametric analysis that considers the location of stiffness irregularities, produced by reducing the column thickness in specific stories, and considering the arrangement of dampers in different stories of the structure. The scale and limited complexity of the model enabled this experimental parametric analysis to consider more system configurations and ground motions than other experimental studies on strongback systems. The impacts of the stiffness irregularities and damper arrangement are evaluated considering the resulting maximum story and roof drift of the structure as well as changes in the structure's first natural frequency and first mode damping coefficient. Data from these tests were used to develop an understanding of how the dynamic behavior and response of the structure changes due to the stiffness irregularities and damper arrangement with and without the strongback.

This paper is organized as follows. Section 2 describes the primary structure and strongback used in this experimental study. Section 3 presents the system configurations considered to investigate the effects of stiffness irregularities and the arrangement of dampers in the structure. Furthermore, this section describes the ground motions considered and the instrumentation used to measure the response of the structure. The results of the experimental parametric investigation are presented and discussed in Section 4, where they are divided into a study investigating the effects of stiffness irregularities and a study investigating the impact of damper arrangements. In Section 5, the results of the studies are summarized, and conclusions are presented.

4.2 PHYSICAL MODEL

The physical model used in this work was a four-story structure (referred to as the primary structure) with a strongback attached to it. An isometric view of the physical model is shown in **Figure 4-1** and **Figure 4-2** shows an elevation view of the physical model and is annotated with key dimensions. Details on the structure dimensions not shown in **Figure 4-1** and **Figure 4-2** can be found in the design drawings for this structure (Lifsey et al., 2023). Tests were performed on this physical model with and without the strongback attached to the primary structure. In order to avoid damage and enable a large parametric study with this model, this structure was designed to remain elastic during testing.

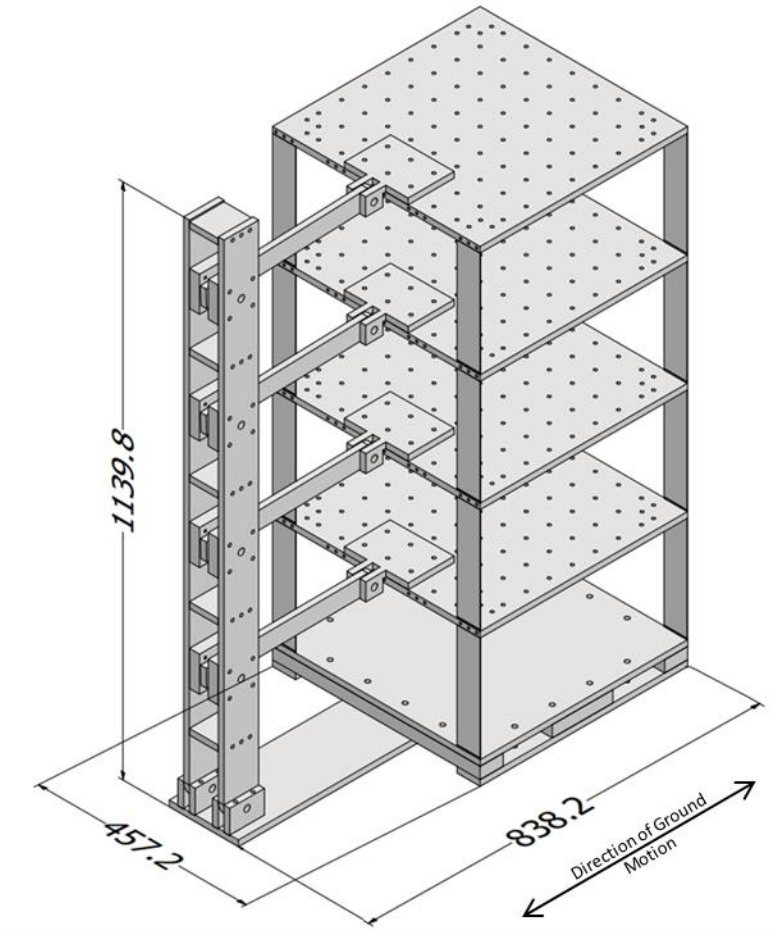


Figure 4-1: Isometric view of the physical model of the primary structure with the strongback– units are mm

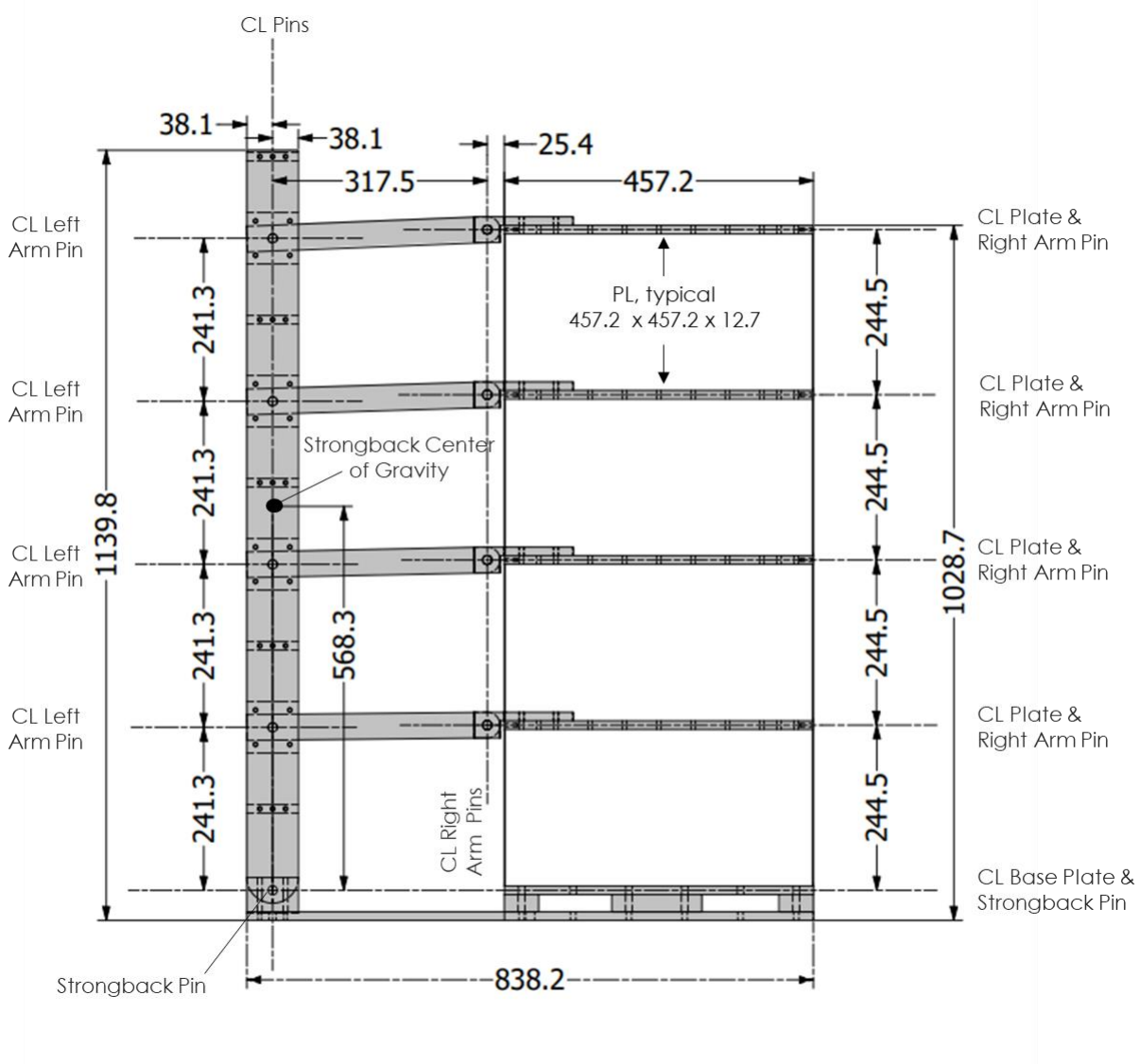


Figure 4-2: Dimensioned elevation view of the primary structure with the strongback – units are mm, CL = centerline

Each of the four floors and the base of the primary structure was a 457.2 mm x 457.2 mm x 12.7 mm 6061-T6511 aluminum plate. Grade 1095 spring steel columns were located in the corners of the structure and bolted to the sides of the plate, forming a moment-resisting connection. The columns were 50.8 mm wide and had a thickness of either 1.575 mm (original thickness) or 1.067 mm (reduced thickness). The columns were oriented in the same direction such that the overall structure was flexible in one lateral direction and stiff in the orthogonal lateral direction, and the connections were such that the bending span of the columns was the clear story height. The c(ACI, 2011)enter-to-center height of each story was 244.5 mm and the clear story height was 231.8 mm. The flexural rigidity, EI, of the spring steel columns, was determined through a three-point bending test as EI = 3.205 N-m^2 and 1.049 N-m^2 for the original and reduced thickness columns, respectively.

The strongback was constructed from two 76.2 mm wide and 12.7 mm thick aluminum plates. The plates were joined together by several connector pieces. The strongback was pinned at the base using a partially threaded bolt. The centerline of the strongback pin was at the same elevation as the centerline of the base plate. The strongback was attached to the primary structure at each floor with aluminum link arms with cross-sectional dimensions of 38.1 mm width and 12.7 mm thickness that were pinned at the strongback (left arm pin) and brackets (right arm pin). The brackets were rigidly connected to the floor plates. The centerline of the right arm pins was at the same elevation as the centerline of the floor plates. Due to a design error, the center-to-center spacing of the left arm pins was 241.3 mm, less than the story height of the primary structure, resulting in the arms being slightly tilted when the structure is in its undeformed position. The strongback was oriented such that it rotated about its base pin with motion in the flexible direction of the primary structure.

The mass of each floor, including associated hardware (e.g., the bracket, but not the link arm), was 8.083 kg. The mass of each of the original thickness columns was 0.154 kg. The mass of each of the reduced thickness columns was 0.113 kg. The mass of each link arm was 0.576 kg. The mass of the strongback, including associated hardware, was 10.156 kg. The center of gravity of the strongback was 568.3 mm above the center of the strongback pin. In cases when the strongback is not present, the strongback, link arms, and associated hardware were removed, but the brackets connected to the floor plates remained.

The dampers used in this study were shock absorbers that were repurposed from an intended use in hobby radio-controlled cars. These devices provide damping through the dynamic motion of a plunger through an oil-filled chamber. The dampers were filled with 30-weight oil, which was determined to be an appropriate viscosity based on a preliminary investigation. The properties of each of the four dampers used in this study were characterized in a separate single-degree-of-freedom test structure subjected to shaped random ground motion. Each damper was pin connected to two sets of aluminum mounts fixed to the test structure's top and bottom plates. From these tests, the average effective viscous damping provided by a single damper was identified to be 77±23 Ns/m. The variability in the estimated effective viscous damping existed for the different dampers as well as the same damper in repeated trials.

A pair of aluminum brackets were used to connect each damper between floors of the primary structure. The mass of a single damper with brackets and associated hardware was 0.733 kg. When considering a distributed arrangement of the dampers, a damper was placed in each story of the primary structure at the centerline of the floor and orientated in the flexible direction of the structure. When considering concentrated arrangements of the dampers, all four dampers were placed in a single story, arranged symmetrically along the centerline of the floor, and orientated in the flexible direction of the structure**. Figure 4-3** shows photos of the dampers connected in a story of the structure in the concentrated and distributed configurations.

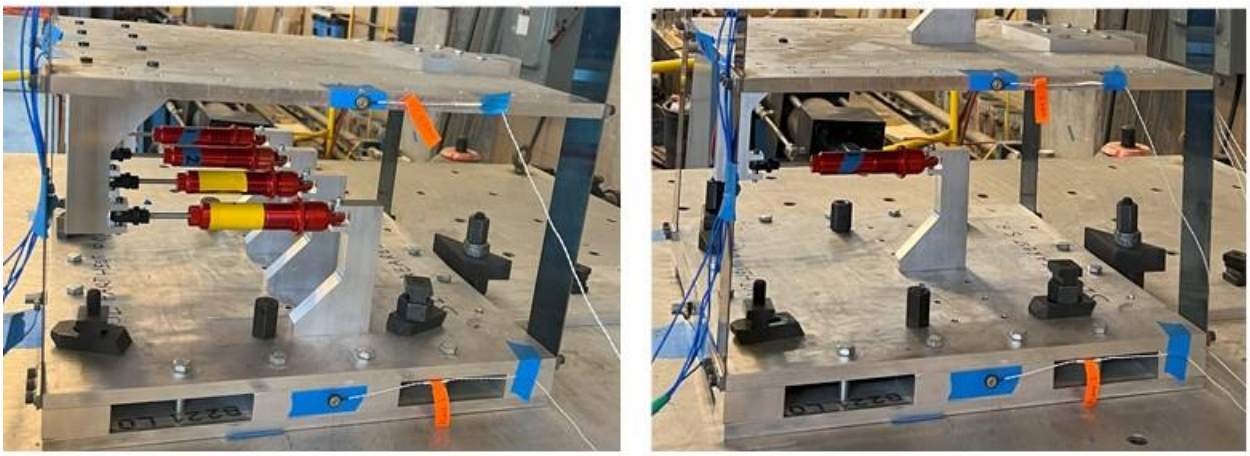


Figure 4-3: Dampers connected in a story of the structure. Left- Concentrated arrangement in the first story, Right- Distributed arrangement showing first story only.

4.3 DESCRIPTION OF EXPERIMENTAL TESTS

This section describes the structure configurations, ground motions, and data collected during the experimental tests.

4.3.1 Structure Configurations

Table 4-1 shows the system configurations utilized for the experimental testing. To investigate the impact of stiffness irregularities on the dynamic performance of the model structure, tests were performed for configurations where reduced thickness columns were installed in lieu of the original thickness columns in a single story. There were eight such configurations, four (one for each story) times two (with and without strongback). Additionally, two configurations (with and without strongback) with all original thickness columns were tested as a control. No dampers were used in any of the tests investigating stiffness irregularities.

To investigate the impact of damper arrangement, tests were performed for configurations where all four dampers were installed in a single story. There were eight such configurations, four (one for each story) times two (with and without strongback). Additionally, two configurations (with and without strongback) with the dampers distributed one per story were tested as a control. Original thickness columns were used in all stories for all tests investigating damper arrangement.

As seen in **Table 4-1**, SI1, SI2, SI3, and SI4 refer to configurations without the strongback and with the stiffness irregularity in the first, second, third, and fourth stories, respectively. NSI refers to the configuration with no stiffness irregularity in the primary structure and without the strongback. DC1, DC2, DC3, and DC4 indicate configurations without the strongback and dampers concentrated in the first, second, third, and fourth stories, respectively. DDA refers to the distributed damper configuration where all stories have one damper and without the strongback. The same configurations, but with the strongback, are denoted with "-SB" appended to the configuration name.

Table 4-1: System configurations for stiffness irregularity and damper arrangement tests

Test Type	Strongback Config.	Config. Name	Column thickness at Each Story				Number of Damper at Each Story			
			1st	2nd	3rd	4th	1st	2nd	3rd	4th
Stiffness Irregularity (SI)	No Strongback	SI1	R	O	O	O	---	---	---	---
		SI2	O	R	O	O	---	---	---	---
		SI3	O	O	R	O	---	---	---	---
		SI4	O	O	O	R	---	---	---	---
		NSI	O	O	O	O	---	---	---	---
	Strongback (SB)	SI1-SB	R	O	O	O	---	---	---	---
		SI2-SB	O	R	O	O	---	---	---	---
		SI3-SB	O	O	R	O	---	---	---	---
		SI4-SB	O	O	O	R	---	---	---	---
		NSI-SB	O	O	O	O	---	---	---	---
Damper Arrangement	No Strongback	DC1	O	O	O	O	4	---	---	---
		DC2	O	O	O	O	---	4	---	---
		DC3	O	O	O	O	---	---	4	---
		DC4	O	O	O	O	---	---	---	4
		DDA	O	O	O	O	1	1	1	1
	Strongback (SB)	DC1-SB	O	O	O	O	4	---	---	---
		DC2-SB	O	O	O	O	---	4	---	---
		DC3-SB	O	O	O	O	---	---	4	---
		DC4-SB	O	O	O	O	---	---	---	4
		DDA-SB	O	O	O	O	1	1	1	1
O: Original column thickness R: Reduced column thickness										

4.3.2 Ground Motions

A 6 degree-of-freedom shake table at the University of Tennessee was used to provide ground motions for this testing. This table is 1.2 m x 1.2 m and was designed and built by Shore Western Manufacturing.

To avoid biasing the results of this study towards a single earthquake record, six seismic ground motions were used to assess the differences in the seismic response of the structural configurations shown in **Table 4-1**, specifically story and roof drift. The six records chosen were recorded from historic events and were obtained from the Pacific Earthquake Engineering Research Center (PEER) ground motion database (Ancheta et al., 2014), and some have been widely used for shake table testing (Alemdar and Al-Gaadi, 2022; Fahnestock et al., 2021; Teh and Venkatratnam, 2015; Maree et al., 2015; Lu et al., 2012; Lignos, 2008; Lu et al., 2008; Li et al., 2006). In all cases, only component A, as denoted in the PEER database, of the recorded ground motions was used. These ground motions were applied as unidirectional horizontal motions by the shake table in the flexible direction of the structure. The records were scaled down separately to an amplitude that resulted in significant motion of the physical model without damaging it. While the shake table is unable to perfectly replicate each of the ground motions, an iterative process was used before testing the structure to produce shake table commands that largely reproduce the desired ground motions. The properties of the six recorded historic seismic ground motions are provided in **Table 4-2.**

Table 4-2: Identifying information and properties of ground motions used for shake table tests

No.	**Earthquake name**	**Station**	**Year**	**Mag.**	**Unscaled PGA max (g)**	**Scaled % used for the test**
1	Northridge	Beverly Hills-Mulhol	1994	6.7	0.52	15
2	Kobe, Japan	Shin-Osaka	1995	6.9	0.24	20
3	Imperial Valley	El Centro Array #11	1979	6.5	0.38	30
4	Manjil, Iran	Abbar	1990	7.4	0.51	30
5	Chi-Chi, Taiwan	CHY101	1999	7.6	0.44	20
6	Landers	Coolwater	1992	7.3	0.42	20

In addition to the recorded seismic ground motions, a shaped white noise loading was employed to examine the dynamic properties of the model structure, especially its first natural frequency and first mode damping ratio. This type of load was chosen for evaluating the structure's dynamic properties as the longer duration and broadband nature of this loading allowed for estimating the system's frequency response functions with more clarity and definition. The white noise loading was generated from a 300-second random acceleration that was subjected to a lowpass filter with a cutoff frequency of 200 Hz. This load was also applied as ground motion by the shake table in the flexible direction of the structure. The white noise was scaled such that the maximum response of the structure when subjected to the white noise was comparable to that for the recorded ground motions.

Each of the seven ground motion records (six seismic records and one shaped white noise) was applied to each of the 20 structure configurations **(Table 4-1**). As a result, 140 shake table tests were performed for this study.

4.3.3 Instrumentation and Data Acquisition

PCB model 352C33SN accelerometers connected to a data acquisition system with a sampling rate of 10,240 Hz were used to capture the acceleration of the ground (shake table) and the acceleration of each floor of the structure. The accelerometers were mounted to the middle of the side of each floor plate and the base plate. These accelerometers measured the acceleration in the structure's flexible direction, which was the primary direction of motion. Additionally, two accelerometers were mounted on top of the strongback and orientated to measure along both horizontal directions. These acceleration measurements were primarily used to estimate the structures' natural frequency and damping.

The displacement response of each floor plate, the base plate, and the strongback were captured using an NDI Optotrak, an optical measurement system that tracks emitted infrared light from markers placed on these components. This system used a sampling rate of 50 Hz. The absolute position of each marker was measured in three dimensions with a separate data acquisition system and synchronized with the acceleration measurements in post-processing. The motion of the structure in its flexible direction was extracted from the three-dimensional marker position data. These displacement measurements were used to calculate the resulting story and roof drifts.

The arrangement of the accelerometers and infrared markers on the structure is shown in **Figure 4-4.**

The system response to the white noise was used to estimate the structure's first-mode natural frequency and damping ratio for each system configuration. Numerical frequency response functions were estimated between the roof absolute acceleration and the base absolute acceleration using the tfestimate function in MATLAB (The MathWorks Inc, 2020a). Curve fitting was then used to match a single degree-of-freedom analytical dynamic model to the numerical frequency response functions produced from the experimental data using the system identification toolbox in MATLAB (The MathWorks Inc, 2020b). This curve fit only considered the frequency response function values within ±0.5 Hz of an initial estimate of the first mode frequency. Finalized system first mode damping and natural frequency estimates were then extracted from the natural frequency and damping ratio of the fit analytical single-degree-of-freedom model.

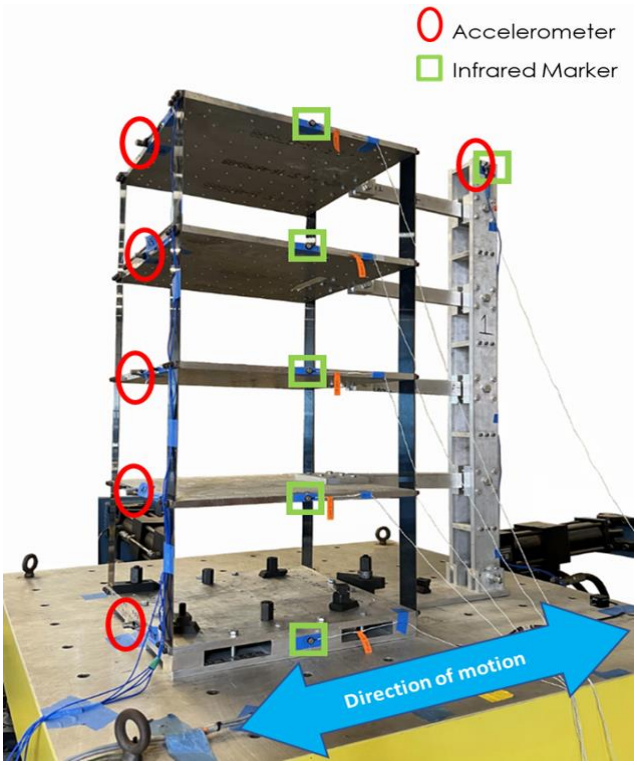


Figure 4-4: Primary structure with the strongback on the shake table with annotations highlighting the instrumentation

4.4 RESULTS AND DISCUSSION

The experimental results and discussion thereof are divided into two parts. The first part presents and discusses results from the stiffness irregularity study and the second part presents and discusses results from the damper arrangement study.

4.4.1 Stiffness Irregularity

The first natural frequency for each of the ten system configurations in the stiffness irregularity study (**Table 4-1**), as determined from the acceleration data from the shaped white noise tests, is shown in **Figure 4-5.** This data shows that reducing the stiffness of a story decreases the natural frequency regardless of the presence of a strongback. However, with a strongback the decrease is less pronounced. For both with and without a strongback, the decrease in natural frequency is, in general, more pronounced as reduced thickness columns are positioned in progressively lower stories of the structure. With all original thickness columns (i.e., configurations NSI and NSI-SB), the estimated first mode frequency of the structure with the strongback is lower than without the strongback. This result is due to the additional mass provided to the system by the strongback and not the presence of a decrease in stiffness resulting from the strongback. Shifts in the first mode frequency due to stiffness irregularities are shown in **Figure 4-5** with and without the strongback.

These results show much greater consistency in the first mode frequency results for the configurations with the strongback. Specifically, the difference between the highest and lowest first natural frequency is shown to be 0.77 Hz without a strongback and 0.30 Hz when the strongback is utilized. These results suggest that the strongback can limit the impact of stiffness irregularities on the dynamic properties of the system, which may lead to more stable and predictable performance under different loading conditions.

Figure 4-6 shows the response of all the structure configurations in the stiffness irregularity study to the seven different ground motions. For each data point in **Figure 4-6**, the maximum story drift is calculated over the duration of the test and over all the stories. As seen from this figure, there is a wide range of results from the different configurations of the structure to the ground motions.

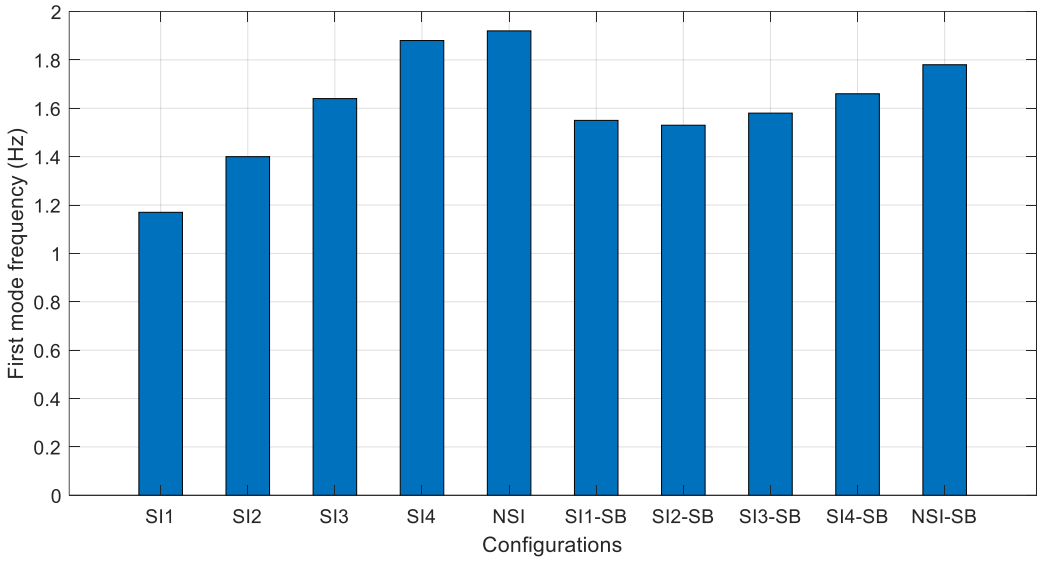


Figure 4-5: Estimated first mode frequency of the structure with and without the strongback given the structural configurations used for the stiffness irregularity study

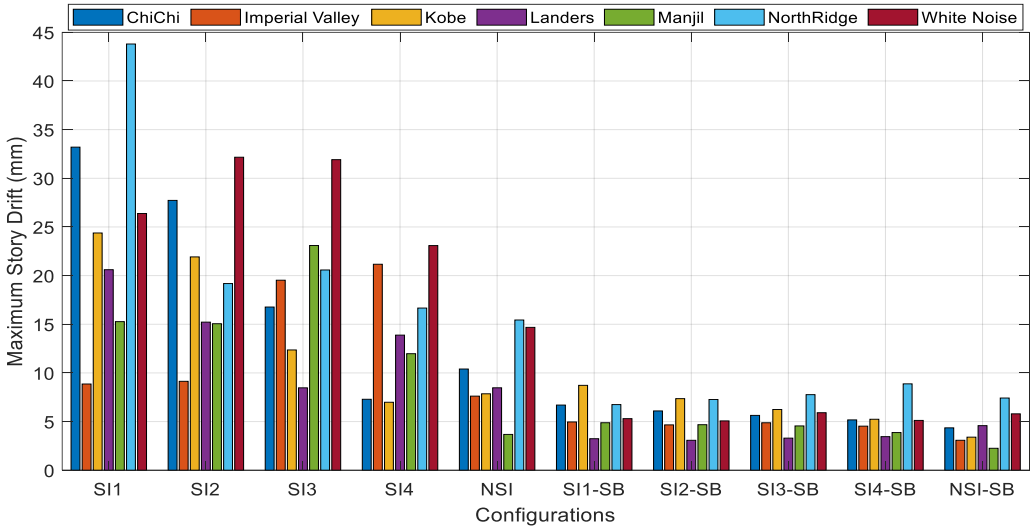


Figure 4-6: Maximum story drift from tests in the stiffness irregularity study.

As expected due to the varying nature and frequency content of the ground motions, no one configuration yields the maximum or minimum story drifts for all of the ground motions. **Figure 4-6** does show that, in general, the presence of a strongback results in a significant reduction in the maximum story drift. While some of this reduction in maximum story drift is related to the stiffness effects of the strongback, much of this reduction can be attributed to the increased effective damping in the structure as a result of friction in the pinned joints of the strongback. While increased damping is present with the strongback in this experimental model, the strongback itself would not significantly increase damping in a realistic structure as it would not be designed to be an energy dissipating element. To compensate for the damping differences in the structure with and without the strongback, the maximum story drifts for all configurations and ground motions were normalized and plotted in **Figure 4-7**. For each ground motion, the maximum story drift was normalized by dividing by the maximum story drift from configuration NSI (for configurations without the strongback) or NSI-SB (for configurations

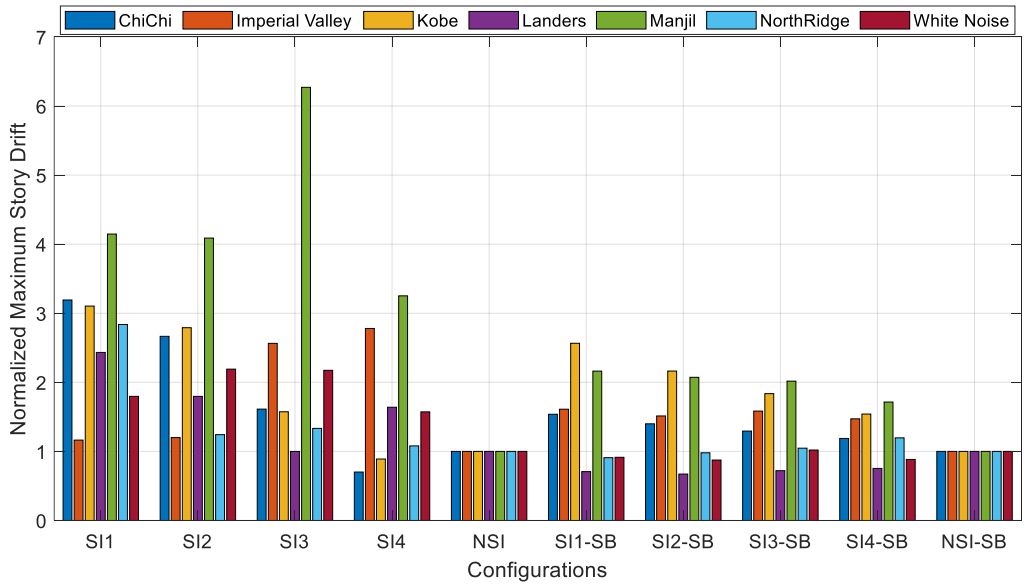


Figure 4-7: Normalized maximum story drift from tests in the stiffness irregularity study. Normalization of results from each record are performed with respect to the NSI configuration story drift results for systems without the strongback and with respect to the NSI-SB configuration story drift results for systems with the strongback

with the strongback). The use of this normalization enables identification of the impact of the stiffness irregularity on the maximum story drift, controlling for differences in mass and damping. The results in show that with and without the strongback, the maximum story drift, in general, increases with the presence of a stiffness irregularity and that the increase in maximum story drift grows as the stiffness irregularity is positioned lower in the structure. Furthermore, in general, the normalized maximum story drift is higher for the structure without the strongback: the peak normalized maximum drift without the strongback is 6.27 and the peak with the strongback is 2.57. There are a number of counter-examples to the general trends discussed in the previous paragraph. This is not unexpected due to the complex interaction between the dynamics of the structure and the ground motions, which both vary in frequency content. Given this variability, rather than comparing individual test results, the average and standard deviation of the results can be considered.

The average normalized maximum story drift with a stiffness irregularity is 2.25 for configurations without a strongback and 1.37 for configurations with a strongback. The standard deviation for configurations with a stiffness irregularity is 1.22 for configurations without a strongback and 0.52 for configurations with a strongback. These results show that, while the strongback is not guaranteed to have a beneficial effect; on average, it greatly reduces normalized maximum story drifts resulting from the presence of the stiffness irregularities considered.

The maximum roof drifts for all configurations and ground motions were normalized in the same manner as for The maximum roof drifts for all configurations and ground motions were normalized in the same manner as for **Figure 4-7** and are plotted in **Figure 4-8**. The peak normalized maximum roof drift without the strongback is 3.25, which is much lower than the peak normalized maximum story drift without the strongback which was 6.27, and the peak normalized maximum roof drift with the strongback is 2.57, which, when rounded, is the same as the peak maximum story drift value with the strongback.

Furthermore, the average normalized maximum roof drift for configurations with a stiffness irregularity was found to be 1.38 for configurations without a strongback and 1.33 for configurations with a strongback. The standard deviation of the normalized maximum roof drift for configurations with a stiffness irregularity was found to be 0.68 for configurations without a

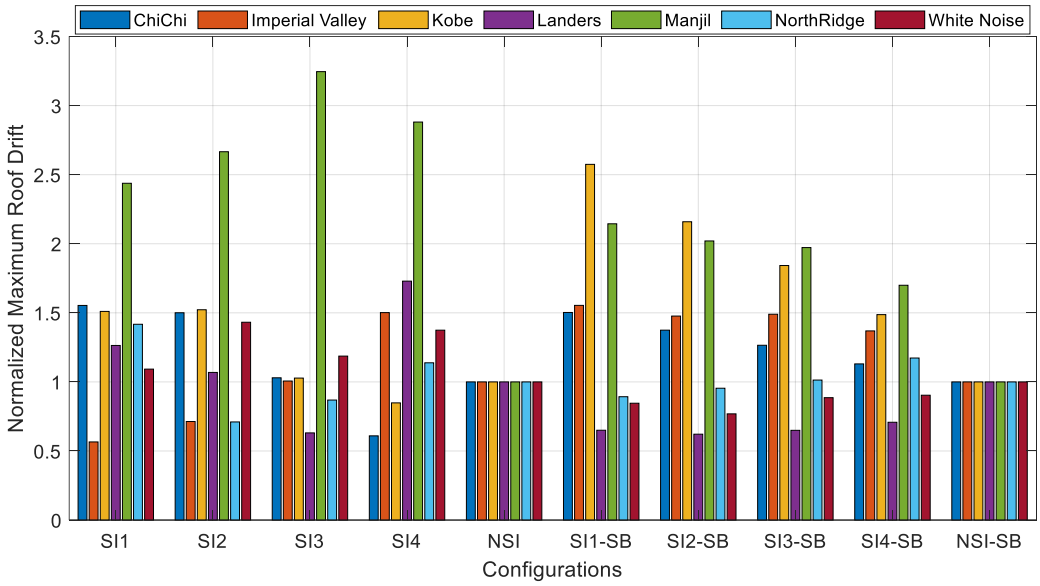


Figure 4-8: Normalized maximum roof drift from tests in the stiffness irregularity study. Normalization of results from each record are performed with respect to the NSI configuration roof drift results for systems without the strongback and with respect to the NSI-SB configuration roof drift results for systems with the strongback

strongback and 0.53 for configurations with a strongback. The consistency of the resulting normalized maximum story drift and maximum roof drift with the strongback indicates that the strongback imposes nearly uniform story drifts despite stiffness irregularities. In contrast, the large difference in normalized maximum story and roof drift values without the strongback is indicative of deformation concentrations.

Figure 4-9 shows the maximum drift for each story over the length of the excitation for all configurations in the stiffness irregularity study, with and without the strongback, and for all seismic records. This figure shows that, without the strongback, the maximum story drift is observed at the story with the stiffness irregularity. However, when a strongback is utilized, the drift is largely uniformly distributed across all stories for all seismic records. Even in the case where there is no stiffness irregularity, the presence of the strongback yields significantly more uniform story drift distribution. The results indicate that regardless of the position of the stiffness irregularity, the strongback effectively achieves uniform distribution of drift along the height of the structure.

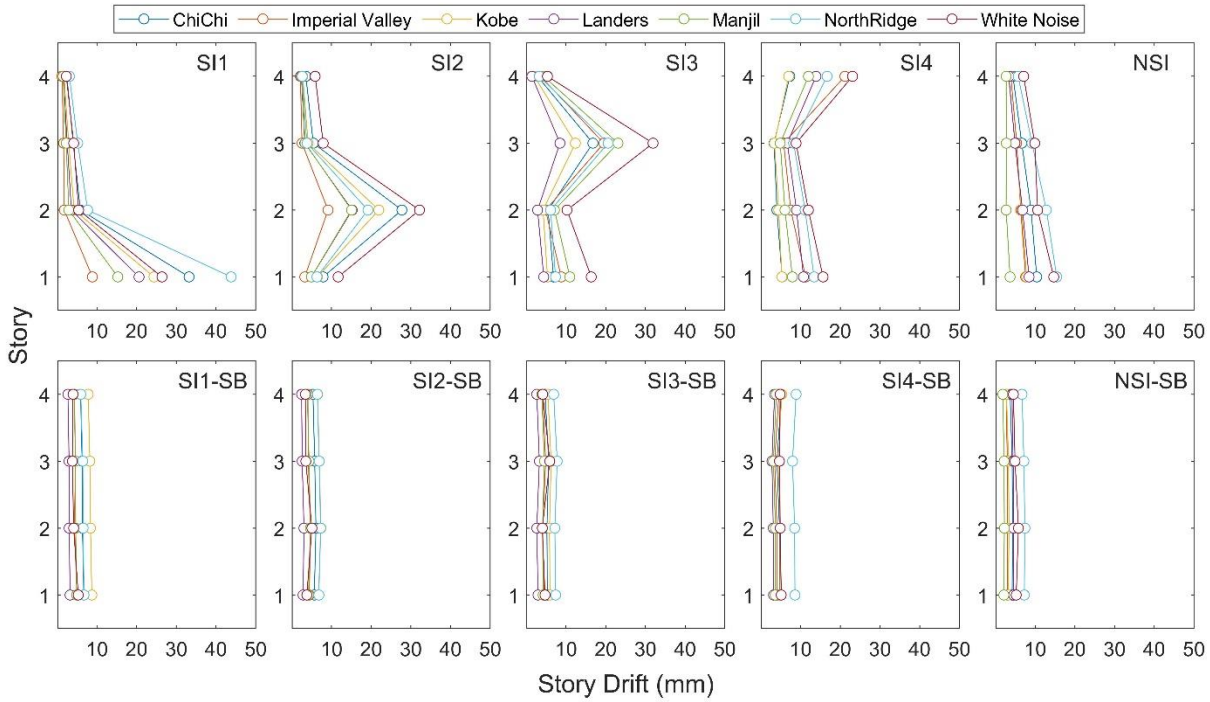


Figure 4-9: Story drifts with and without strongback for all configurations in the stiffness irregularity study and for all seismic records

4.4.2 Damper Arrangement

The first natural frequency for each of the ten system configurations in the damper arrangement study (**Table 4-1**), as determined from the acceleration data from the shaped white noise tests, are shown in **Figure 4-10**. Comparing the frequencies of configurations DDA and DDA-SB in Comparing the frequencies of configurations DDA and DDA-SB in **Figure 4-10** and configurations of NSI and NSI-SB in **Figure 4-5**, it is seen that the addition of the dampers leads to a small change in the first-mode frequency. While the addition of viscous damping does not typically change the natural frequency of structures, the dampers used in this work did not add solely pure viscous damping; rather, the dampers and their mounts have an associated mass and physical dampers have a complicated restoring force that includes stiffness effects. The results in The results in **Figure 4-10** shows that the first mode natural frequency increases as the location of the concentrated dampers moves down the height of the structure; however, these changes in first mode frequency are small compared to the changes observed in **Figure 4-5** for the different locations of reduced thickness columns. Additionally, the results in Additionally, the results in **Figure 4-10** show that the first natural frequency is lower for configurations with the strongback, which is expected due to the additional mass of the strongback.

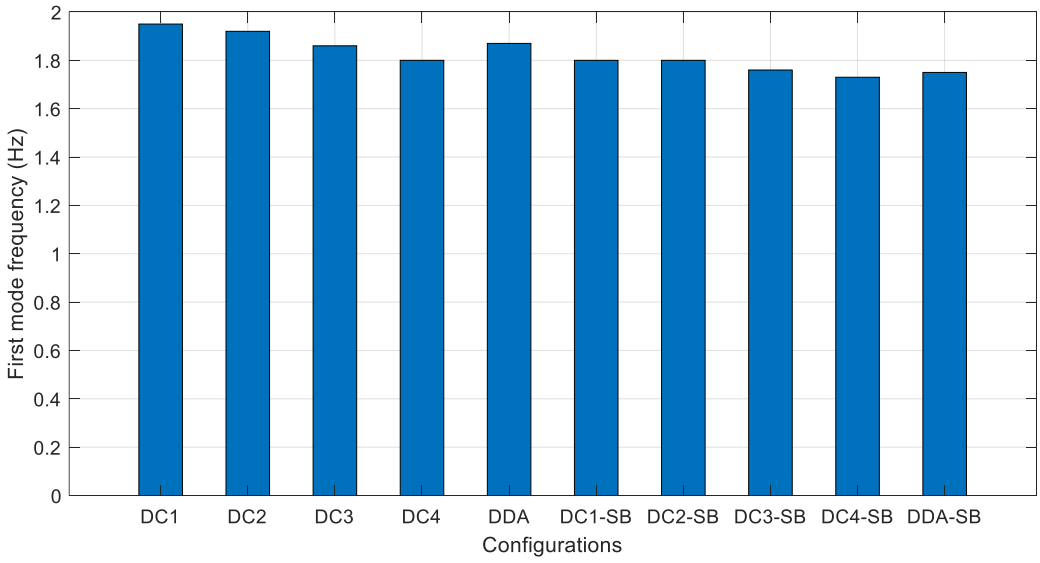


Figure 4-10: Estimated first mode frequency of the structure with and without the strongback given the structural configurations used for the damper arrangement study

The estimated damping associated with each configuration's first natural frequency was produced using the results with the white noise loading and are shown in **Figure 4-11.** This figure shows that with the strongback there is much higher first mode damping, which is the expected result for this model due to added frictional effects from the pins of the strongback at the base and its connections to each floor. **Figure 4-11** also shows that the estimated damping for the configurations without the strongback change significantly with some of the concentrated damper configurations having higher estimated damping than the distributed configuration and some having lower estimated damping. In contrast, the estimated damping with the strongback is more consistent when comparing the estimated values from the concentrated and distributed damper configurations.

Figure 4-12 shows the maximum story drift calculated from the response of all the structure configurations in the damper arrangement study to the seven different ground motions considered. To compensate for the damping differences in the structure with and without the strongback, the maximum story drifts for all configurations and ground motions were normalized and plotted in **Figure 4-13**. For each ground motion, the maximum story drift was normalized by dividing by the maximum story drift from configuration DDA (for configurations without the strongback) or DDA-SB (for configurations with the strongback). The use of this normalization enables identification of the impact of the damper arrangement on the maximum story drift, controlling for differences in mass and damping.

The results in **Figure 4-13** show that the largest and smallest normalized maximum drift without the strongback are 1.56 and 0.54 and the largest and smallest normalized maximum drift with the strongback are 1.22 and 0.88. The average normalized maximum story drift with concentrated dampers was found to be 1.06 for configurations without a strongback and about 1.00 for configurations with a strongback. Additionally, the standard deviation with concentrated dampers was found to be 0.26 for configurations without a strongback and 0.08 for configurations with a strongback. These results show that the placement and concentration of dampers has a large impact on the response of the system without the strongback; furthermore, with the dampers considered in this investigation, this included times where the impact is beneficial and other times where the impact is detrimental. In contrast these results also show that the placement and concentration of dampers has little effect on the system with a strongback.

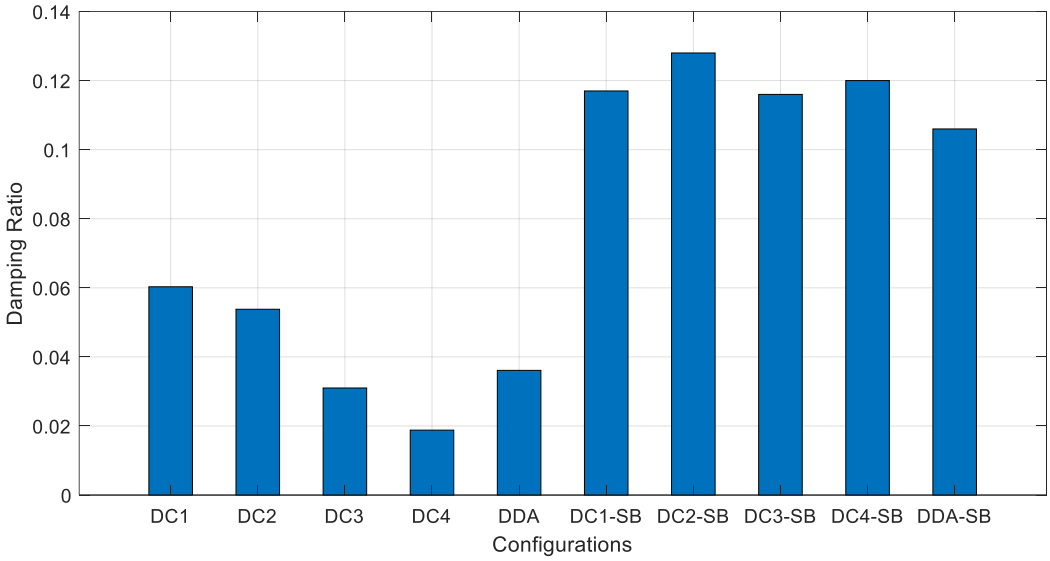


Figure 4-11: Estimated damping ratio of the structure with and without the strongback given the structural configurations used for the damper arrangement study

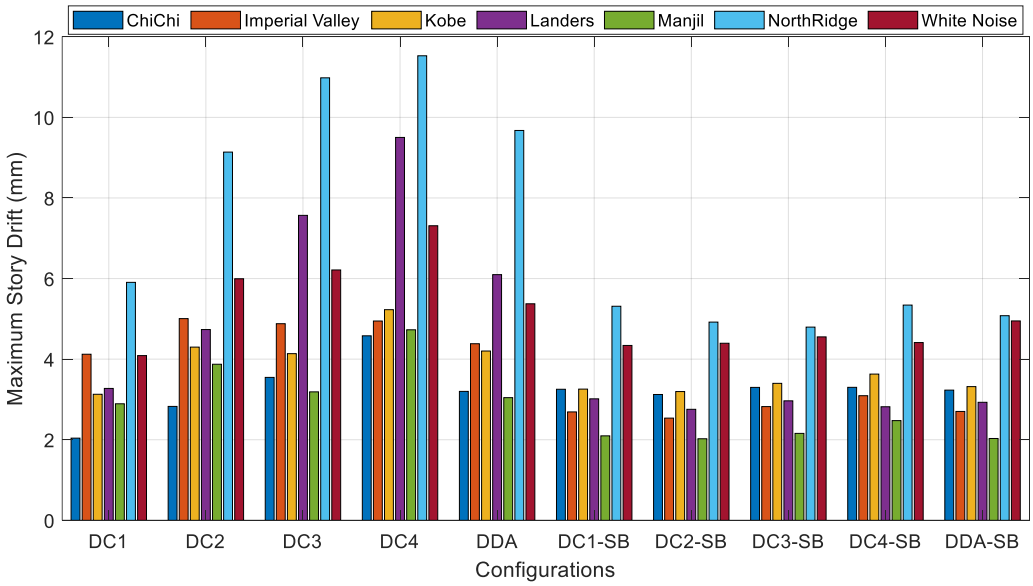


Figure 4-12: Maximum story drift from tests in the damper arrangement study

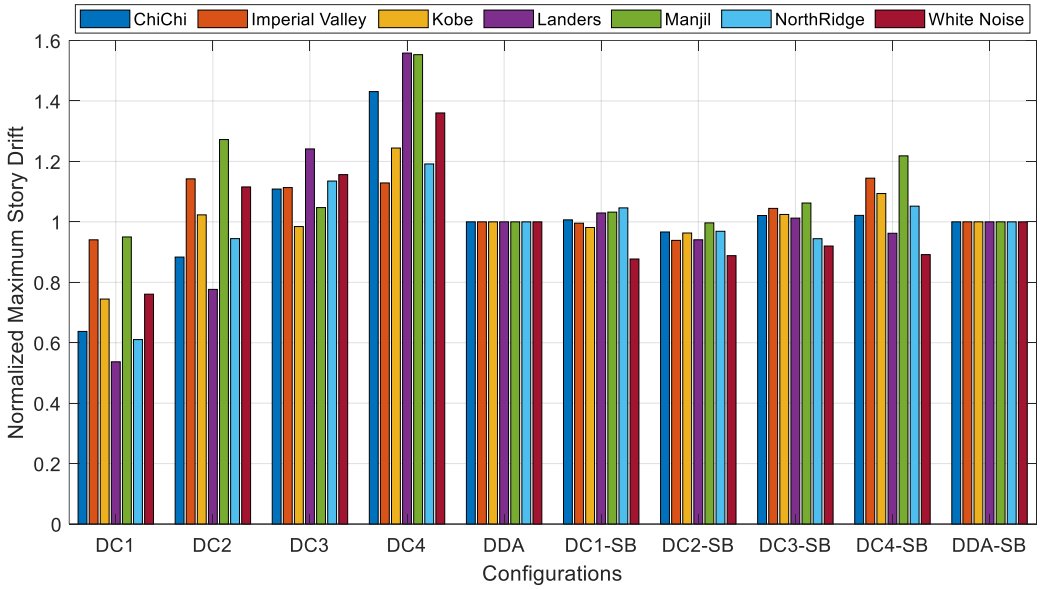


Figure 4-13: Normalized maximum story drift from tests in the damper arrangement study. Normalization of results from each record are performed with respect to the DDA configuration story drift results for systems without the strongback and with respect to the DDA-SB configuration story drift results for systems with the strongback.

The normalized maximum roof drifts for all configurations and ground motions were calculated and are plotted in **Figure 4-14**. For each ground motion, the maximum roof drift was normalized with respect to the distributed dampers and no strongback configuration (DDA) for systems without a strongback and with respect to the distributed dampers with a strongback configuration (DDA-SB) for systems with a strongback. From the results in **Figure 4-14**, the average normalized maximum roof drift with concentrated dampers was found to be 1.04 for configurations without a strongback and 1.01 for configurations with a strongback. The standard deviation of the normalized maximum roof drift with concentrated dampers was found to be 0.26 for configurations without a strongback and 0.06 for configurations with a strongback. The consistency of the resulting normalized maximum story drift with the maximum roof drift both with the strongback and without the strongback indicates that this concentration of dampers does not lead to a large increase in concentration of localized story drift, which was seen considering stiffness irregularities.

Figure 4-15 shows the story drifts for all configurations in the damper arrangement study, with and without the strongback, and for all seismic records. This figure shows that, without the strongback, there are differences in the patterns and amplitudes of maximum story drift observed

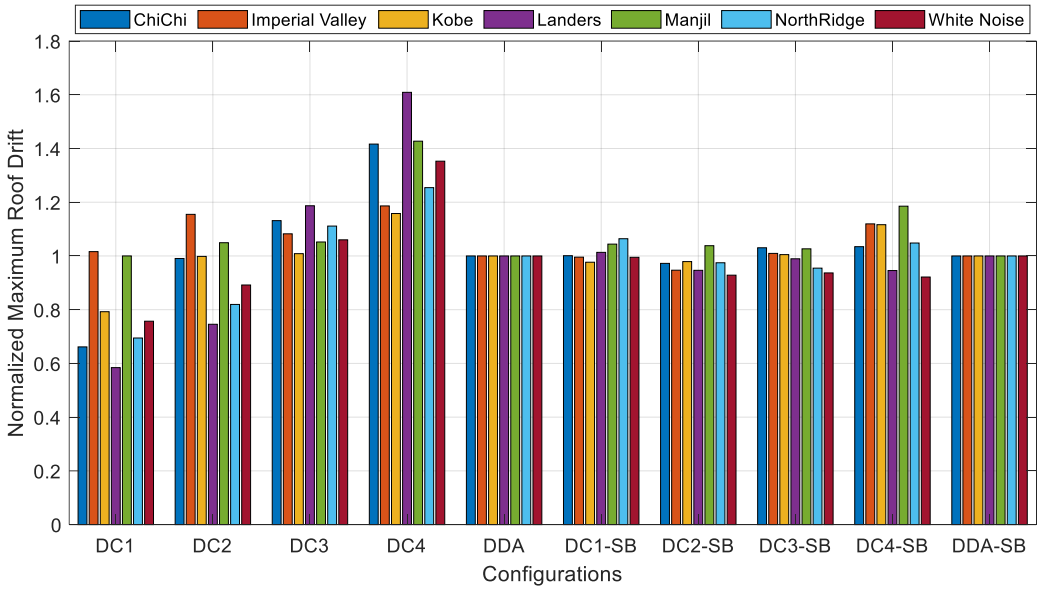


Figure 4-14: Normalized maximum roof drift from tests in the damper arrangement study. Normalization of results from each record are performed with respect to the DDA configuration roof drift results for systems without the strongback and with respect to the DDA-SB configuration roof drift results for systems with the strongback

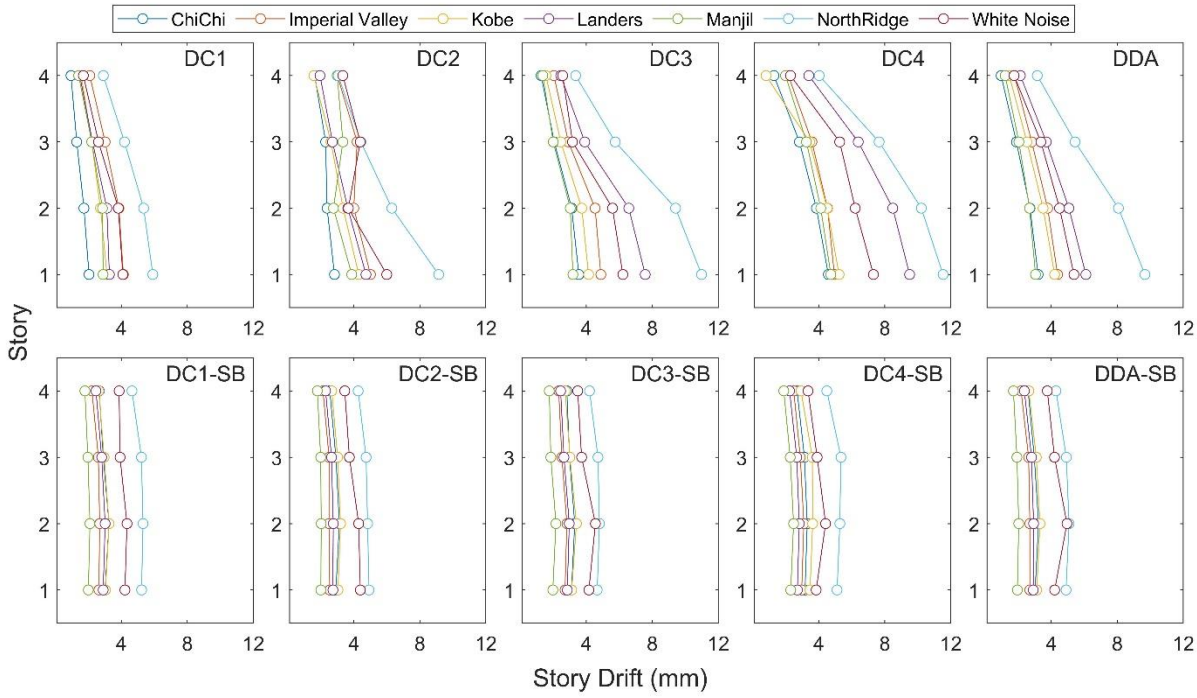


Figure 4-15: Story drifts of structure with and without strongback for all damper arrangement configurations and for all seismic records

for the different damper arrangements, but, in general, story drifts are more concentrated in the lower stories of the structure. However, when a strongback is utilized, the drift is largely uniformly distributed across all stories for all seismic records and damper arrangements and the damper arrangement has a smaller impact on the amplitudes of the story drift.

4.5 CONCLUSIONS

The main focus of this work was to explore the impacts of damper arrangement and the location of soft story vertical stiffness irregularities on the dynamic behavior and properties of a structure with a strongback. The investigation was carried out through experiments conducted on a small-scale four-story structure that was subjected to ground motion generated by a shake table. This small-scale structure was tested with and without an attached strongback. The location of stiffness irregularities resulting from a reduction in column thickness at specific stories and the distribution of dampers at various stories of the structure were separately varied in the experiments. Maximum story and roof drift of the structure and the changes in its first natural frequency and damping were evaluated. As expected, due to the complex interaction of varying structural dynamics and ground motion dynamics, large variability in the results were observed considering the different ground motions. However, based on the results of this work, the following conclusions can be made:

- Without the strongback, the first mode frequency of the structure changed significantly depending on the location of the stiffness irregularity at different stories in the structure. In contrast, the inclusion of the strongback, a stiff elastic spine, resulted only in small changes in first mode frequency when evaluating the structure with stiffness irregularities at different stories.
- Without the strongback, the maximum story drifts were measured to be much higher on average than compared to with the strongback, even when controlling for the additional mass and damping of the strongback in the model.
- In both the stiffness irregularity study and the damper arrangement study, it was observed that the use of the strongback resulted in a largely uniform distribution of story drift along the

height of the structure regardless of the stiffness irregularity or damper arrangement considered.

- The inclusion of the strongback resulted in consistency in the estimated first mode damping and maximum story drift when evaluating the structure with different damper arrangements.

The strongback's ability to protect against soft story vertical stiffness irregularities, regardless of their location, presents promising new options for structural design, architectural design, and the remediation of existing structures. Furthermore, the results of this work suggest that, with the strongback, energy dissipation devices can achieve similar levels of effectiveness if they are distributed throughout a structure or concentrated at one level or perhaps concentrated in a single large device. A topic of investigation that logically follows on the results of this study is the behavior of strongbacks combined with innovative energy dissipation devices that are well-suited to being concentrated. Also, the development of design methods for strongback systems that consider various distributions of energy dissipation devices and intentional stiffness irregularities is still needed.

Chapter 5 : IMPACT OF A TUNED JOINT ON THE BEHAVIOR OF A SEGMENTAL STRONGBACK

The effectiveness of continuous strongback systems can diminish in taller buildings due to elevated force demands caused by higher-mode effects. Segmenting the strongback has been proposed as a means to alleviate these demands while retaining the drift-controlling benefits of the system. Although numerical studies have shown that segmental strongbacks can reduce internal forces without compromising overall performance, most previous research has idealized the connections between segments as perfectly pinned joints. This simplification neglects the influence of joint stiffness on force distribution, drift patterns, and energy dissipation, particularly under varying seismic demands.

To address these limitations, this chapter presents a two-phase investigation aimed at understanding how tuning the joint stiffness between strongback segments can influence seismic performance. The first phase, detailed in Section 5.1, examines the integration of a nonlinear rotational inertial mechanism at the joint. This study investigates how such a mechanism can influence system behavior under varying levels of white noise excitation. This portion of the work is presented in the form of a standalone manuscript, which was accepted for presentation at the International Modal Analysis Conference (IMAC) 2025.

Abolghasemi, S., Wierschem, N., 2025. Exploring the Role of a Nonlinear Rotational Inertial Mechanism at the Joint of a Segmented Strongback Structural System. Presented at the International Modal Analysis Conference (IMAC), Orlando, FL.

The second phase of this investigation, presented in Section 5.2, involves both experimental and numerical studies of segmental strongbacks with linear rotational springs at the joint. Five levels of joint stiffness are evaluated in the physical tests using a 5-story structure model subjected to ground motions. A complementary numerical analysis explores a broader range of stiffness values under an expanded suite of seismic ground excitations to assess trends and potential for drift control and moment reduction.

Together, the two phases presented in this chapter aim to fill critical gaps in the current understanding of segmented strongback systems by evaluating the role of joint stiffness and advanced joint mechanisms in shaping structural response. The findings offer insight into practical design modifications that can be employed to optimize performance while maintaining simplicity and adaptability in real-world applications.

5.1 EXPLORING THE ROLE OF A NONLINEAR ROTATIONAL INERTIAL MECHANISM AT THE JOINT OF A SEGMENTED STRONGBACK STRUCTURAL SYSTEM

5.1.1 Introduction

Seismic events can induce soft story mechanisms, which jeopardize the structural integrity of buildings. To mitigate this risk, a promising approach involves integrating a stiff, elastic spine, commonly referred to as a "strongback," that extends vertically throughout the structure and is anchored at the base. This spine ensures a more uniform displacement profile across the building's height, helping to prevent concentrated damage and premature failure (Faramarzi and Taghikhany, 2021; Simpson and Mahin, 2018). Research on strongbacks has shown that structures equipped with strongbacks exhibit more controlled story drifts, enhancing the overall seismic resilience by delaying or preventing soft story collapse (Fahnestock et al., 2021; Hu et al., 2021; Simpson and Mahin, 2018).

One means that has been investigated to improve the performance of buildings with strongbacks is the incorporation of structural control devices. Various types of structural control devices, including friction spring dampers with recentering capabilities, shear-type steel dampers, and viscous dampers, have been implemented in spine-supported structures to absorb seismic energy and reduce drift. For instance, Hu et al. (2021) integrated friction spring dampers along the height of a steel structure with rigid spines, effectively mitigating drift and ensuring the structure's return to its original position. Other approaches, such as those by Qu et al. (2012), used shear-type dampers in steel-reinforced concrete frames, distributed along multiple stories. Palermo et al. (2021b) explored configurations of viscous dampers at varying heights and found that the strongback's ability to impose uniform drift patterns allows for more flexibility in damper placement. Experimental investigations, such as that by Abolghasemi et al. (2024b), further demonstrated that strongbacks can reduce the sensitivity of structural performance to the placement of dampers, making the system less reliant on precise damper positioning. This flexibility in the arrangement of structural control devices, combined with the strongback's ability to impose uniform drift, significantly enhances the overall seismic resilience of the structure.

Rotational inertial mechanisms are another type of structural control device that have been investigated when incorporated into strongback systems. Rotational inertial mechanisms convert translational motion into rotational motion and in the process can add large mass effects to the systems they are incorporated into. Abolghasemi et al. (2024a) investigated linear rotational inertial mechanisms, known as an inerter, incorporated into a structure with a strongback as interstory devices. A similar nonlinear rotational inertial mechanism can produce variable mass effects that can be used to disrupt the formation of resonant conditions investigated linear rotational inertial mechanisms, known as an inerter, incorporated into a structure with a strongback as inter story devices. A similar nonlinear rotational inertial mechanism can produce variable mass effects that can be used to disrupt the formation of resonant conditions (Sarkar and Wierschem, 2024b); however, this device has not been investigated in combination with strongback systems.

A key unresolved issue with strongbacks is the tendency for higher mode effects to result in large forces in the strongback and high floor accelerations. These undesirable results occur because the higher modes of vibration conflict with the pattern of uniform story drift that the strongback tries to impose on the structure. A proposed solution is to divide a continuous vertical spine of the strongback into two or more segments along the height of the structure that are pin connected. This segmentation approach, known as the segmented strongback, has been introduced to improve retrofit cost efficiency (Balazadeh-Minouei et al., 2018) and structural performance (Chen et al., 2019b, 2018; Tremblay et al., 2014), particularly in taller buildings. Previous numerical studies on segmented spines have demonstrated that dividing the spine into multiple segments effectively reduces the force demand on each segment while still maintaining control over the overall drift of the structure (Tremblay et al., 2014).

The concentrated motion at the joint of a segmented strongback presents an opportunity to incorporate a structural control device that could enhance system performance. This research investigates the use of a nonlinear rotational inertial mechanism at the joint in a segmented strongback system. This device introduces mass effects into the system by converting translational motion into rotational motion, with a nonlinear ball-screw mechanism enabling the adjustment of these mass effects based on the ball-screw shaft design and the response

amplitude. This study provides experimental validation through shake table tests on a 5-story structure equipped with a segmented strongback and a nonlinear rotational inertial mechanism.

5.1.2 Model and Properties

5.1.2.1 Structure

The experimental setup utilized in this work consists of a model five-story structure with a segmented strongback, as shown in **Figure 5-1**. Each of the five floor plates, including the base plate, measured 457.2 mm by 457.2 mm with a thickness of 12.7 mm and has a mass of approximately 8 kg. To provide lateral and vertical support, a total of 20 spring steel columns were installed, each having dimensions of 50.8 mm in width and 1.575 mm in thickness. These columns were oriented and connected such that the structure remained flexible in one lateral direction while maintaining stiffness in the orthogonal direction. The vertical spacing between each floor, measured from plate center to center, was 244.5 mm, with a clear story height of 231.8 mm. The flexural rigidity (EI) of the spring steel columns was calculated through a three-point bending test, yielding a value of 3.205 $N \cdot m^2$.

The lower portion of the segmented strongback system is composed of two aluminum plates measuring 76.2 mm by 546.1 mm by 12.7 mm that are rigidly tied together and pinned at the base of the structure. The lower portion of the segmented strongback is connected with a pin joint to two additional plates of 76.2 mm by 884.3 mm by 12.7 mm that are rigidly tied together and form the upper portion of the strongback. A close up view of the joint of the segmented strongback is shown in **Figure 5-1**-Right. Fixturing has been incorporated near the joint of the segmented strongback to allow for the connection of the rotational inertial mechanism, which is described below.

The strongback was connected to the main structure at each floor through structural link components that include an inline load cell to measure lateral force transferred between the strongback and the rest of the structure. To minimize friction during testing, needle bearings were installed at the pin joints, while thrust bearings were applied at other key connection points. This ensured that the system operated smoothly during dynamic loads and testing conditions.

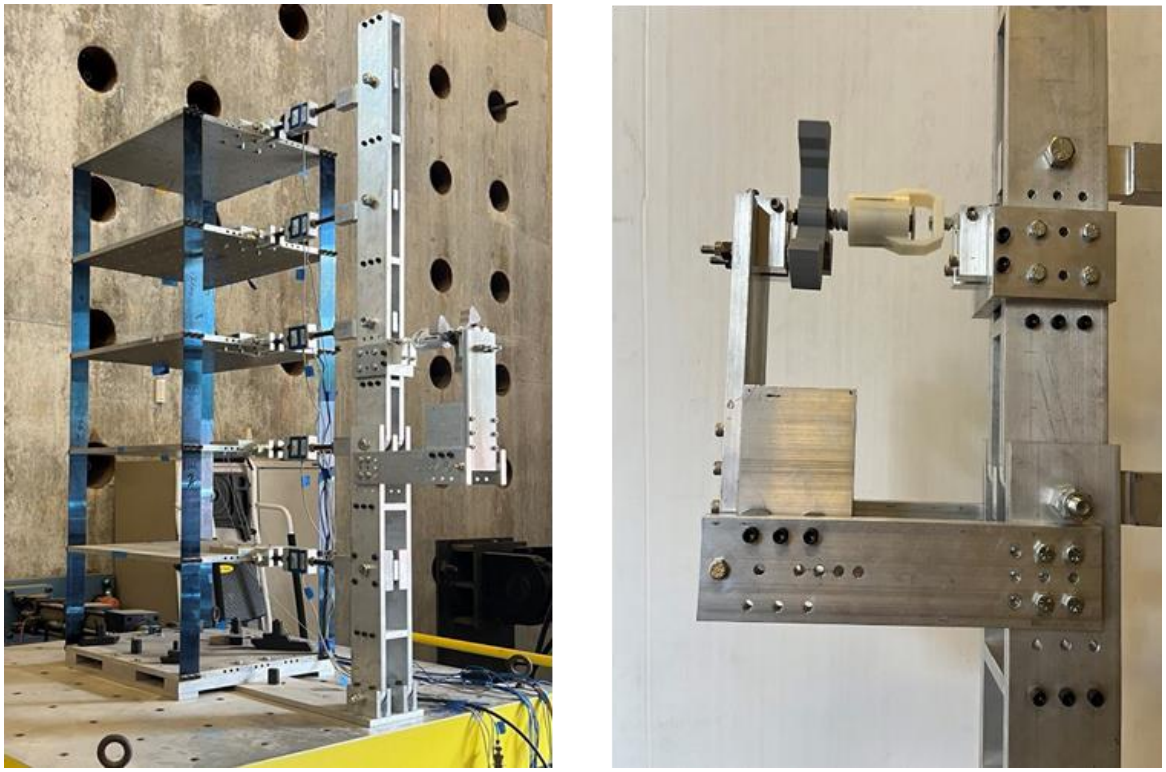


Figure 5-1: Five-story structure with segmented strongback (Left) overall view (Right) close up view of segmented strongback joint and rotational inertial mechanism installed across the joint

5.1.2.2 Rotational Inertial Mechanism

The nonlinear rotational inertial mechanism used in this study is based on a ball-screw design. As standard ball-screw designs rely on a fixed pitch, a modified ball-screw design was required for this study. The ball-screw-based nonlinear rotational inertial mechanism developed by the research team for this study is shown in **Figure 5-2**. The ball-screw in this device converts relative translational motion between the ends of the device into rotational motion as the threaded shaft moves over a group of ball bearings that are in a fixed position in the device's outer nut (see **Figure 5-2c**). The device's shafts have three starts; thus, there are three ball bearings at this fixed location. As the ball bearings in the outer nut support the shaft at a single location, alone they would allow for undesirable pivoting about this location. A second location where the shaft is supported is provided by ball bearings in the inner nut, which is placed inside the outer nut (see **Figure 5-2a**). To allow for shafts with different fixed pitches and shafts with variable pitch, the inner nut has ball bearings on its exterior that enables the inner nut to change location inside the outer nut.

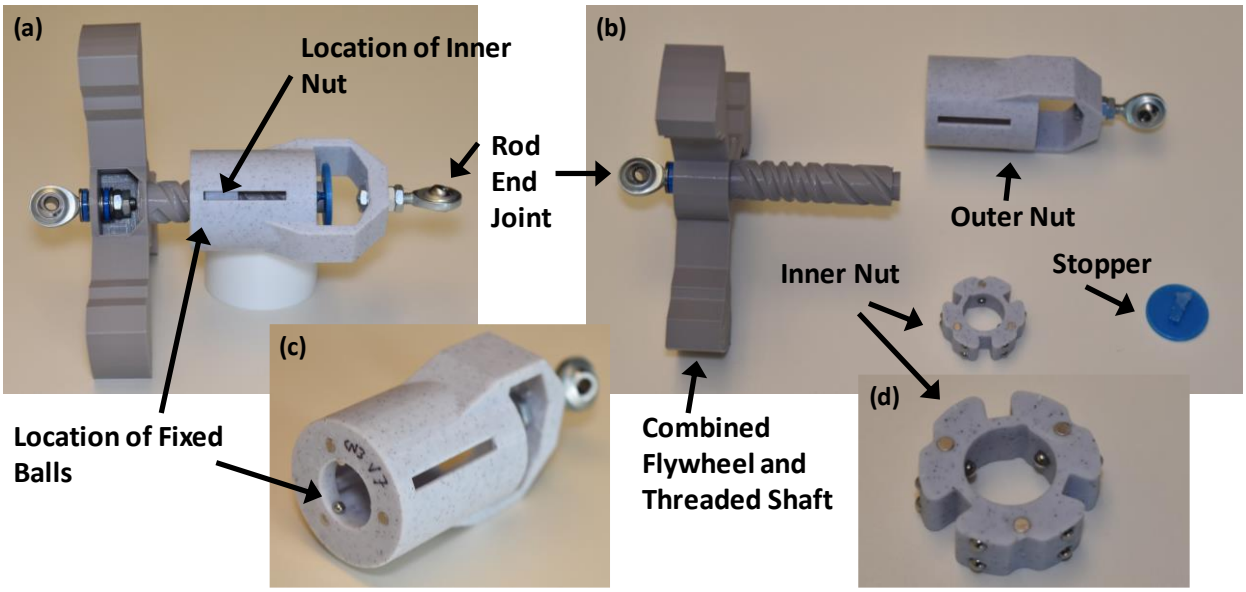


Figure 5-2: Ball-screw-based nonlinear rotational inertial mechanism (a) assembled device (b) disassembled device (c) close up view of outer nut for the ball-screw and its fixed ball bearings (d) close up view of the inner nut

Additional features of the nonlinear rotational inertial mechanism developed by the research team is a stopper and its rod ends. The stopper is connected to the end of the device's shaft and provides a mechanical stop to prevent the shaft from pulling out of the inner or outer nut. However, the amplitudes considered during testing are limited such that this stopper is not engaged. With the rod ends, the device is connected at the joint of the strongback with shoulder bolts acting as pins. These rod ends allow for the necessary in plane rotation of the device to accommodate the geometry of the structure's motion as well as allows for only axial forces to be transmitted by the device.

The inertance of the device is calculated as $b = I * (2 * pi/L)\text{^}2$, where I is the rotational inertia of the rotating components and L is the lead of the ball-screw, the translational distance required for the ball-screw to produce 1 rotation. Note that the shafts pitch is calculated as the lead value divided by the number of starts of the shaft, in this case 3. While different shaft threading is considered, the rotational inertia of all the integrally fabricated shafts and flywheels is approximately 153.4 kg-mm^2.

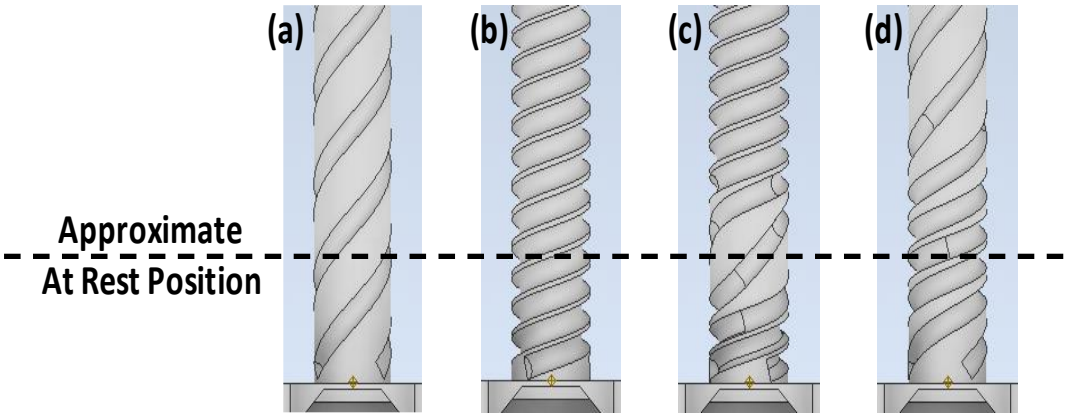


Figure 5-3: 3D models of different shafts used in the ball-screw-based rotational inertial mechanism with approximate at rest position of the fixed ball bearings of the outer shaft shown (a) Low Inertance (b) High Inertance (c) Low to High Inertance (d) High to Low Inertance

The four shafts used in this work are shown in **Figure 5-3**. For these four shafts, two major lead values are considered, 45 and 14.4 mm. These correspond to inertance values of 3.0 and 29.2 kg; referred to as low and high inertance, respectively. **Figure 5-3a** shows a model of the low inertance shaft. **Figure 5-3b** shows the high inertance shaft. The shaft in **Figure 5-3c** transitions between low inertance at low amplitudes of response to high inertance at high amplitudes. The shaft in **Figure 5-3d** transitions between high inertance at low amplitudes of response to low inertance at high amplitudes.

5.1.3 Test Setup

The four cases of rotational inertial mechanism configurations that are described above (Low Inertance, High Inertance, Low to High Inertance, and High to Low Inertance) are utilized in testing of the structure. An additional No Inerter case is considered in which the rotational inertial mechanism is removed from the joint of the segmented spine. In this case, the direct connection between the segments of the strongback is solely a pin.

Shaped white noise ground motion was applied in the structure's flexible direction with a shake table, with four different amplitudes, 30%, 40%, 50%, and 60% of the full amplitude of the noise were used for tests with each configuration. In total, 20 tests were conducted.

To capture the acceleration data during testing, PCB model 352C33SN accelerometers were employed and interfaced with a data acquisition system operating at a sampling rate of 5120 Hz.

These accelerometers were strategically mounted at the center of the side of each floor plate and the base plate, aligning with the flexible direction of the structure, which represented the primary axis of motion. The recorded acceleration data from the shake table (ground acceleration) and the top floor of the structure was used to produce experimentally estimated system frequency response function (FRF) curves.

Five Interface s-type load cells were used at each floor level, attached to the structural link between the floors and the segmented strongback, to measure the lateral force transferred between the strongback and the rest of the structure. This force is collected with a sampling rate of 5120 Hz.

An NDI Optotrak optical measurement system was utilized to capture the displacement response of the floor plates, base plate, and strongback. This system tracked infrared light emitted from markers placed on the components and recorded their absolute positions in three dimensions. Operating at a sampling rate of 100 Hz, the Optotrak system provided precise positional data, which was collected through a separate data acquisition system. The data from the displacement measurements were synchronized with the acceleration data during post-processing. The structure's motion in the flexible direction was extracted from the three-dimensional marker positions, enabling the calculation of the story drifts and roof drifts.

5.1.4 Analysis

Findings from the experimental tests with varying amplitudes of white noise conducted on the five-story structure equipped with a segmented strongback and the different configurations of a rotational inertial mechanism are presented here.

FRFs estimated from the measured ground acceleration to the acceleration of the top floor of the structure are plotted in **Figure 5-4** for the five configurations considered. Several key observations can be made. The first mode frequency remained constant across all configurations and the peak of this first mode remains similar for all configurations. This indicates that the fundamental mode is largely unaffected by changes in inertance. In contrast, large changes are observed with the second mode. The second mode peak was almost completely suppressed in the High Inertance and High to Low Inertance cases. While still present, the second mode peak is reduced in the Low Inertance case compared to the No Inertance case and even further reduced

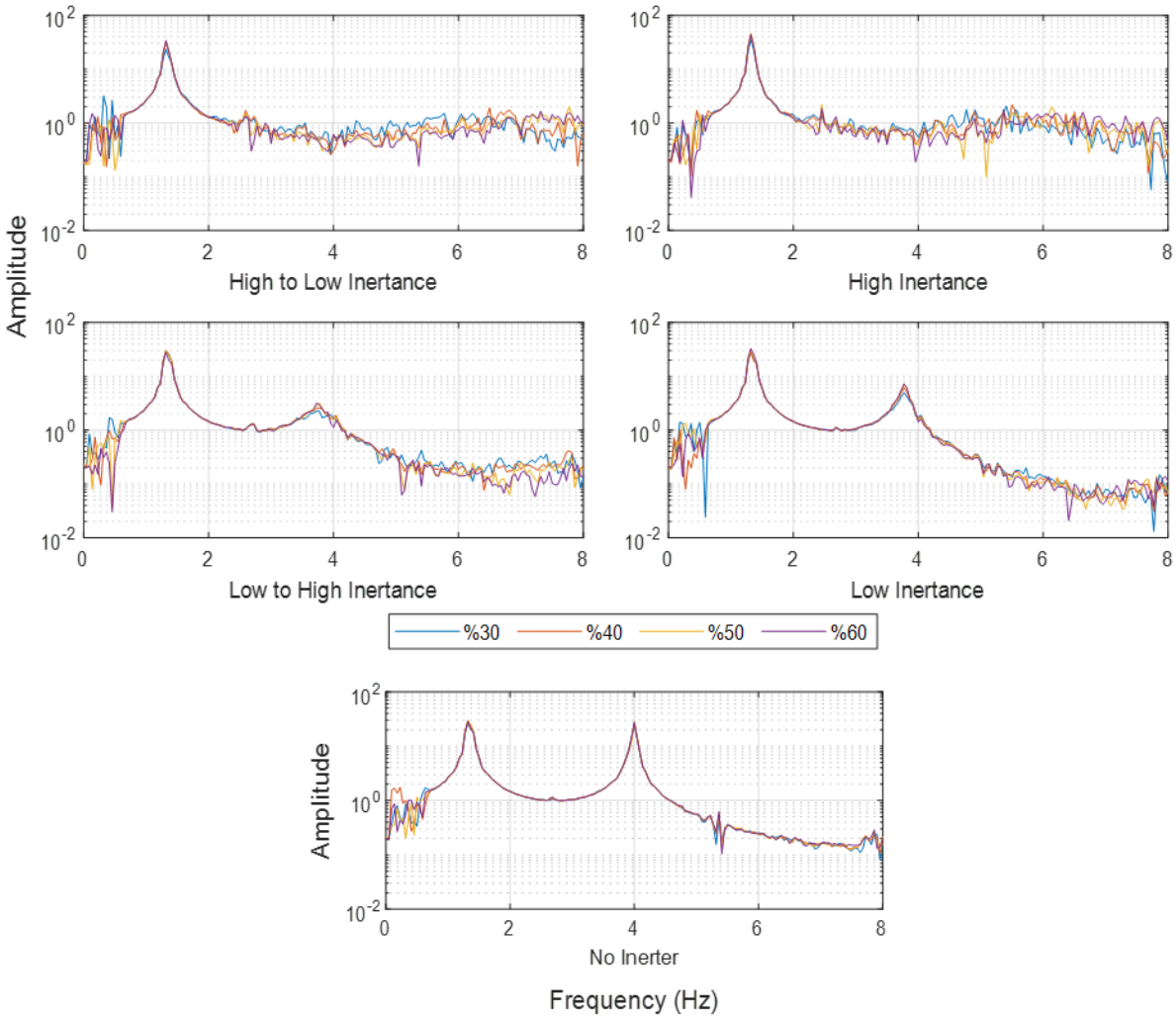


Figure 5-4: Frequency response functions from ground acceleration to fifth-floor acceleration of all configurations for all amplitudes.

in the Low to High Inertance case. Furthermore, the frequency of the second mode is noticeably shifted lower for the Low Inertance and Low to High Inertance cases compared to the No Inertance case. Additionally, it is observed that the higher frequency (above 4 Hz) floor of the FRFs is significantly raised for the High Inertance and High to Low Inertance cases.

The maximum story drift was calculated and then normalized with respect to the No Inerter case for each load amplitude and then plotted in **Figure 5-5.** All configurations, except for the High Inertance case, exhibited lower maximum story drift than the No Inerter case. The Low to High

Inertance case yielded the lowest maximum story drift for most amplitudes, demonstrating a better overall performance in minimizing drift among all configurations. Despite that the effective inertance provided the nonlinear rotational inertial mechanism is designed to vary with response amplitude, the Low to High case displayed the most consistent normalized story drift results across the varying load amplitudes. The only configuration for the rotational inertial mechanism that resulted in worse maximum story drift performance, compared to the No Inerter case, is the High Inertance case.

Figure 5-6 presents the maximum story drift for each story for all of the configurations at all the loading amplitudes tested. These results show that, even in the High Inertance case, the drift response shows the gradation and jump in story drift that is typical of a segmented strongback. This is in contrast to the increasingly uniform drift that would result if a segmented strongback had a stiffness element placed at the joint between segments. Instead, the segmented response persisted with the rotational inertial mechanism, highlighting the inertance's role in modifying the second mode response without making the strongback behave as if it was composed of only a single segment.

Figure 5-7 presents the maximum story acceleration for different configurations normalized with respect to the No Inerter case for each load amplitude. The No Inerter case exhibits the highest story acceleration across all load amplitudes by a significant margin. The Low to High Inertance case has the best performance, but it is largely similar to the normalized performance of the Low Inertance and High to Low Inertance cases.

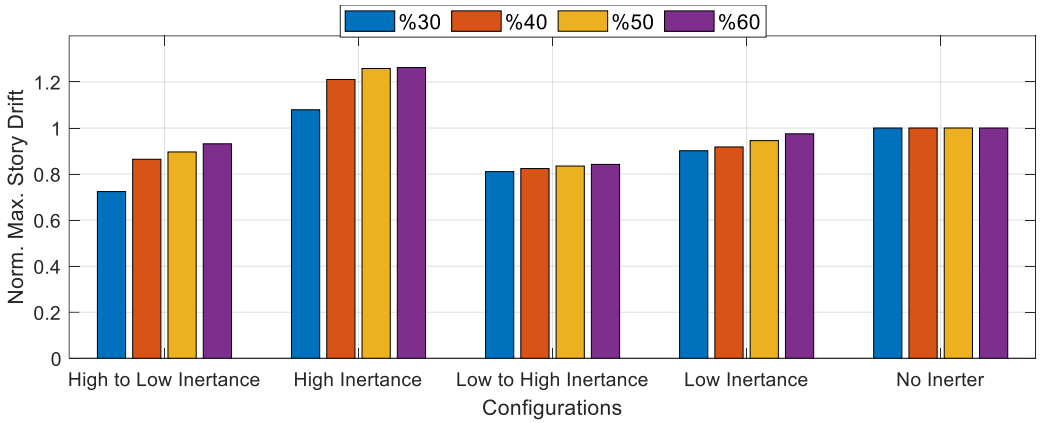


Figure 5-5: Normalized maximum story drift of all configurations with respect to the No Inerter case for all amplitudes

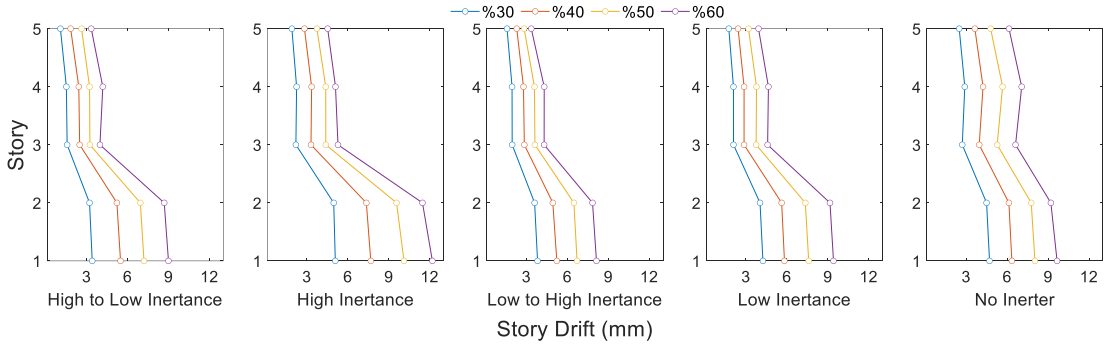


Figure 5-6: Story drifts of all configurations for all amplitudes

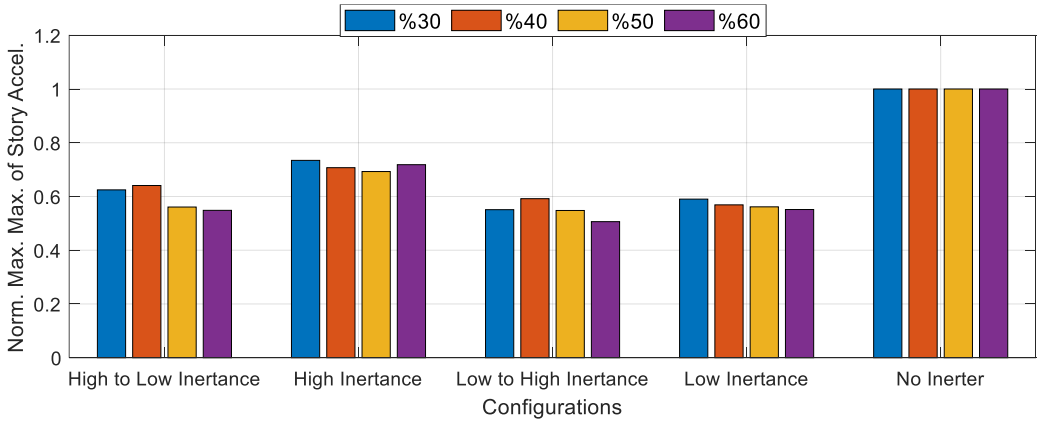


Figure 5-7: Normalized maximum story acceleration of all configurations with respect to the No Inerter case for all amplitudes

Figure 5-8 presents the maximum force measured in the links connecting the strongback and the rest of the structure for the different configurations normalized with respect to the No Inerter case for each load amplitude. These results show that the Low to High Inertance case consistently minimizes the normalized maximum link force. Additionally, while the other added inertance cases force, the High Inertance case shows a significant increase in normalized force.

5.1.5 Conclusion

The dynamic response of a five-story model structure with a segmented strongback was experimentally investigated with various configurations of a modified ball-screw based nonlinear rotational inertial mechanism placed across the joint between the strongback's segments (Low Inertance, High Inertance, Low to High Inertance, High to Low Inertance, and No Inerter). This system was subjected to a shaped white noise over a range of amplitudes and the dynamic response of the system for each of the configurations of the rotational inertial mechanism were assessed through measurements of floor acceleration, link force, story drift, and resulting frequency response function (FRF) curves. The key results of this study are.

- The second mode of the system was attenuated and shifted in the Low to High Inertance and Low Inertance cases, but completely suppressed in the High to Low Inertance and High Inertance cases.

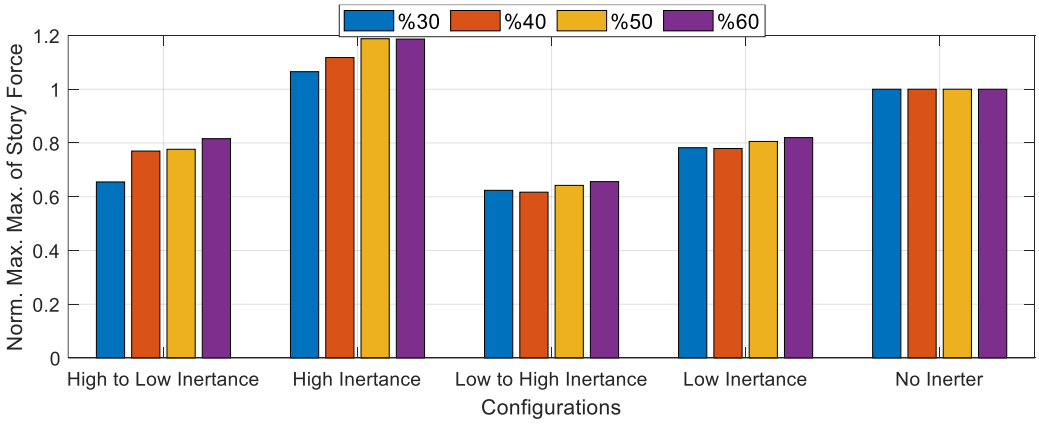


Figure 5-8: Normalized maximum link force of all configurations with respect to the No Inerter case for each load amplitude

- Segmented response persisted with the rotational inertial mechanisms, highlighting the inertance's role in modifying the second mode response without making the strongback behave as if it was composed of only a single segment.
- The Low to High Inertance case consistently outperformed the others cases considered and reduced the maximum story drift, story acceleration, and link force compared to the No Inerter case.
- The High Inertance case improved the maximum story acceleration compared to the No Inerter case, but had higher maximum story drift and link force response.
- Large amplitude dependency was expected in the Low to High Inertance case and High to Low Inertance case due to the varying pitch of the ball-screw shafts used in the rotational inertial mechanisms in these cases, but was not observed.

Overall, the results of this study suggest that improved performance is possible when utilizing a rotational inertial mechanism in the joint of a segmented strongback. This encourages the further study of these combined systems. An avenue of interest for future work is if strongly amplitude dependent behavior can be achieved with different variable pitch ball-screw shaft designs.

5.2 SEGMENTAL STRONGBACK WITH LINEAR JOINT STIFFNESS

The findings of the experimental portion of the second phase with a segmental strongback with different linear joint stiffnesses were presented at the 2024 Engineering Mechanics Institute (EMI) Conference. Below are the findings of the experimental portion of phase 2.

Abolghasemi, S., N. Wierschem, and M. Denavit. 2024b. “Experimental Study of Segmental Elastic Spines with Joint Stiffness for Buildings.” Engineering Mechanics Institute Conference. Chicago, IL, https://dx.doi.org/10.13140/RG.2.2.12432.62727 (Abstract only).

5.2.1 Experimental Investigations

5.2.1.1 Model and Configurations

The five-story structure model with an attached segmented strongback described in **Section 3.1** was used in this study. This strongback features a pin at the second-floor level that utilizes ball bearings to ensure smooth, low-friction rotation. To examine how joint stiffness impacts the behavior of the segmented strongback system, a relative rotation versus rotational stiffness diagram **(Figure 5-9**) was produced with data extracted from the SAP2000 model across a stiffness range. This diagram aided in selecting an appropriate range of rotational stiffness for designing a linear beam, as illustrated in **Figure 5-10.**

The relationship between linear beam properties and joint rotational stiffness was analytically calculated and experimentally validated. (Barley et al., 2024).

$$K_\theta = \frac{12EI}{L} \tag{5-1}$$

Where:

K_θ = rotational stiffness at the joint

E = modulus of elasticity of the beam

I = moment of inertia of the beam

L = length of the beam

Table 5-1 lists system configurations by stiffness levels, with linear beams designed to achieve these levels for testing the segmented strongback system's stiffness effects.

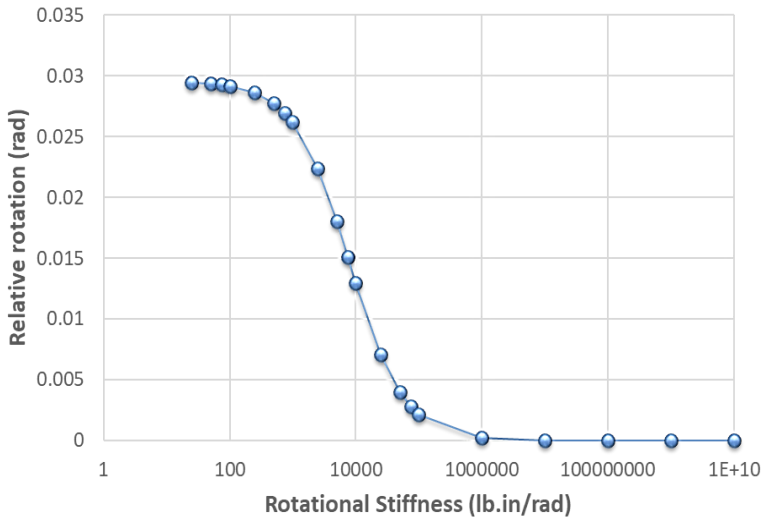


Figure 5-9: Relative rotation changes respect to a range of rotational stiffness diagram

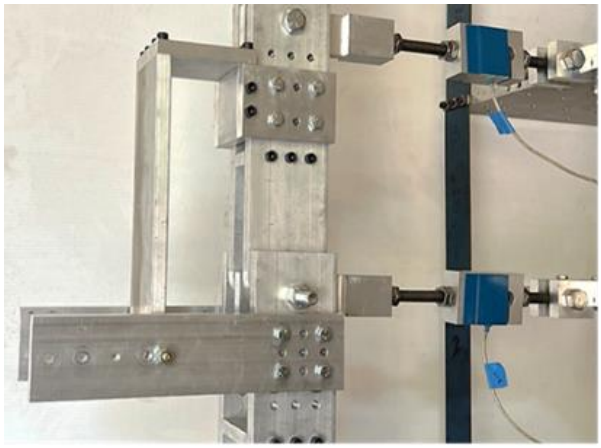


Figure 5-10: Linear beam design for joint stiffness between two segments of the segmented strongback model

Table 5-1: Test system configurations and associate properties

Name	Configuration	L (in)	W (in)	Stiffness (lb.in/rad)
No SS	No segmented strongback	-	-	-
SS L0	Seg. strongback without beam at joint	-	-	~ 0
SS L1	Seg. strongback + 0.042” thick beam at joint	5	3	1209
SS L2	Seg. strongback + 0.062” thick beam at joint	3	3	6481.33
SS L3	Seg. strongback + double 0.062” thick beam at joint	3	3	12962.66
SS L4	Seg. strongback + 0.125” thick beam in parallel at joint	3.5	3	45527.34
SS L5	Seg. strongback + 0.5” thick beam at joint	2.5	3	509906.25

5.2.1.2 Experimental Results and Discussions

The measured ground acceleration and the top floor acceleration from the white noise ground motion where utilized to produce estimated frequency response functions for each of the systems considered (**Figure 5-11**). These results indicate that the presence of the segmented strongback decreases the first mode frequency of the system, but that this first mode frequency is not impacted significantly by the stiffness of the joint. In contrast to this, the second mode frequency is greatly impacted by joint stiffness. As joint stiffness increases, the second mode frequency shifts higher and its amplitude simultaneously decreases. At the highest stiffness level (resembling a unit strongback), the second mode frequency is significantly suppressed.

The normalize maximum acceleration, normalize maximum link arm force, and normalize maximum story drift are shown for the ground motions considered in **Figure 5-12**, **Figure 5-13**, and **Figure 5-14**, respectively. For this normalization, the maximum response metric was divided by the maximum response metric from the SSL0 configuration (segmented strongback with no joint stiffness) for each ground motion.

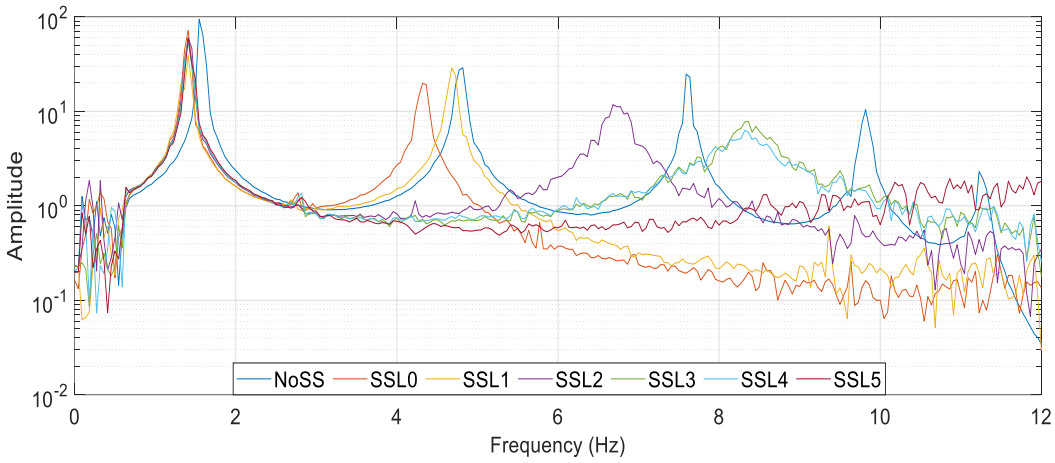


Figure 5-11: Frequency response functions from ground acceleration to fifth-floor acceleration for all system configurations

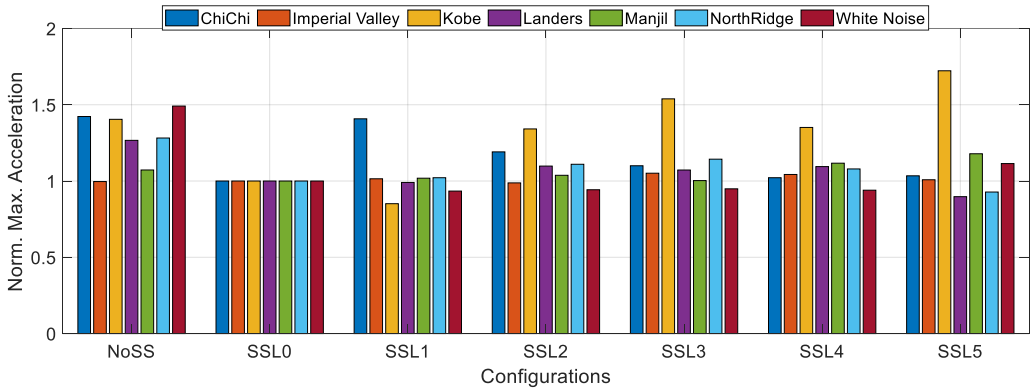


Figure 5-12: Normalized maximum acceleration. Normalization of results from each record are performed with respect to the SSL0 configuration results.

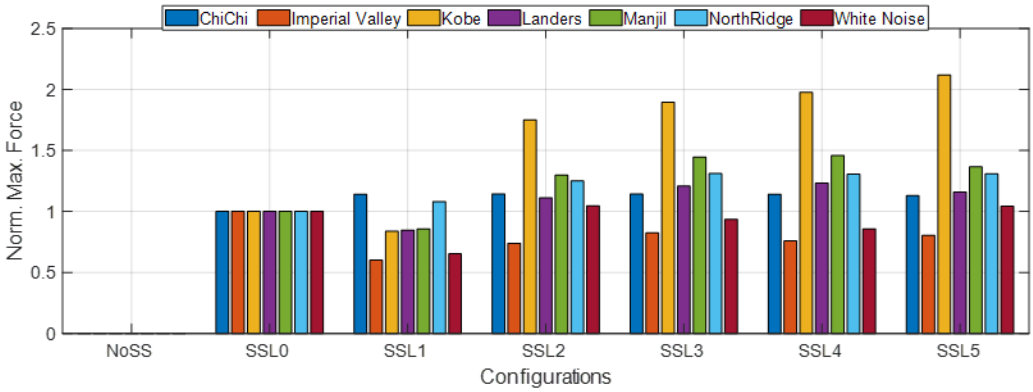


Figure 5-13: Normalized maximum force. Normalization of results from each record are performed with respect to the SSL0 configuration results.

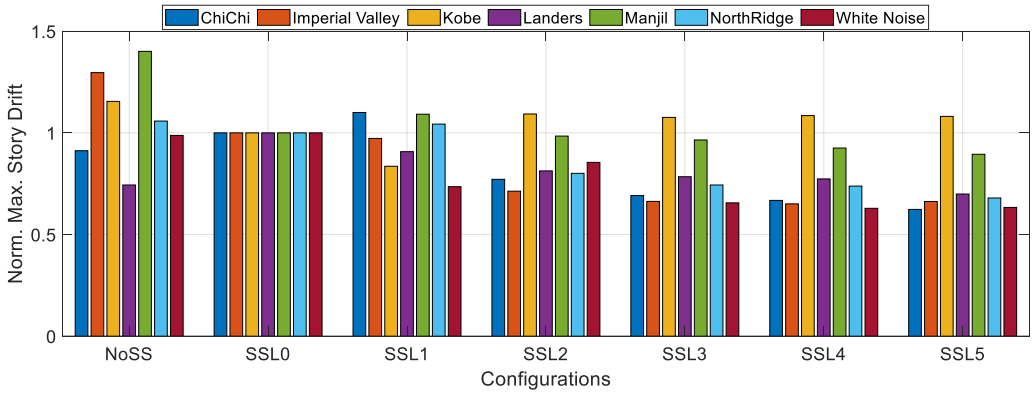


Figure 5-14: Normalized maximum story drift. Normalization of results from each record are performed with respect to the SSL0 configuration results.

The overall trends in these figures show that with increases in the joint stiffness, the normalized maximum force in the link arms goes up and the normalized maximum story drift is reduced. However, while there are overall trends, significant counter examples are seen for individual ground motions. Furthermore, there are times when no trends are apparent at all. For example, there is not a clear trend related to how increasing joint stiffness effects normalized maximum floor acceleration in the structure or the relative benefits of the NoSS and SSLO configurations on normalized maximum story drift.

5.2.1.3 Conclusion

Based on this study's findings, increased joint stiffness impacted the segmented strongback configuration in several ways:

- The first mode frequency remained unaffected by different configurations, while the second mode frequency shifted higher as joint stiffness increased.
- Link arm maximum force demand generally increased with increased joint stiffness.
- Maximum story drift generally decreased as joint stiffness approached that of a unit spine.

While some trends in the results have been identified, confidence in these trends is limited due to scatter in the data. The shifting of the second mode frequency due to joint stiffness, combined with the unique spectral characteristics of each earthquake record, suggests that the structural response is strongly influenced by specific earthquake characteristics. Further numerical analysis

with a larger set of ground motions may provide insights into the potential for establishing clearer results.

5.2.2 Numerical Investigations

To complement the experimental findings and further explore the impact of joint stiffness on structural behavior, a numerical analysis was conducted. This analysis focused on evaluating how variations in the rotational stiffness at the joint between strongback segments affect seismic performance, including interstory drift, floor acceleration, and moment demand in the spine. The use of a numerical model in this analysis enables a broader and more controlled parametric investigation that would be difficult to achieve experimentally. In shake table testing, each ground motion must be processed and repeated multiple times to ensure accurate signal reproduction, making the testing of large suites of records extremely time-consuming. Performing large suites of ground motions for each joint stiffness level would require considerable time and resources. Additionally, it is nearly impossible to isolate and eliminate unintended damping effects in the physical structure and joint assembly during experiments. In contrast, the numerical model allows for precise control of system parameters, including a wide range of joint stiffness values, and enables consistent analysis under a full suite of ground motions records without the confounding effects of physical damping. Moreover, the numerical approach allows for the simulation of more realistic structural systems and loading conditions, extending beyond the limitations of the scaled experimental model.

The numerical model is based on a realistic structure, as described in detail in Chapter 3. The segmental strongback was modeled by idealizing the joint as a rotational spring. The details of this modeling approach are provided in the following section. A range of joint stiffness values, from zero to very high, was considered to capture broader trends and assess system sensitivity. Each configuration was subjected to a suite of ground motions, described in **Section 3.2.6**, representing a variety of seismic intensity levels and frequency content. The analysis was performed using MATLAB, with preliminary validation conducted in SAP2000. The simulation results are used to observe general trends in system behavior and to identify potential limitations associated with the modeling assumptions.

5.2.2.1 Mathematical Model of the System

The numerical model used in this study builds upon the unit strongback model previously described in **Chapter 3**. In addition to the baseline configuration, a rotational spring was introduced at the joint between the strongback segments to simulate a tunable connection. The moment developed at the joint is defined as $M = k_j \times \theta$, where k_j is the rotational stiffness and θ is the relative angle of rotation of the segments at the joint. To incorporate this joint behavior into the global system, a 2×2 stiffness matrix representing the rotational spring stiffness was added to the global stiffness matrix where the joint is located at second floor.

$$K_{Rotational} = \begin{bmatrix} k_j & -k_j \\ -k_j & k_j \end{bmatrix} \tag{5-2}$$

This modification introduces an additional degree of freedom associated with the rotational spring. As a result, the five-story strongback beam model expands from 12 degrees of freedom to 13 degrees of freedom, as shown in Equation (9). Static condensation is then applied, allowing the analysis to focus on the primary translational degrees of freedom. This approach enables the investigation of how varying joint stiffness, k_j , influences structural response while maintaining consistency with the modeling framework established in Chapter **3**.

$$K = \frac{12EI}{L^3}\begin{bmatrix} 12 & 6L & -12 & 6L & 0 & 0 & 0 & 0 & 0 & 0 & 0 & 0 & 0 \\ 6L & 4L^2 & -6L & 2L^2 & 0 & 0 & 0 & 0 & 0 & 0 & 0 & 0 & 0 \\ -12 & -6L & 24 & 0 & -12 & 6L & 0 & 0 & 0 & 0 & 0 & 0 & 0 \\ 6L & 2L^2 & 0 & 8L^2 & -6L & 2L^2 & 0 & 0 & 0 & 0 & 0 & 0 & 0 \\ 0 & 0 & -12 & -6L & 24 & -6L & 6L & -12 & 6L & 0 & 0 & 0 & 0 \\ 0 & 0 & 6L & 2L^2 & -6L & 4L^2+k_j & -k_j & 0 & 0 & 0 & 0 & 0 & 0 \\ 0 & 0 & 0 & 0 & 6L & -k_j & 4L^2+k_j & -6L & 2L^2 & 0 & 0 & 0 & 0 \\ 0 & 0 & 0 & 0 & -12 & 0 & -6L & 24 & 0 & -12 & 6L & 0 & 0 \\ 0 & 0 & 0 & 0 & 6L & 0 & 2L^2 & 0 & 8L^2 & -6L & 2L^2 & 0 & 0 \\ 0 & 0 & 0 & 0 & 0 & 0 & 0 & 12 & -6L & 24 & 0 & -12 & 6L \\ 0 & 0 & 0 & 0 & 0 & 0 & 0 & 6L & 2L^2 & 0 & 8L^2 & -6L & 2L^2 \\ 0 & 0 & 0 & 0 & 0 & 0 & 0 & 0 & 0 & -12 & -6L & 12 & -6L \\ 0 & 0 & 0 & 0 & 0 & 0 & 0 & 0 & 0 & 6L & 2L^2 & -6L & 4L^2 \end{bmatrix} \tag{5-3}$$

To validate the numerical model, its results were compared with those from a segmental strongback system with an ideal pinned joint when $k_j = 0$, as well as with a SAP2000 model incorporating a rotational spring at the segmental joint.

5.2.2.2 Numerical Analysis

This section introduces the numerical analysis measures considered for the study of the segmental strongback system with a tunable joint. To evaluate the seismic performance of the structural system, three key parameters are considered:

- Maximum Absolute Floor Acceleration:

The peak absolute acceleration is selected for each floor throughout the ground motion duration. This measure reflects the potential for damage to nonstructural components.

- Maximum Story Drift:

The maximum relative lateral displacement between adjacent floors, is computed for each story. This parameter is used to assess deformation demands and potential structural damage.

- Maximum Bending Moment in the Strongback:

The peak moment developed in the strongback element is tracked to evaluate internal force demands. This measure is particularly important for understanding how joint stiffness affects moment distribution within the spine.

For each joint stiffness configuration and response parameter, the median of the maximum values across suite of ground motion records (44 records) is reported for each joint stiffness value. The use of the median helps represent typical system behavior while reducing the influence of outlier ground motions with unusually large or small responses.

To evaluate the influence of joint stiffness on seismic performance, a normalized root-mean-square (RMS) value was also computed for each of the key response measures, enabling consistent comparison across different joint stiffness levels. While maximum values show the single highest demand experienced during an earthquake, RMS values provide insight into how strong the response was overall during the entire shaking. In other words, the RMS reflects how much the structure was responding on average, not just at the peak. Together, these measures provide a more comprehensive view of structural performance by identifying not only extreme demands but also the overall energy input and cumulative response experienced by the system.

For story drift and floor acceleration, the RMS value was calculated for each story and each floor, respectively. The maximum RMS across all stories or floors was then selected to represent the system's overall drift and acceleration response for a given configuration. For moment demand, the maximum moment in the strongback was tracked at each time step, and the RMS of these peak moment values was computed to capture the sustained force levels within the spine throughout the ground motion duration.

Each response metric was evaluated for a range of joint stiffness values, k_j , and across the full suite of ground motions. To allow for meaningful comparison, all computed RMS values were normalized by the corresponding RMS values obtained from the ideal pinned-joint configuration, $k_j = 0$. This normalization highlights the relative effectiveness of each joint stiffness level in reducing or amplifying seismic response metrics, with values below one indicating improved performance compared to the configuration with ideal pin at the joint in segmental strongback. The results reveal how joint stiffness influences drift control, acceleration levels, and internal moment demand, and provide insight into potential trade-offs when tuning the joint for seismic performance. Trends observed across ground motions and stiffness levels are discussed in detail below.

5.2.2.3 Results and Discussion

Acceleration Response: The results for both maximum absolute acceleration and normalized RMS acceleration indicate that floor acceleration response is relatively insensitive to changes in joint stiffness. As shown in **Figure 5-15**, the variation in acceleration is more strongly influenced by the specific ground motion than by the joint stiffness itself, suggesting that the response is highly earthquake-dependent. **Figure 5-16** further supports this observation: while some results show improved performance compared to the ideal pinned-joint case and others perform worse, the overall trend—represented by the median line—demonstrates limited sensitivity to changes in joint stiffness. Once again, the results appear to be strongly earthquake-dependent, with certain ground motions yielding better acceleration performance and others worse, but with relatively minor variation observed in the median across different joint stiffness values. Additionally, the results suggest that as joint stiffness increases, effectively transitioning the

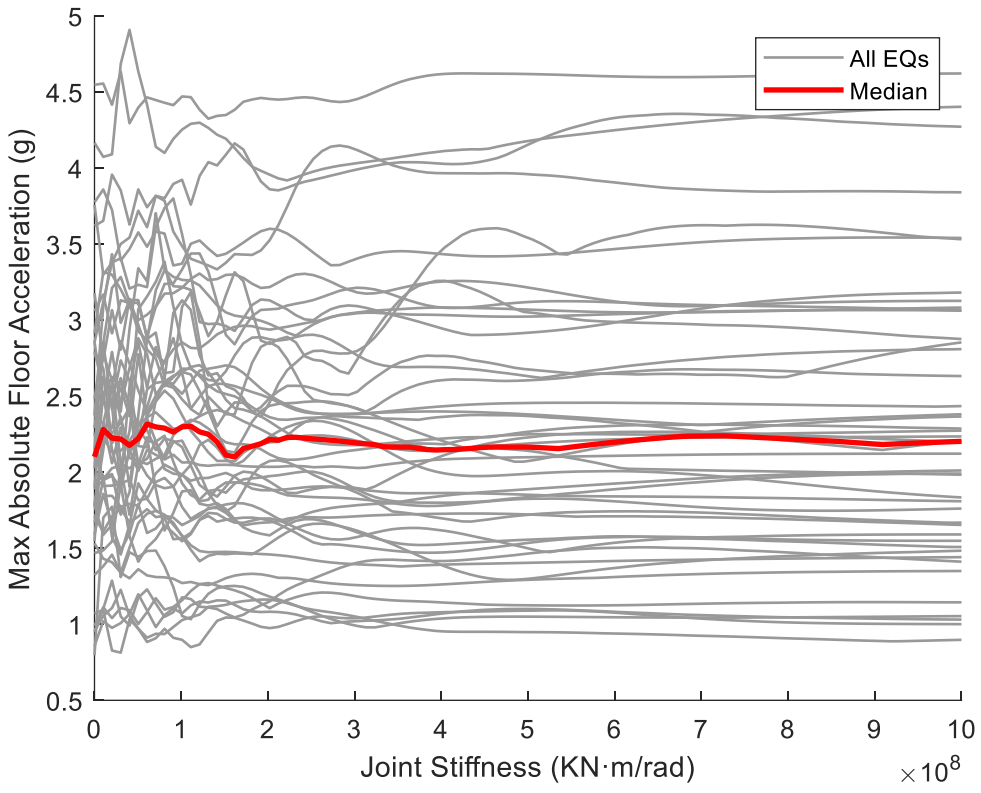


Figure 5-15: Maximum absolute floor acceleration (g) for a 5-story structure with a segmental strongback pinned at the second floor, across a range of linear joint stiffness values (kN·m/rad). Each gray line represents results from one ground motion record; the red line shows the median response across all records. Acceleration values were computed by identifying the maximum floor acceleration for each joint stiffness value per record.

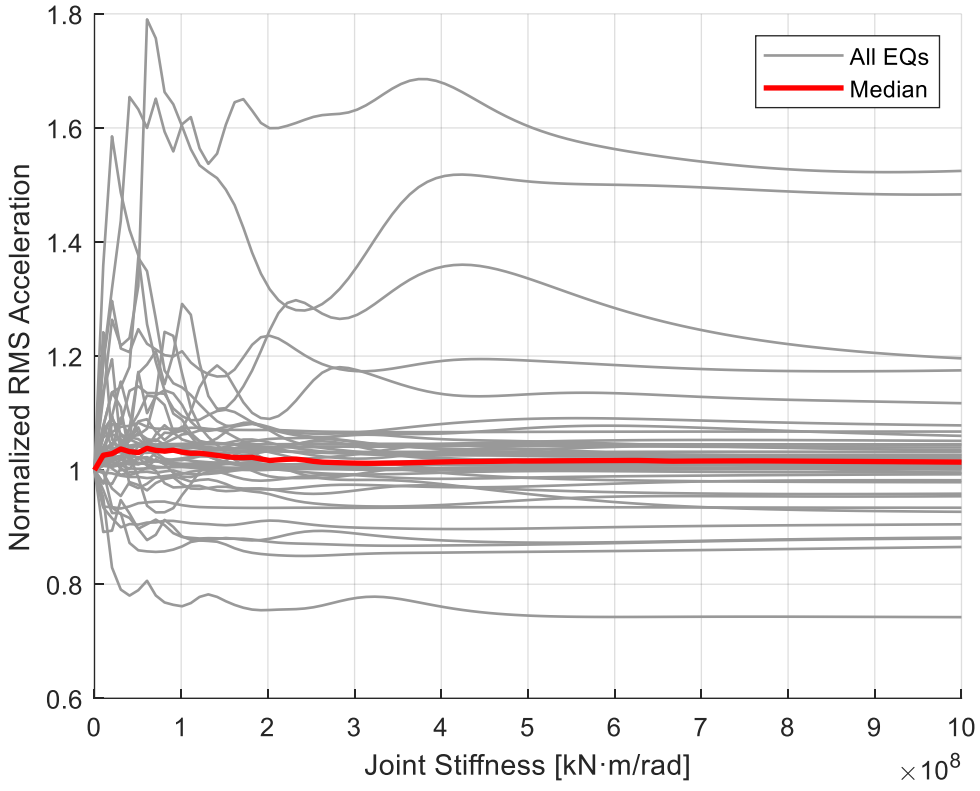


Figure 5-16: Normalized RMS of maximum floor acceleration for a 5-story structure with a segmental strongback pinned at the second floor, across a range of linear joint stiffness values (kN·m/rad). For each record, the time history of the maximum floor acceleration at each time step was computed, and its RMS was calculated for each joint stiffness. Gray lines represent individual records, while the red line shows the median normalized RMS across all ground motions, with normalization relative to the zero joint stiffness case.

segmented strongback toward a continuous (unit) strongback, the acceleration response becomes more consistent across ground motions, indicating a stabilizing effect at higher stiffness levels.

Moment in the elastic spine: **Figure 5-17** illustrates the effect of joint stiffness on the maximum moment demand in the elastic spine. The results show that even a modest increase in joint stiffness leads to a significant rise in moment demand, with the values reaching a plateau for k_j greater than approximately 3×10^8 kN·m/rad. Unlike the acceleration results, where relatively little sensitivity to joint stiffness was observed, the moment consistently increases with higher joint stiffness across all ground motions (**Figure 5-18** and **Figure 5-19**). The magnitude of this increase, however, varies considerably between earthquake records. In some cases, the normalized moment increases by as little as 50% (e.g., from 1.0 to 1.5), while in others it exceeds 400% (e.g., from 1.0 to over 5.0). These findings highlight a key trade-off: while adjusting joint stiffness can influence drift behavior, it also results in a substantial and highly variable increase in moment demand in the elastic spine.

Story drift: **Figure 5-19** and **Figure 5-20** show that introducing joint stiffness in the segmental strongback consistently reduces the maximum interstory drift compared to the ideal pinned-joint configuration across all ground motions. While some variation exists across records, the extent of this variability is relatively modest compared to that observed in acceleration and moment responses. Most of the drift reduction occurs when the joint stiffness is below approximately 2×10^8 kN·m/rad. Beyond this threshold, additional increases in joint stiffness result in minimal changes to interstory drift, indicating that the system behavior begins to converge toward that of a unit strongback and reaches a performance plateau.

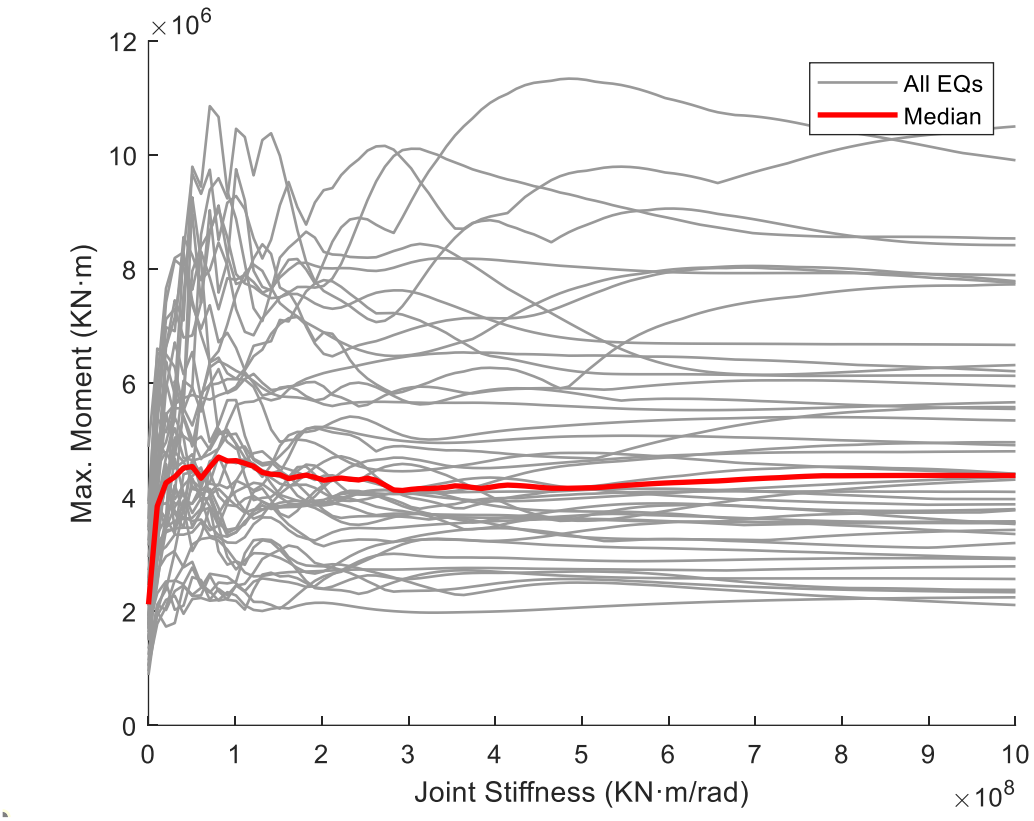


Figure 5-17: Maximum moment demand (KN.m) in the spine for a 5-story structure with a segmental strongback pinned at the second floor, across a range of linear joint stiffness values (kN·m/rad). For each ground motion, the maximum moment in the spine was identified for each joint stiffness value. Gray lines represent results from individual records, and the red line shows the median of maximum moments across all ground motions.

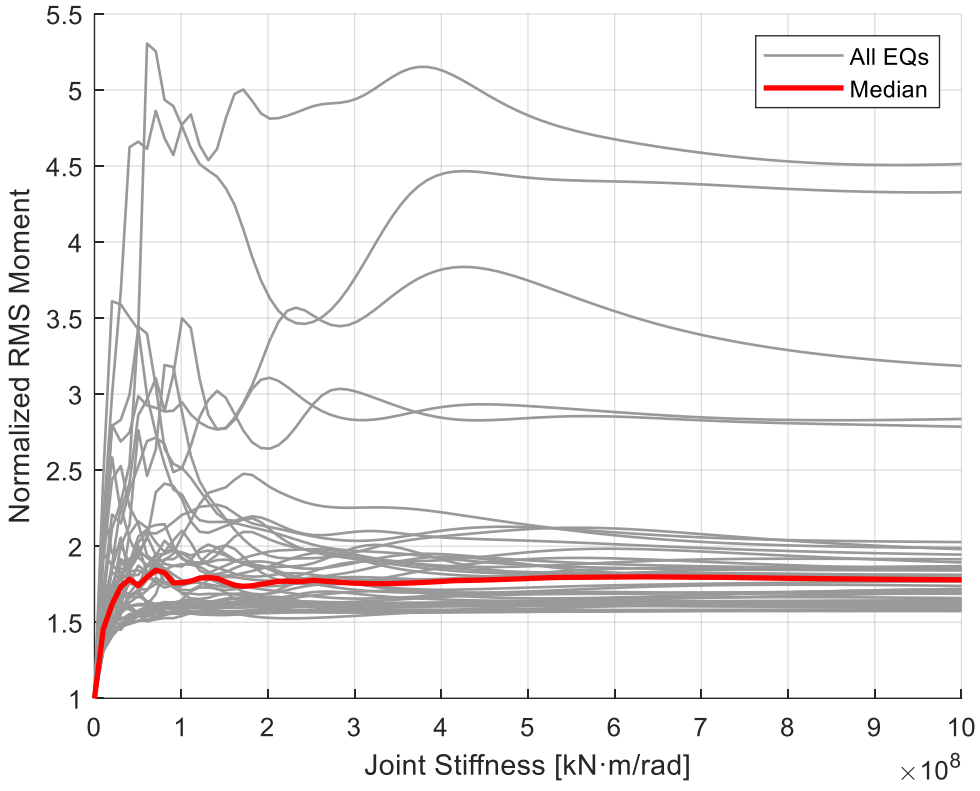


Figure 5-18: Normalized RMS moment in the spine for a 5-story structure with a segmental strongback pinned at the second floor, across a range of linear joint stiffness values (kN·m/rad). For each ground motion, the maximum spine moment at each time step was tracked to construct a time history of maximum moment, from which the RMS was computed. Results are normalized relative to the zero joint stiffness case across all joint stiffnesses for each record; the red line represents the median across all records.

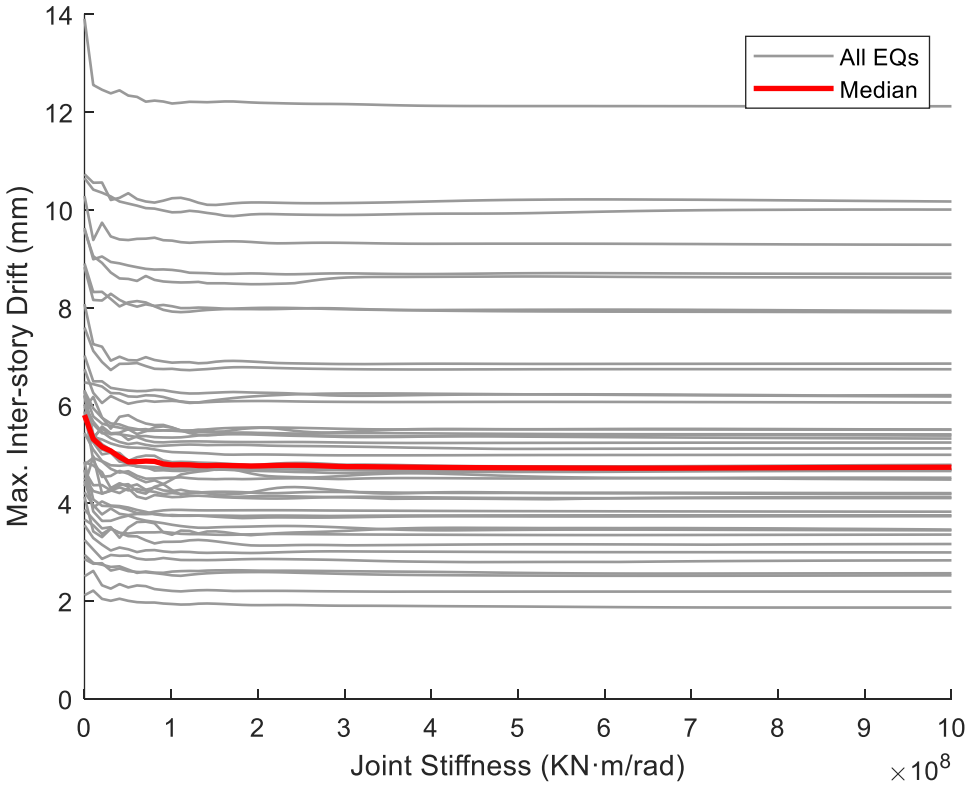


Figure 5-19: Maximum interstory drift (mm) for a 5-story structure with a segmental strongback pinned at the second floor, evaluated across a range of linear joint stiffness values (kN·m/rad). For each ground motion, the maximum interstory drift was extracted for every joint stiffness value. Gray lines represent individual ground motions, while the red line indicates the median drift across all records.

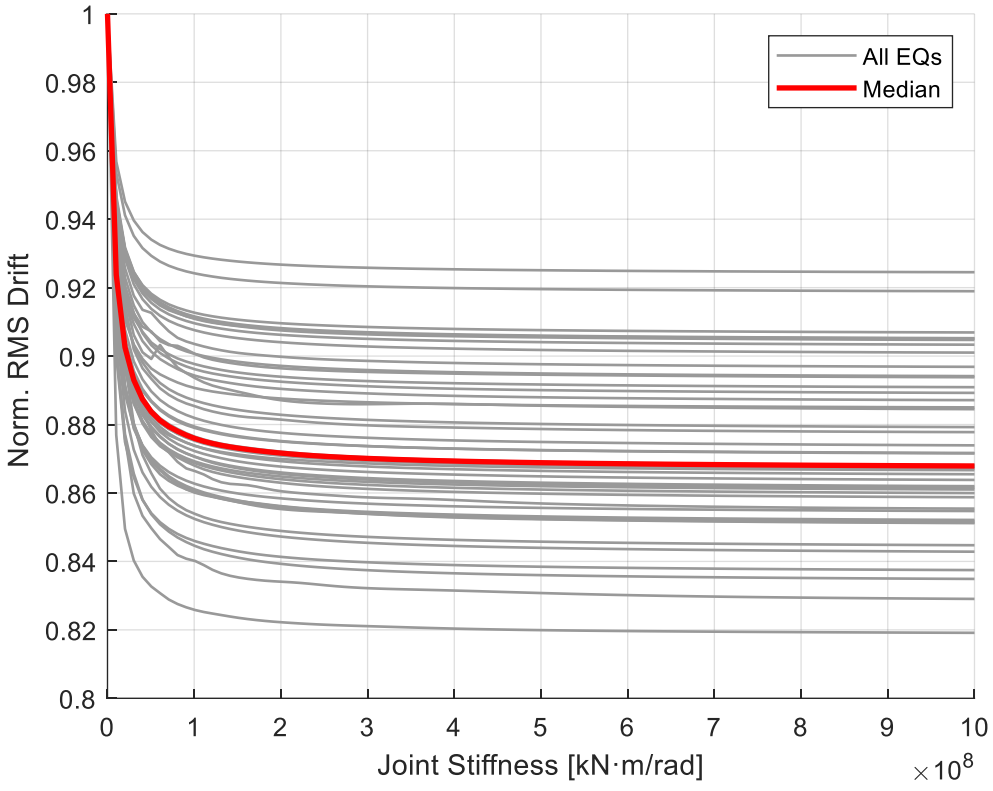


Figure 5-20: Normalized RMS of maximum interstory drift for a 5-story structure with a segmental strongback pinned at the second floor, across a range of linear joint stiffness values (kN·m/rad). For each ground motion, the time history of the maximum interstory drift across all stories was extracted, and its RMS was computed for each joint stiffness value. Gray lines indicate individual records, and the red line represents the median normalized RMS, with normalization performed relative to the zero joint stiffness case.

To better understand the trade-offs between different response measures, the median normalized RMS values for acceleration, interstory drift, and moment were plotted together for all joint stiffness values (**Figure 5-21**). The results show that there is no clear point where adding linear joint stiffness significantly improves drift performance without also increasing moment demand. In the best case, when the joint stiffness is less than about 0.1×10^8 kN·m/rad, the interstory drift is reduced by less than 10 percent, while the moment increases by less than 20 percent compared to the ideal pinned-joint configuration. It is important to note that this evaluation is based on normalized RMS results, and the actual percentage of increase or decrease can vary depending on the specific ground motion. These results suggest that it is difficult to achieve meaningful drift reduction using a tuned joint without introducing a noticeable increase in moment demand on the spine.

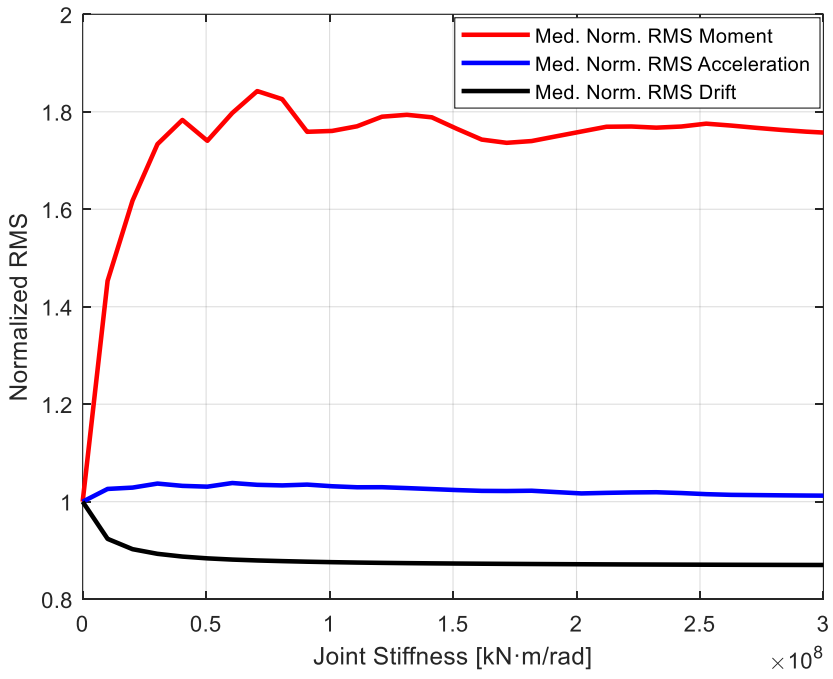


Figure 5-21: Median normalized RMS values of maximum floor acceleration, interstory drift, and moment for a 5-story structure with a segmental strongback pinned at the second floor, across a range of linear joint stiffness values (kN·m/rad). Each response measure was normalized with respect to the zero joint stiffness case, and the median was computed across all ground motions. The combined plot highlights the trade-offs between acceleration, drift, and moment responses as joint stiffness varies.

5.2.2.4 Conclusion

This study investigated the impact of introducing a linear joint stiffness at the joint of a segmented strongback system. The goal was to evaluate whether adjusting joint stiffness could improve seismic performance by reducing interstory drift without significantly increasing other structural demands. Key findings include:

- Floor acceleration showed minimal sensitivity to joint stiffness, with earthquake characteristics having a more dominant effect on response.
- Moment demand in the spine increased significantly with added joint stiffness, reaching a plateau for higher k_j values.
- Interstory drift consistently decreased as joint stiffness increased, with the majority of improvement occurring in lower k_j values.
- Increasing joint stiffness consistently reduced interstory drift but also led to a simultaneous and often substantial increase in moment demand, highlighting a trade-off between drift control and force amplification in the spine.

Overall, this investigation suggests that tuning the joint stiffness of a segmented strongback using a linear joint stiffness offers limited performance improvement and presents trade-offs between drift control and increased internal force demand. These findings highlight the limitations of linear joint stiffness in optimizing system behavior and suggest the need for more adaptive solutions, such as nonlinear joint mechanisms, to better balance drift control and force demand in segmented strongback systems.

Chapter 6 : INERTIAL STRONGBACK: COMPARING THE BEHAVIOR AND PERFORMANCE OF DISTRIBUTED INERTERS AND A TRADITIONAL STRONGBACK

Strongback systems are widely recognized for their ability to mitigate soft-story behavior by promoting a more uniform story drift profile across building heights. This drift uniformity not only enhances global ductility but also suppresses displacement demands associated with higher vibration modes. However, despite these advantages, higher-mode effects can still introduce significant force demands on the strongback and lead to elevated floor accelerations. While previous studies have examined the performance of various energy dissipation and passive control devices in structures with strongback, the integration of inerters within strongback-equipped systems has received little attention, aside from the segmental strongback configurations explored in Chapter 5.

The experimental portion of this chapter, detailed in **Section 6.1**, is presented in the form of a manuscript titled “Experimental Study on the Impact of an Elastic Spine in a Structure with Inerter-Based Devices”, which was published in the proceedings of the 18th World Conference on Earthquake Engineering (WCEE). This study examines the dynamic response of a scaled structural model equipped with distributed inerters and an elastic spine under controlled excitation.

Abolghasemi, S., Sarkar, A., Manson, C., Wierschem, N. and Denavit, M.D., 2024. “Experimental study on the impact of an elastic spine in a structure with inerter-based devices”. Proceedings of the 18th World Conference on Earthquake Engineering.

Subsection 6.2, titled “Numerical study of hybrid seismic control using segmental elastic spine and distributed inerters” presents a version of a manuscript that is intended for submission to a journal. This section expands the investigation by conducting numerical analysis on a more realistic structure and evaluating a broader range of configurations and response metrics. In particular, this study assesses how distributed inerters compare to strongbacks in terms of controlling story drift, floor acceleration, and moment demands. Additionally, the research evaluates the potential benefits of hybrid systems that combine the two strategies, offering insights into how inertial and stiffness-based control mechanisms can complement each other in improving overall seismic performance.

6.1 EXPERIMENTAL STUDY ON THE IMPACT OF AN ELASTIC SPINE IN A STRUCTURE WITH INERTER-BASED DEVICES

6.1.1 Introduction

A recently proposed earthquake engineering strategy is coupling a primary structural system with a stiff elastic spine that runs the full height of the structure and is pinned at the base of the structure. The result of the addition of an elastic spine to a structural system, referred to subsequently in this work as a spine, is a nearly uniform drift profile along the height of the structure (Chen et al., 2018; Hu et al., 2021; Simpson and Mahin, 2018).

One of the key benefits of the nearly uniform drift profile that results from the spine is the prevention of soft story mechanisms that may lead to premature failure of the structure; thus, the inclusion of a spine often leads to a more ductile overall response in structures (Faramarzi and Taghikhany, 2021; Simpson and Mahin, 2018). The effectiveness of spines in structures has been studied numerically (Alavi and Krawinkler, 2004; Lai and Mahin, 2015; Qu et al., 2012) and experimentally (Abolghasemi et al., 2024b; Chen and Tagawa, 2023; Ma et al., 2013). The effect of the spine's stiffness on its performance has been investigated (Chen et al., 2018; Lin et al., 2019), and design methodologies have been proposed (Chen et al., 2017; Simpson and Mahin, 2017).

The application of different types of energy dissipation devices and passive control devices in structures with spines has also been investigated. Hu et al. (2021) suggested the adoption of friction spring dampers with recentering capabilities that were distributed throughout the height of a steel structure featuring a pair of rigid spines. In a different approach, Qu et al. (2012) investigated the efficacy of shear-type steel dampers, which were distributed along the height of an eleven-story steel-reinforced concrete frame with pin-supported walls. Similarly, Wang et al. (2023) examined a pin-supported wall frame structure and explored the implementation of hysteretic and viscoelastic dampers within this framework. Furthermore, Palermo et al. (2021a) numerically investigated a structure equipped with a spine, examining various configurations of viscous dampers within the system. These configurations included dampers positioned at every story, at selected stories, and concentrated at the base of the spine in a vertical configuration. The findings of this work showcased another key benefit of the elastic spine, as it indicated that the

presence of the spine facilitated an enhancement in the seismic performance effectiveness across the different viscous damper configurations. Otherwise stated, the largely uniform story drifts resulting from the spine allow for more freedom in arranging (e.g., distributing throughout a structure vs. concentrating at one level) energy dissipation or passive control devices in structures. Abolghasemi et al. (2024b) later conducted an experimental investigation on the impact of the arrangement of dampers in a structure with an elastic spine, referred to as a strongback, considering distributing throughout a structure vs. concentrating at one level. This experimental study had similar conclusions and found that the effective damping ratio, maximum story drift, and roof drift of the structure are significantly less sensitive to the location or arrangement of dampers in the presence of the strongback.

Inerters and inerter-based control devices have been considered as part of systems for mitigating the response of structures to earthquakes (Ma et al., 2021b); however, these devices have not been studied for use in structures with spines. Inerters are two-terminal mechanical devices that produce resistive force proportional to the relative acceleration between their terminals. The proportionality constant of inerters has the same units as mass and is referred to as inertance. Physical mechanisms, including ball-screws and rack and pinion assemblies, can be used to realize inerters by converting translational motion into the rotational motion of a flywheel (Smith, 2012, 2002b; Swift et al., 2013b). This conversion allows inerters to produce large mass effects even though they may have a relatively small physical mass. For example, Sugimura et al. studied a device that has a flywheel with a physical mass of 560 kg that was capable of generating an effective mass of 5,400,000 kg (Sugimura et al., 2012a). Due to its significant mass amplification capacity, inerters have been suggested for incorporation into a variety of vibration control systems (Di Egidio et al., 2021b; Giaralis and Petrini, 2017b; Hwang et al., 2007b; Javidialesaadi and Wierschem, 2019b; Nakamura et al., 2014b).

While the effectiveness of different arrangements of energy dissipation and passive control devices in structures with spines has been investigated previously, the combination of inerters and a spine has not been previously considered. The inerter is fundamentally different than other structural control devices in that the intrinsic damping that is present in a realistic inerter is accompanied by large mass effects. Thus, the inerter's effect on a structure with a spine is unknown, as well as how various arrangements of inerters impacts the performance and behavior

of the structure with and without a spine. For this investigation, a four-story primary structure with and without a spine was tested on a shake table using both recorded seismic and white noise ground motions. Configurations where inerters are installed at each story and configurations where multiple inerters are installed at a single story are examined. The impact of the combination of the spine and the different inerter configurations is evaluated by examining the structure's dynamic properties and response to the ground motions.

6.1.2 Physical Model

A four-story model structure composed of a primary structure with an attached spine was used to conduct this experimental study. An isometric representation of the physical model is presented in **Figure 6-1a**. Important details regarding this physical model are described in the following paragraphs; further details can be found in a document that includes this physical model's design drawings (Lifsey et al., 2023). This physical model was tested with different inerter configurations and with and without the spine attached to the primary structure.

This primary structure consists of five 457.2 mm x 457.2 mm x 12.7 mm aluminum floor plates, including the base and 16 spring steel columns with a width of 50.8 mm and thickness of 1.575 mm. The connections of the columns were made such that the bending span of the columns was equal to the clear story height, and the columns were orientated in the same direction so that the overall structure was flexible in one horizontal direction and ridge in the orthogonal horizontal direction. Each story measured 244.5 mm from center to center, while the height of the clear story was 231.8 mm.

The spine was constructed from two 76.2 mm x 1114.4 mm x 12.7 mm aluminum plates. The plates were joined together by several connector pieces. The spine was pinned at the base using a pair of partially threaded bolts. A combination of needle roller bearings and thrust bearings were utilized at the base pin to minimize the effect of friction in this pin. The base plate's centerline and the spine pin's centerline were at the same height. The orientation of the spine and the base pin was such that the spine rotated about this pin, given the motion of the structure in its flexible direction. Aluminum link arms measuring 38.1 mm in width and 12.7 mm in thickness, attached at the spine (left arm pin) and at brackets that were rigidly connected to the floor plates (right arm pin), were used to connect the spine to the primary structure at each floor. Needle roller

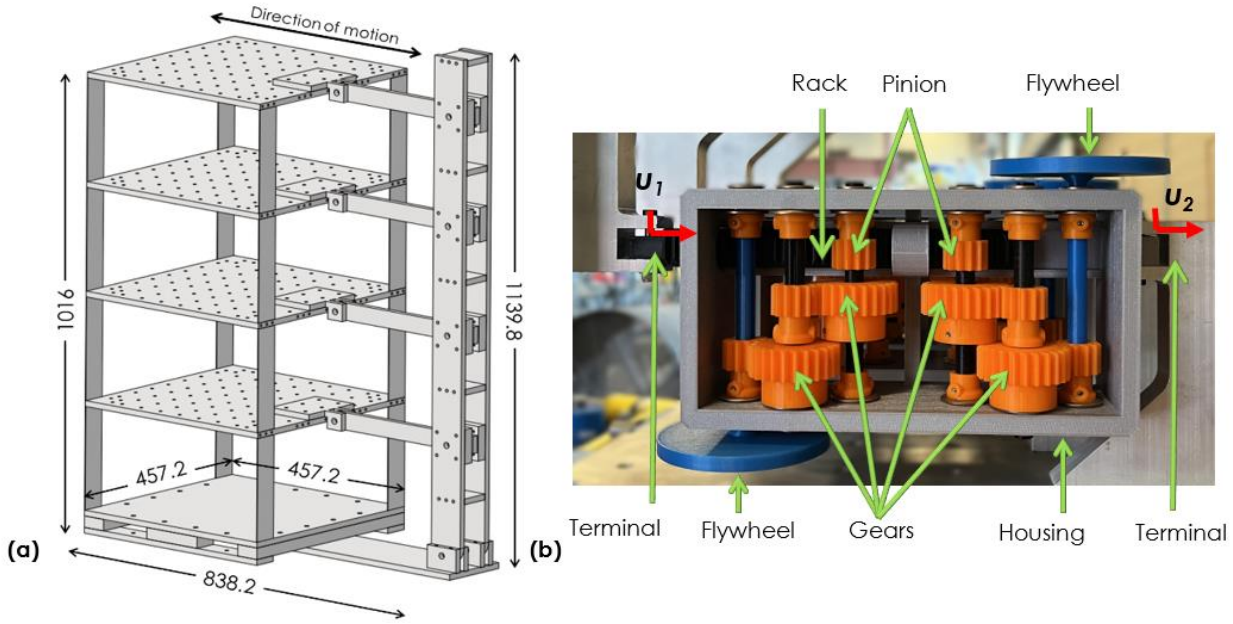


Figure 6-1: (a) Isometric view of the physical model of the primary structure with the spine – units are mm, (b) inerter used in this study with annotations identifying its components

bearings were used in the holes in the link arms at these pins to reduce friction. The centerline of the right arm pins was at the same elevation as the centerline of the floor plates.

Each floor weighed 8.083 kg when the related hardware (such as the bracket but not the link arm) was included. Each column weighed 0.154 kg. Each link arm weighed 0.576 kg. The spine weighed 10.156 kg when all the hardware was included. The spine's center of gravity was located 568.3 mm above the center of the spine's pin. The brackets attached to the floor plates remained in situations when the spine was not present, but the spine, link arms, and related hardware were removed.

The inerter in this study contains a pair of flywheels and a gearbox, which is comprised of a rack and pinion assembly and multiple gears in a housing (see **Figure 6-1b**). These inerters were fabricated predominantly via 3D printing with polylactic acid filament. The rack of the inerter, which is connected to one of the terminals of the device, slides within the inerter's housing along a linear path towards the other terminal, which is connected to the housing. The relative movement of the rack causes the pinion to rotate within the housing. The rotational velocity of the flywheels is further increased with a connected second set of gears. The rotational velocity of

the flywheels and the relative velocity of the structure between the connection points of the inerter are related as follows:

$$\dot{\theta} = \alpha\left(\dot{u}_2 - \dot{u}_1\right) \tag{6-1}$$

where $\dot{\theta}$, $(\dot{u}_2 - \dot{u}_1)$, and α represent the rotational velocity of the flywheels, the relative velocity of the structure between the connection points of the inerter, and α is the coefficient governing this relationship, respectively. α for a rack and pinion mechanism with multiple gears is shown in **Equation (6-2)** where *n* is the number of gears; r_i and r_{pi} are the radius of the ith gear and its corresponding pinion, respectively; and r_f and r_{pf} are the flywheel radius, and radius of the flywheel pinion, respectively.

$$\alpha = \frac{{r_f}^2}{{r_{pf}}^2}\left(\prod_{i=1}^{n}\frac{{r_i}^2}{{r_{pi}}^2}\right) \tag{6-2}$$

The expression for the restoring force provided by an ideal inerter is

$$F = b\left(\ddot{u}_2 - \ddot{u}_1\right) \tag{6-3}$$

where the inerter is subjected to equal and opposite forces *F* at terminals 1 and 2 with accelerations $\ddot{u}_1$ and $\ddot{u}_2$. The coefficient on the relative acceleration term, *b*, in **Equation (6-3)** is known as the inertance and is equal to the effective mass provided by the ideal inerter. In addition to ideal inerter behavior, intrinsic friction in the rack and pinion mechanism will cause the relative motion of the inerter to result in energy dissipation.

Sets of aluminum brackets were utilized to connect the inerters within the stories of the primary structure; each bracket and associated connection hardware has a mass of 0.31 kg. The mass of a single inerter is 0.372 kg, with 0.06 kg of that mass associated with the flywheels and their attached axles. The inertance produced by the device was calculated to be 8.62 kg based on the geometry of the mechanism and the density of the materials utilized. The resulting mass amplification ratio as calculated by the inertance divided by the mass of the inerter is 22.0;

alternatively, the mass amplification ratio as expressed as the inertance divided by the mass of only the flywheels and attached axles of the inerter is 141.

An additional second inerter configuration is considered that is identical to the configuration shown in **Figure 6-1b**, except the device's axles with integrated flywheels have been replaced with axles without a flywheel. The result of this is an inerter that still has intrinsic friction but produces much less mass effects.

In this study, four inerters were attached in a variety of configurations to the primary structure: concentrated and distributed. When the inerters were concentrated in a single story, all four inerters were installed within a single story, following a symmetrical layout along the centerline of the floor. In contrast, when they were distributed, the four inerters were installed on the centerline of each story of the primary structure. In both arrangements, they aligned to engage in motion with the flexible direction of the structure. Photographs of the primary structure with the inerters concentrated in a single story and in the distributed arrangement are provided in **Figure 6-2.**

6.1.3 Description of Experimental Tests

This section provides an overview of the structural configurations, ground motions, and data collection procedures used in the experimental testing.

6.1.3.1 System Configurations

Table 6-1 shows the system configurations employed in the experimental testing. These configurations include scenarios where all four inerters were concentrated in a single story, an arrangement with the inerters evenly distributed in each story, an arrangement with the inerters without flywheels evenly distributed in each story, and an arrangement where the inerters were removed from the primary structure. Each of these configurations was evaluated both with and without the spine, resulting in a total of fourteen distinct structural configurations for this investigation.

(a)  (b) 

Figure 6-2: (a) Primary structure with distributed inerter arrangement, (b) Primary structure with concentrated inerter arrangement

Table 6-1: System configurations for experimental tests

	Spine Config.	Config. Name	Number of Inerters at Each Story			
			1st	2nd	3rd	4th
Inerter Arrangement	Without	IC1	4	---	---	---
		IC2	---	4	---	---
		IC3	---	---	4	---
		IC4	---	---	---	4
		ID	1	1	1	1
		INFD	1	1	1	1
		NI	---	---	---	---
	With	IC1-S	4	---	---	---
		IC2-S	---	4	---	---
		IC3-S	---	---	4	---
		IC4-S	---	---	---	4
		ID-S	1	1	1	1
		INFD-S	1	1	1	1
		NI-S	---	---	---	---

The notation used to identify the configurations in **Table 6-1** is also used when presenting the results of this study. IC1, IC2, IC3, and IC4 signify setups without the spine, where inerters are concentrated in the first, second, third, and fourth stories, respectively. ID refers to the distributed inerters configuration, where each story is equipped with one inerter, and this configuration is assessed in the absence of the spine. INFD refers to distributed inerters but with no flywheel utilized. NI is the configuration without an inerter attached. The same configurations, but with the inclusion of the spine, are indicated by appending "-S" to the respective configuration name.

6.1.3.2 Ground Motions

Ground motions for these tests were generated using a six-degree-of-freedom shake table located at the University of Tennessee. A set of six distinct seismic ground motions (see **Table 6-2**) was employed to ensure a comprehensive evaluation and limit bias resulting from a single earthquake when assessing variations in the seismic response of the structural configurations.

The selected ground motions were recorded from historic seismic events and were sourced from the Pacific Earthquake Engineering Research (PEER) Center ground motion database (Ancheta et al., 2014). Only component A of the recorded ground motions was utilized. These ground motions were applied as unidirectional horizontal accelerations by the shake table; this direction of loading and motion is indicated in **Figure 6-1**. To ensure the physical model would not be damaged, thus enabling reuse for multiple tests, each of the selected ground motion records was individually scaled down. Detailed information regarding the properties of the six recorded seismic ground motions is presented in **Table 6-2.**

The white noise ground motion record was scaled such that it induced a maximum structural response similar to that from the scaled seismic ground motion records. All seven ground motion records, including six seismic records and one shaped white noise, were applied in the flexible direction of the structure to each of the fourteen structure configurations listed in **Table 6-1**. This resulted in a total of 98 shake table tests, providing an assessment of seismic responses across different structural setups and loading scenarios.

Table 6-2: Information on ground motions used for shake table tests

No.	Earthquake name	Station	Year	Mag.	Unscaled PGA max (g)	Scaled % used for the test
1	Northridge	Beverly Hills-Mulhol	1994	6.7	0.52	20
2	Kobe, Japan	Shin-Osaka	1995	6.9	0.24	50
3	Imperial Valley	El Centro Array #11	1979	6.5	0.38	40
4	Manjil, Iran	Abbar	1990	7.4	0.51	60
5	Chi-Chi, Taiwan	CHY101	1999	7.6	0.44	40
6	Landers	Coolwater	1992	7.3	0.42	50

6.1.3.3 Instrumentation and Data Acquisition

Accelerometers attached to the base and floors of the structure (**Figure 6-3**) were used to measure ground (shake table) accelerations and floor-level accelerations of the structure in its primary direction of motion. These measurements are used to estimate frequency response functions, as well as the structure's first mode frequency and damping ratio.

An NDI Optotrak optical measurement system was used to measure the position of each floor plate and the base plate by tracking the infrared light emitted from small markers attached to these components (**Figure 6-3**). These measurements were then used to calculate story drifts.

The system response to the white noise was used to estimate the structure's frequency response function, first mode frequency, and damping ratio for each system configuration. Numerical frequency response functions were estimated between the roof absolute acceleration and the base absolute acceleration using the tfestimate function in MATLAB (The MathWorks Inc, 2020a). Curve fitting was then used to match a single degree-of-freedom analytical dynamic model to the numerical frequency response functions produced from the experimental data using the system identification toolbox in MATLAB (The MathWorks Inc, 2020b).



Figure 6-3: Physical model with instrumentation: accelerometers and infrared markers

6.1.4 Results and Discussion

In this section, the results of the experimental shake table tests are presented and discussed. Frequency response functions (FRFs) are used to examine the dynamic behavior of the different inerter and spine system configurations. Additionally, maximum values from time history responses to the multiple ground motions are utilized to compare the performance of the different configurations.

Figure 6-4 shows the FRFs from the ground acceleration to the fourth-floor acceleration using data measured during the shaped white noise tests for each of the 14 configurations tested (**Table 6-1**). The different inerter configurations have different impacts on the dynamics of the system without the spine. Focusing on the first mode of the structure, which appears as a peak in each FRF near 1.8 Hz, without the spine, the different inerter configurations result in variations in the magnitude of the shift in this peak to lower frequencies and the reduction in the amplitude of this peak in comparison to the NI case. With the spine, the inerter configurations result in a relatively consistent shift in the first mode frequency and amplitude in comparison to the NI-S case. With and without the spine, the use of distributed inerters without a flywheel, INFD, and INDF-S, results in a shift of the first mode frequency and a reduction of the peak that is small in comparison to the changes seen with the use of distributed inerters with a flywheel, ID, and ID-S.

To provide a quantitative evaluation of the shifts in the first mode seen in **Figure 6-4**, **Figure 6-5** shows the frequency of the first mode for each of the fourteen system configurations. The system frequencies seen in this figure were determined from fit models produced near the first mode of the FRFs from the ground acceleration to the fourth-floor acceleration using data obtained during the shaped white noise tests. For both with and without the spine, the lowest first mode frequencies are seen with the inerters concentrated in the first story or distributed throughout the structure. However, the results indicate a greater consistency in the first mode frequency with the spine for the configurations with inerters. The average of the first mode frequency of each set of configurations, excluding the no inerter and distributed inerters with no flywheel cases, are 1.88 Hz without the spine and 1.64 Hz with the spine. The standard deviation of these results is 0.25 Hz without the spine and 0.026 Hz with the spine.

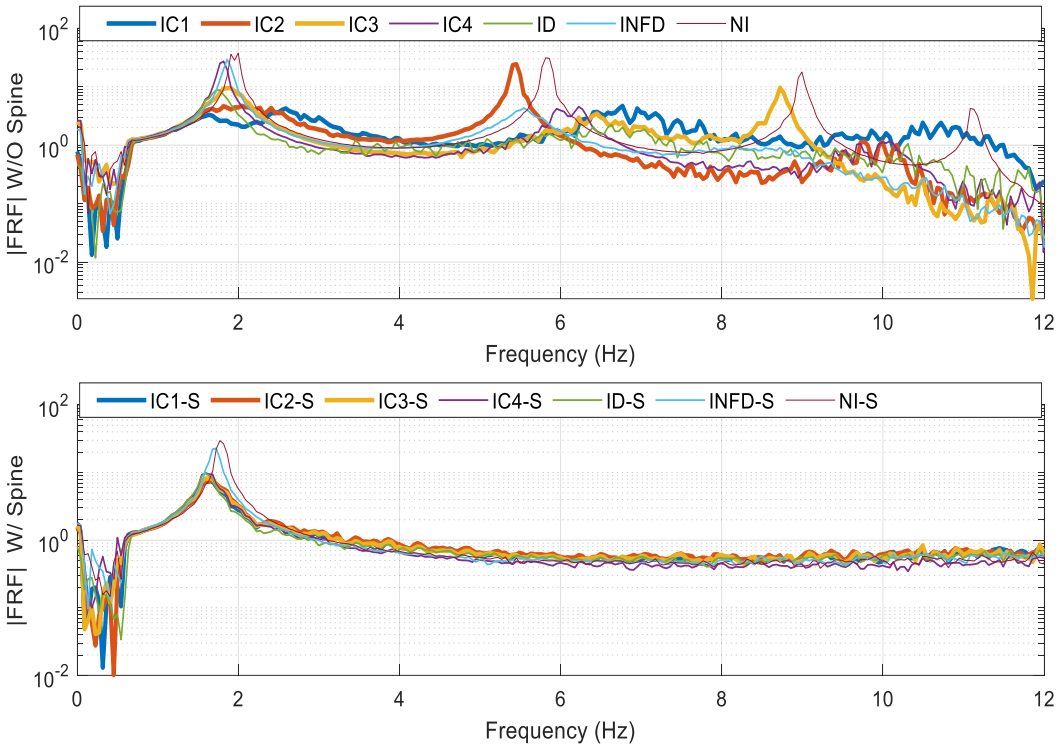


Figure 6-4: Frequency response functions from ground acceleration to fourth-floor acceleration for all system configurations

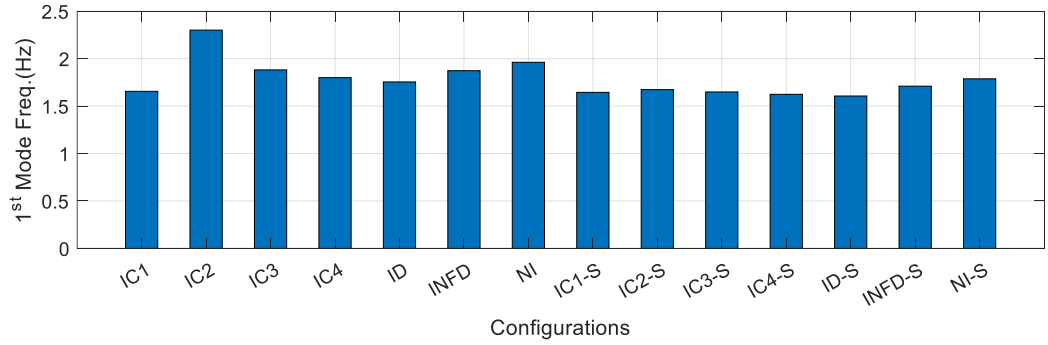


Figure 6-5: First mode frequency estimated by system identification for structure with and without spine and for all inerter configurations

Estimated damping values associated with the first mode frequency of each configuration were also determined from fit models produced near the first mode of the FRFs from the ground acceleration to the fourth-floor acceleration using data obtained during the shaped white noise tests and are shown in **Figure 6-6**. The first mode damping ratio of the NI and NI-S configurations were 0.0165 and 0.0228, respectively. These results show the low intrinsic damping in the system, but that the structure with the spine has marginally higher damping, likely due to friction in the added pins. With the inerters without the flywheel distributed throughout the structure, the damping ratio increased to 0.0203 for the INFD case and 0.0277 for the INFD-S case. With the inerters (with a flywheel), the estimated damping without a spine significantly varies for the different inerter configurations. Some concentrated inerter configurations exhibit higher estimated damping than the distributed configuration (ID), and others have lower estimated damping values. In contrast, the estimated damping values with the spine show greater consistency for the different inerter configurations. The average first mode damping ratio of each set of configurations, excluding the no inerter and distributed inerters with no flywheel cases, are 0.089 without the spine and 0.064 with the spine. The standard deviation of these results is 0.090 without the spine and 0.028 with the spine.

The natural frequency and damping changes shown in **Figure 6-5** and **Figure 6-6** provide a good view of the overall system behavior shown in **Figure 6-4** for the structures with a spine. The reason for this is that the drift pattern imposed by the spine suppresses the majority of the other global dynamics of the system. In contrast, the same is not true without the spine.

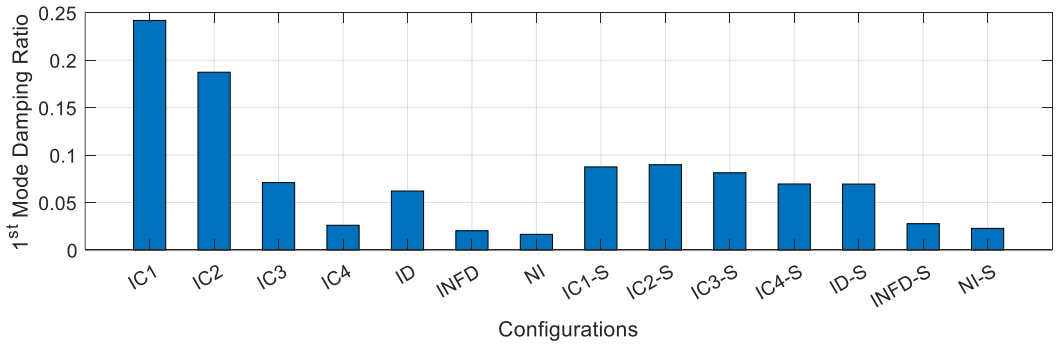


Figure 6-6: First mode damping ratio estimated by system identification for structure with and without spine and for all inerter configurations

As shown in **Figure 6-4**, without the spine, the different inerter configurations cause much more complicated changes in the systems. While larger effective damping is seen in most modes of the structure with the inerters and no spine, there are cases where modes with much less damping are seen, such as the mode near 5.5 Hz for IC2 and the mode near 8.5 Hz for IC3.

Figure 6-7 shows the maximum story drift that results from the different system configurations for each of the seven ground motions considered. These results show that the inclusion of inerters significantly reduced the maximum story drift in the structure when compared to cases where no inerter was attached. This observation holds true with and without the spine. Furthermore, these results show that for the structure with a spine similar maximum story drift was observed with the different inerter configurations (IC1-S, IC2-S, IC3-S, IC4-S, and ID-S). In contrast, large variations in maximum story drift were observed for the inerter configurations without a spine (IC1, IC2, IC3, IC4, and ID). **Figure 6-7** also shows the maximum story drift results normalized with the results from the INFD configuration for systems without a spine and the results from the INFD-S configuration for systems with a spine. This normalization is done to account for changes in system response when the flywheels of the inerter produce significant mass effects. It is clear from these normalized results that with the spine, the performance of the inerters is consistent and almost always better than the no flywheel case. Without the spine, there are much larger variations in effectiveness based on inerter configuration and ground motion.

Figure 6-8 presents the maximum absolute acceleration response for the different system configurations for the ground motions. When processing these time-history results, a lowpass filter with a cut off frequency of 100 Hz was used. The presence of a spine led to an increase in the maximum absolute acceleration compared to cases without a spine. Unlike the story drift results, there are no clear trends showing the presence or configuration of inerters improves the maximum acceleration performance of the structure.

Figure 6-9 shows plots of the maximum drifts for each story of the structure for each of the 14 configurations. This figure shows that the spine was able to impose a nearly uniform set of peak story drifts that is not seen in most cases for the structure without the spine. Furthermore, this figure shows how the magnitude of story drifts changes for the different configurations of inerters (with flywheels) without the spine, but that these drifts remain more consistent with the spine.

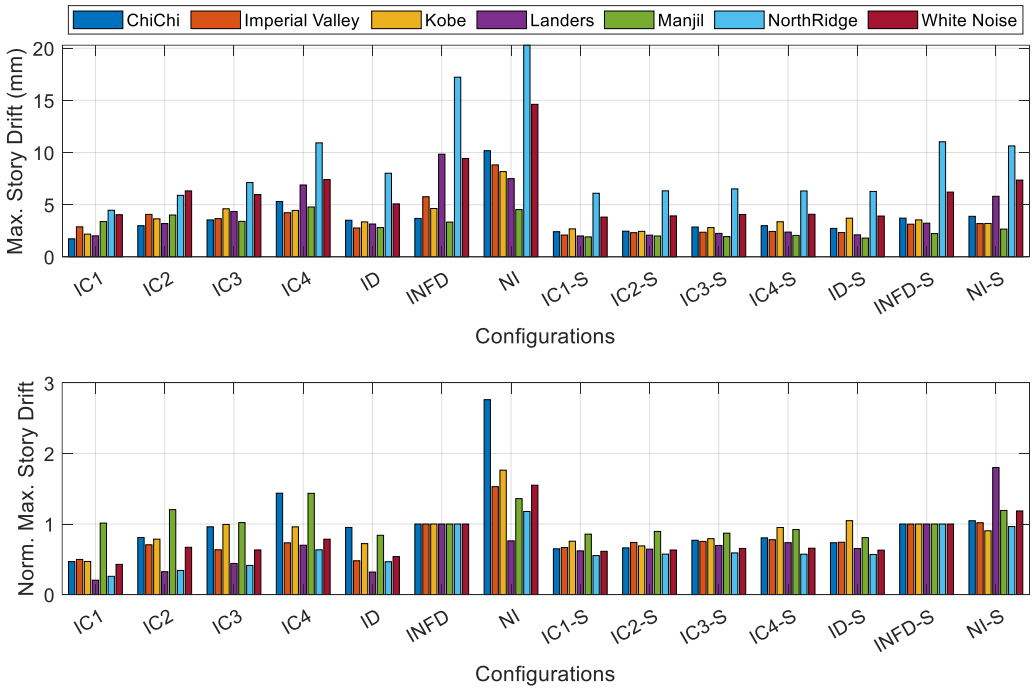


Figure 6-7: Maximum story drift and normalized maximum story drift results. Results were normalized with reference to the maximum story drift of the INFD configuration (for systems without a spine) and the INFD-S configuration (for systems with a spine)

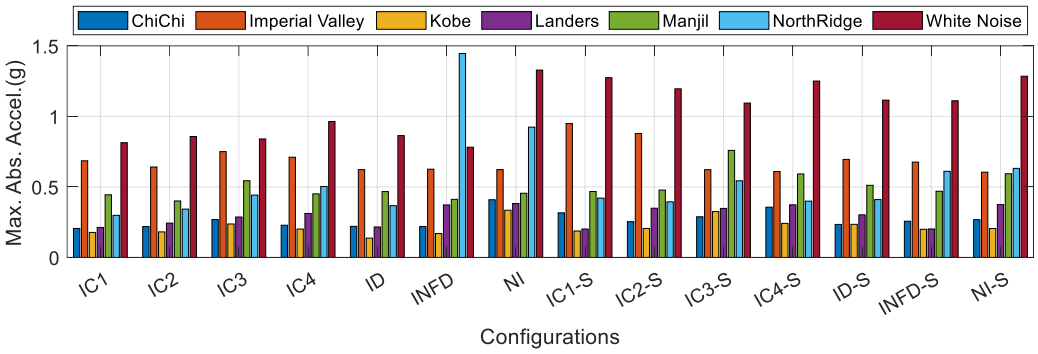


Figure 6-8: Maximum absolute acceleration results

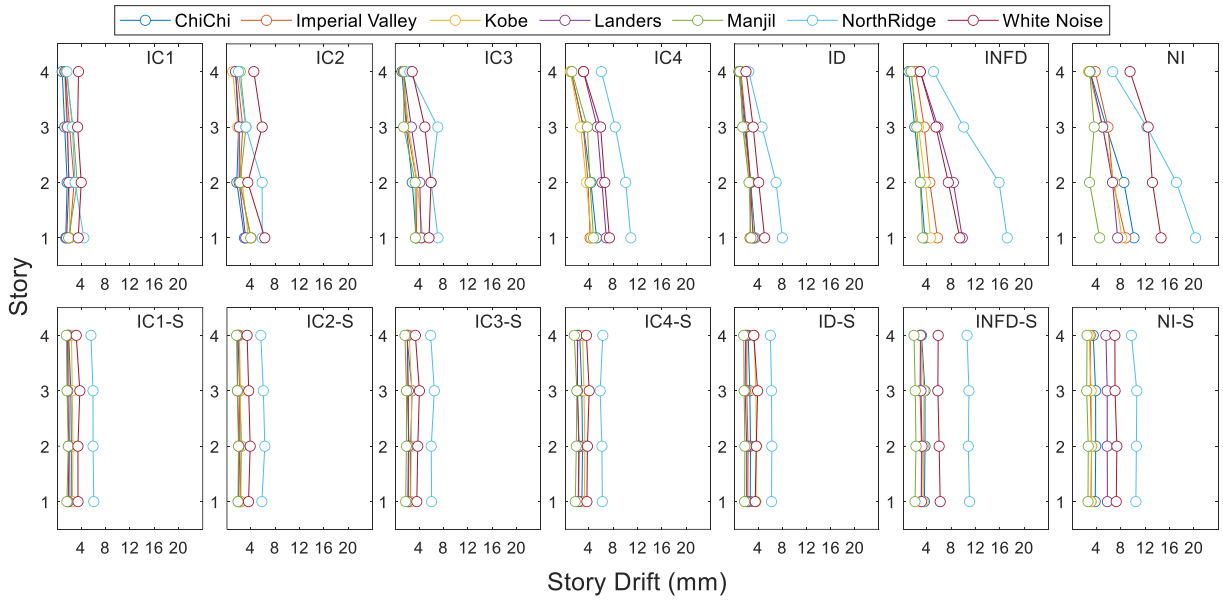


Figure 6-9: Maximum drifts for each story of the structure with and without spine for all inerter configurations

6.1.5 Conclusion

Inerters are a type of passive control device that can produce large effective mass by exploiting the conversion of translational motion to localized rotational motion. An experimental study was conducted on a small-scale four-story structure to investigate the behavior of a structure combining inerters and an elastic spine. Several configurations with inerters, including those where inerters are concentrated in a single floor and those where inerters are distributed across all floors, were tested with and without a spine using ground motions generated by a shake table. The key findings of this work are:

- The inclusion of inerters led to decreases in maximum story drift in most cases, but had no clear effect on maximum absolute acceleration.
- Inclusion of the spine led to a largely uniform distribution of story drift throughout the height of the structure, irrespective of the inerter configuration. In contrast, the story drift distribution varied widely for the inerter configurations without the spine.
- Without the spine, there was large variability in the effectiveness of the different inerter configurations and the impact of these configurations on the dynamic properties of the structure.

- With the spine and when the flywheels were attached, the different inerter configurations had largely similar effects on structural performance and dynamic properties.

The findings from this study indicate that when a spine is used, inerters can achieve comparable levels of effectiveness, whether they are distributed throughout a structure or concentrated in a single story. Further investigation into alternative inerter-based devices, especially tuned-inerter devices, is encouraged by these results. Tuned-inerter devices, which resemble tuned mass dampers in behavior, provide an effective and lightweight passive control option; however, they have not been utilized much in practice as they typically need to be distributed throughout a structure. This work shows that the addition of a spine may allow the concentration of tuned-inerter devices while still maintaining their effectiveness.

6.2 NUMERICAL STUDY OF HYBRID SEISMIC CONTROL USING SEGMENTAL ELASTIC SPINE AND DISTRIBUTED INERTERS

6.2.1 Introduction

Earthquakes continue to pose a significant threat to the safety, functionality, and resilience of built infrastructure. The devastating impacts of past seismic events have underscored the critical need to advance our understanding of how structures respond to earthquake excitations (Kramer and Stewart, 2024; Shokrgozar-Yatimdar et al., 2024). Strategies have been developed to improve the performance of structures subjected to seismic demands, both statically and dynamically. These include enhancements in structural strengthening, improved ductility and energy dissipation capacity, and the integration of control devices to mitigate seismic response.

6.2.1.1 Elastic Spine

Premature failure due to soft story formation undermines the structural integrity and ductile response of buildings, often resulting in significant repair costs and delays in restoring the structure's operational use (AISC, 2018; Sabelli, 2001). Among various seismic protection strategies, elastic spine (ES) has emerged as a promising concept to minimize damage by preventing or reducing the of soft-story mechanism by integrating a rigid vertical truss or stiffening elements (Faramarzi and Taghikhany, 2021; Simpson and Mahin, 2018). This concept

has been developed under various alternative terms in the literature, such as spine frame (Chen et al., 2022; Hu et al., 2021; Takeuchi et al., 2015), hinged wall (Alavi and Krawinkler, 2004), stiff rocking core (Slovenec et al., 2017), rocking steel shear wall (Djojo et al., 2014; Eatherton et al., 2014) , and vertical rigid truss (Palermo et al., 2021a; Simpson and Mahin, 2018).

While experimental studies on ES systems remain relatively limited (Abolghasemi et al., 2024b; Chen and Tagawa, 2023; Ma et al., 2013; Simpson and Mahin, 2018), a substantial body of numerical research has been dedicated to evaluating ES-like configurations and their effectiveness in seismic performance enhancement (Alavi and Krawinkler, 2004; Chen et al., 2017, 2018; Faramarzi and Taghikhany, 2021; Lai and Mahin, 2015; Palermo et al., 2021a; Qu et al., 2012; Talley et al., 2024). Designing ES systems remains a complex task in seismic engineering. Although nonlinear response history analysis offers detailed insight, it is difficult to implement in practice. As a result, alternative methods have been proposed to simplify the design process. For example, Simpson and Rivera Torres (2021) introduced a modal pushover-based approach, and Martin and Deierlein (2021) proposed a modified superposition technique—both of which aim to address higher-mode effects and the partial yielding behavior that often occurs in ES-equipped structures. In parallel, the plastic mechanism control theory (Montuori et al., 2022) has shown potential for achieving desired global deformation patterns. Despite their conceptual value, these simplified procedures have not yet been formalized within existing design codes, and practical guidance for their implementation remains limited.

Parametric studies have shown that ES are more effective in mitigating inter-story drift concentrations in low- and mid-rise buildings than in high-rise structures. They are particularly beneficial in buildings that exhibit flexural-type deformation behavior. However, ESs are more effective when used in shear-type buildings, assuming uniform story stiffnesses over the building heights (Lin et al., 2019). Studies show that stiffness of the ES and the structure it is attached are both important and impacts the behavior of combined system (Chen et al., 2017; Lin et al., 2019). Simpson and Mahin (2018) explicitly investigated the effect of a ES in structures with a single-story stiffness reduction; however, they did not explore how the vertical location of the soft-story irregularity influences structural response. Building on this, Abolghasemi et al. (2024b) conducted an experimental study on a small-scale four-story structure to examine the

effect of stiffness irregularity location on ES performance. Their results indicated that the structural response was largely insensitive to the vertical position of the stiffness irregularity.

In addition, several studies have examined the effects of integrating energy dissipation and control devices alongside ES systems to enhance seismic performance. Qu et al. (2012) and Wang et al. (2023) investigated shear-type, hysteretic, and viscoelastic dampers in pin-supported wall frames. Hu et al. (2021) used friction spring dampers with recentering capabilities along the height of a steel structure with dual spines. Palermo et al. (2021a) evaluated various viscous damper configurations—distributed, selective, and base-concentrated—demonstrating that the presence of a ES improves the flexibility and effectiveness of damper arrangements by promoting uniform drift across stories. Abolghasemi et al. (2024b) experimentally examined how damper configuration—whether distributed across stories or concentrated at a single story—affects the performance of ES structures. The findings revealed that key response metrics, including effective damping ratio, story drift, and roof drift, showed minimal sensitivity to the damper arrangement in the presence of an ES.

Despite ES effectiveness in promoting uniform drift and mitigating soft-story mechanisms, ES systems face a key limitation: their interaction with higher-mode vibrations. These higher modes often introduce force and acceleration demands that conflict with the intended uniform drift pattern, leading to elevated internal forces in the ES and increased floor accelerations (Fahnestock et al., 2021; Wang et al., 2023).

6.2.1.2 Segmental Elastic Spine

While traditional ESs effectively promote uniform drift profiles and mitigate soft-story mechanisms, they also introduce notable challenges—particularly in taller buildings —such as increased force demands and floor accelerations. In particular, continuous spines can attract substantial force and acceleration demands due to higher-mode participation, especially in mid- to high-rise structures. A proposed solution is to divide a continuous vertical spine into two or more segments along the height of the structure that are pin connected (Chen et al., 2012; Tremblay et al., 2014).

This segmentation approach, known as the segmental ES , has been introduced to improve retrofit cost efficiency (Balazadeh-Minouei et al., 2018; Chen et al., 2019b) and structural

performance (Chen et al., 2019b, 2018; Tremblay et al., 2014), when properly design in taller buildings. For example, distributing stiffness across multiple ES segments has been shown to limit story shear and column axial forces, particularly when a minimum number of stories per module is maintained (Chen et al., 2019b).

Energy dissipation devices have also been considered in conjunction with segmental ES. For example, Tremblay et al. (2014) demonstrated that incorporating dampers at the interfaces between spine segments can improve drift control, with performance gains increasing as the number of segments grows. However, beyond this study, research on segmental ES—particularly their integration with control devices—remains limited. Most existing analyses are purely numerical and often rely on idealized assumptions such as perfectly pinned joints, overlooking the potential effects of joint stiffness or nonlinearity. Furthermore, the dynamic behavior of these systems under seismic loading and their interaction with damping mechanisms have not been thoroughly explored. These gaps point to the need for more comprehensive studies, including experimental validation and design guidance, to fully understand and utilize the potential of segmental ES systems.

6.2.1.3 Inerters

The inerter is a two-terminal mechanical device that produces a force proportional to the relative acceleration between its terminals, acting as an inertia amplifier within structural systems. Unlike traditional masses, which are grounded, inerters connect two moving points—allowing them to influence the dynamic behavior of a structure without significantly increasing its physical mass (Sugimura et al., 2012b). These devices have been used as vehicle suspension system. They have been explored for a wide variety of vibration control purposes, including use in vibration absorbers and mounts (Siami et al., 2018; Smith, 2002a), to provide structural damping in buildings (Wang et al., 2010), and as a part of suspension systems for railway vehicles (Jiang et al., 2013).

The unique property of inerter has led to their growing interest in the field of structural control to help mitigate the response of structures to earthquakes (Hwang et al., 2007a; Nakamura et al., 2014a; Giaralis and Petrini, 2017a; Javidialesaadi and Wierschem, 2019a; Di Egidio et al., 2021a; Ma et al., 2021a). Inerters can serve different purposes depending on the structural

control objectives. In some applications, the primary goal is to adjust the natural frequencies of the system, effectively shifting the dynamic characteristics to avoid resonance or to better align with desired performance targets (Beeby et al., 2006; Yu et al., 2001). In other cases, inerters are employed to achieve structural mode control (Zhang et al., 2021), promoting more favorable deformation patterns or reducing localized demands.

Several configurations—such as linear translational inerters and rotational inerters using ball-screw or rack-and-pinion mechanisms—have been developed and experimentally validated (Smith, 2002a; Smith et al., 2012; Swift et al., 2013a). Furthermore, a nonlinear rotational inertial mechanism is a type of nonlinear inerter that can produce variable mass effects that can be used to disrupt the formation of resonant conditions (Sarkar and Wierschem, 2024a). This nonlinearity can be due to geometric nonlinearity (Moraes et al., 2018; Yang et al., 2020), like changes in lead-screw properties, as well as from adjustments in the properties of the device's flywheel (Kushwaha et al., 2020; Mahato et al., 2019).

6.2.1.4 Hybrid Control Strategy

Despite extensive research on ES systems and the growing interest in inerters for structural control, studies that examine the combination of these two strategies are extremely limited. While both mechanisms offer distinct advantages, their potential interaction has yet to be fully explored in the context of building structures. In an experimental study, Abolghasemi et al. (2024a) examined the seismic performance of a four-story structure with and without a ES under various inerter configurations. The results showed that when inerters are combined with an ES, inerters produced uniform distribution of story drift whether distributed across all stories or concentrated at a single level—highlighting the potential for flexible inerter design in ES-equipped systems. However, the study was limited to a 4-story scaled structure with a single inertance value and a restricted set of ground motions, leaving open questions about optimal inerter design and broader applicability under varying seismic scenarios.

This work investigates how hybrid control strategy, combining inerters (with no damping) with ES systems (segmental one specifically), can address the key challenges associated with ES implementation: the large internal demands imposed on the spine and the elevated floor accelerations. These demands arise from a mismatch between the uniform drift pattern enforced

by the ES and the nonuniform deformation shapes of the structure's natural vibration modes. While the first mode already deviates from uniform drift, higher modes further amplify this discrepancy, resulting in increased internal forces and floor accelerations. The effectiveness of this strategy is evaluated through numerical simulations conducted in MATLAB on 4-, 5-, and 6-story structural models. The models include configurations both with and without ESs (including unit and segmental variants), and with and without inerters. For each configuration, the structures are subjected to a suite of seismic ground motions, and their performance is assessed based on story drift, floor acceleration, and moment demands in the ES.

This work is organized as follows. Section 2 describes the mathematical method and numerical model of MDOF structure(s) with attached ES for the numerical study. Section 3 presents the system configurations examined. Furthermore, this section describes the ground motions considered to measure the response of the structure. The results of the numerical investigation are presented and discussed in Section 4. In Section 5, the results of the studies are summarized, and conclusions are presented.

6.2.2 Numerical Model

This section introduces the numerical model used to investigate the performance and efficiency of various ES configurations. Numerical simulations are employed to evaluate a large number of seismic ground motions and system configurations. The model combines a shear structure representation for the main structure with a beam model for the ES. As illustrated in **Figure 6-10**, this simplified model forms the basis for the numerical analysis. The model is implemented in MATLAB and is adaptable to simulate 4-, 5-, or 6-story structures, with the flexibility to incorporate inerters and represent segmental ES with adjustable joint stiffness.

6.2.2.1 Building Model

The three building configurations considered for this study (4,5, and 6 stories), are assumed to represent office buildings with Seismic Design Category (SDC) D and with identical floor plans.

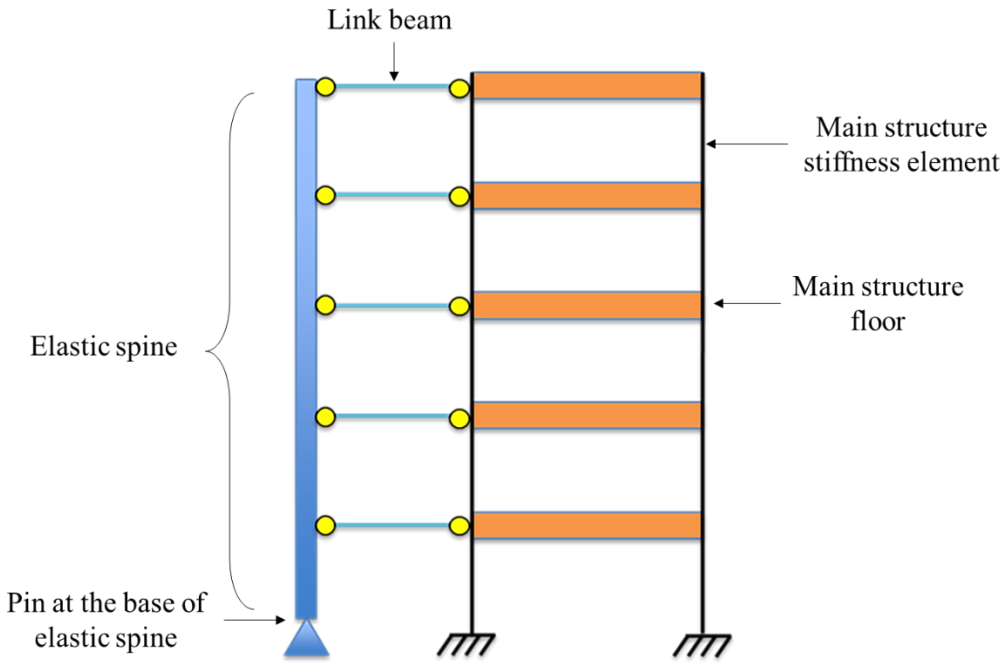


Figure 6-10: Simplified model of five-story structure with elastic spine.

Each story has a height of 4.5 meters. The mass of a typical floor is taken as 500,000 kg, while the roof mass is assumed to be 400,000 kg, representing 80% of the typical floor mass.

Consider a 5-story structure as an example, the general parametric mass matrix as follows, considering the system DOF as displacement relative to the base.

$$Ms = \begin{bmatrix} m & 0 & 0 & 0 & 0 \\ 0 & m & 0 & 0 & 0 \\ 0 & 0 & m & 0 & 0 \\ 0 & 0 & 0 & m & 0 \\ 0 & 0 & 0 & 0 & 0.8m \end{bmatrix} \tag{6-4}$$

In most designs, the inclusion of the ES primarily modifies the stiffness of a structure without significantly increasing the overall mass. As a result, the mass of the ES is excluded from the equations of motion (EOM) only the contribution to the stiffness matrix will be considered. This will allow this study to focus on the stiffness contribution of the ES.

6.2.2.2 Inerter Model

Inertance of inerter, commonly denoted as *b*, is the key parameter defining the behavior of inerters in the system and is incorporated into the models accordingly. It has the same unit as mass and, in the equations of motion, contributes to the system in a similar way by generating a force proportional to the relative acceleration between its two terminals. The restoring force provided by an ideal inerter is expressed as below:

$$F = b\left(\ddot{u}_2 - \ddot{u}_1\right) \tag{6-5}$$

In this study, inertance is incorporated as an additional mass term acting between structural degrees of freedom, which alters the dynamic characteristics of the system. To isolate the effect of inertance on structural response, inerter's damping effects is intentionally excluded from the numerical model. This allows the analysis to focus on the effects of changes in dynamic properties, such as natural frequencies and mode shapes, rather than on energy dissipation. The mass matrix will be modified with the inclusion of distributed inerters (one at each story) and will become nondiagonal.

$$M = \begin{bmatrix} b_1 + b_2 + m & -b_2 & 0 & 0 & 0 \\ -b_2 & b_2 + b_3 + m & -b_3 & 0 & 0 \\ 0 & -b_3 & b_3 + b_4 + m & -b_4 & 0 \\ 0 & 0 & -b_4 & b_4 + b_5 + m & -b_5 \\ 0 & 0 & 0 & -b_5 & b_5 + 0.8m \end{bmatrix} \tag{6-6}$$

where b_i is inertance value of i^{th} story.

6.2.2.3 Main Structure Stiffness and Damping

A linearly decreasing stiffness distribution is applied to the main structure, where the first story has stiffness k, and the stiffness of each subsequent story decreases by a fixed amount of 0.1k. For a structure with n stories (n = 4, 5, or 6), the story stiffnesses are assigned as k, 0.9k, 0.8k, and so on, down to (1 − 0.1 × (n − 1)) k at the top story. This linear reduction reflects the reduction in vertical stiffness with increased story commonly observed in real structural systems.

The stiffness matrix of the main structure, without the ES, is:

$$Ks = \begin{bmatrix} k_1 + 0.9k_1 & -0.9k_1 & 0 & 0 & 0 \\ -0.9k_1 & 0.9k_1 + 0.8k_1 & -0.8k_1 & 0 & 0 \\ 0 & -0.8k_1 & 0.8k_1 + 0.7k_1 & -0.7k_1 & 0 \\ 0 & 0 & -0.7k_1 & 0.7k_1 + 0.6k_1 & -0.6k_1 \\ 0 & 0 & 0 & -0.6k_1 & 0.6k_1 \end{bmatrix} \quad (6\text{-}7)$$

A 5% damping ratio considered for all modes of the structure, and the modal damping matrix calculated accordingly considering no ES or inerters and then converted into a physical damping matrix. This same physical damping matrix is utilized for all subsequent tests with different configurations of inerters and ES.

6.2.2.4 Elastic Spine Model

6.2.2.4.1 ES Stiffness Matrix

A numerical model of the ES based on Euler-Bernoulli beam stiffness was developed for this work. By using the Euler-Bernoulli beam as a basis, shear deformations are neglected when calculating the stiffness contribution of the ES. The stiffness matrix of a single element of a two-node Euler-Bernoulli beam, K, is

$$K = \frac{12EI}{L^3} \begin{bmatrix} 12 & 6L & -12 & 6L \\ 6L & 4L^2 & -6L & 2L^2 \\ -12 & -6L & 12 & -6L \\ 6L & 2L^2 & -6L & 4L^2 \end{bmatrix} \quad (6\text{-}8)$$

where E is the modulus of elasticity, I is the moment of inertia, and L is the length of the beam. Each end of the beam has two DOF: one for displacement and one for rotation. In **Equation (**6-8**)**, the first and third rows correspond to displacement (u), while the second and fourth rows correspond to rotation (θ). For a beam with two elements, three nodes, and six DOF, the stiffness matrix is:

$$K = \frac{12EI}{L^3}\begin{bmatrix} 12 & 6L & -12 & 6L & 0 & 0 \\ 6L & 4L^2 & -6L & 2L^2 & 0 & 0 \\ -12 & -6L & 12+12 & -6L+6L & -12 & 6L \\ 6L & 2L^2 & -6L+6L & 4L^2+4L^2 & -6L & 2L^2 \\ 0 & 0 & -12 & -6L & 12 & -6L \\ 0 & 0 & 6L & 2L^2 & -6L & 4L^2 \end{bmatrix}$$

$$= \frac{12EI}{L^3}\begin{bmatrix} 12 & 6L & -12 & 6L & 0 & 0 \\ 6L & 4L^2 & -6L & 2L^2 & 0 & 0 \\ -12 & -6L & 24 & 0 & -12 & 6L \\ 6L & 2L^2 & 0 & 8L^2 & -6L & 2L^2 \\ 0 & 0 & -12 & -6L & 12 & -6L \\ 0 & 0 & 6L & 2L^2 & -6L & 4L^2 \end{bmatrix} \quad (6\text{-}9)$$

The odd rows of this matrix are associated with nodal and even rows are associated with nodal rotations.

This matrix can be expanded for the 4-story, 5-story, and 6-story model structures in this study considering four, five, or six connected beam elements.

6.2.2.4.2 Static Condensation Method

To combine the spine and primary structure numerical models, the stiffness matrix for the ES is reduced to a nxn matrix, in which n refers to the number of stories in the structure. To reduce this matrix, the Guyan Reduction (GUYAN, 1965) method, also known as static condensation, can be used. This approach reformulates the stiffness matrix based on primary DOFs, DOFs that can be internalized, and retrained DOF and effectively reduces the size of the model while retaining the essential characteristics of the underlying structure.

After condensation, the reduced ES stiffness matrix and can be added to main structure stiffness matrix, Ks.

$$K = K_{reduced} + Ks \quad (6\text{-}10)$$

6.2.2.5 Equation of Motion

The general equation of motion (EOM) for a structure combined with ES is:

$$M\ddot{U} + C\dot{U} + KU = F(t) \tag{6-11}$$

where M is a total mass matrix including inerter (if considered), C is a damping matrix, K is the total stiffness matrix that combines the condensed stiffness matrix of the ES and the main structure stiffness (**Equation (6-10)**), and $F(t)$ is the vector of applied forces on each story.

For segmental ES systems, the same general modeling procedure is followed as in the continuous ES case, with one key modification: the ES is divided into separate segments, and static condensation is performed individually for each segment. The stiffness matrix for each segment is first formulated based on its own boundary conditions, treating the pin connection between segments as an internal constraint. For example, in a 5-story structure with a pin located at the second floor, the ES is divided into two segments: the lower segment contributes a condensed 2×2 stiffness matrix, and the upper segment contributes a condensed 4×4 matrix. These condensed matrices are then assembled into a full 5×5 structural stiffness matrix, ensuring continuity at the pin location. This modular approach allows flexibility in representing various pin locations and segmental configurations while preserving the essential stiffness characteristics of the system.

6.2.3 Analysis Plan

6.2.3.1 Optimization

In this study, optimization is used to determine a proposed distribution of inerters with the goal of improving the performance of a structure equipped with a segmental ES. There are many ways to approach this optimization, depending on the specifics of the goal and how performance is measured. In this work, we focused this optimization on one of the core strengths of the ES system: its ability to shift the dynamics of the systems through added mass effects.

The optimization of the inters used for this work was set up to shift the first and second mode shapes of the system. Specifically, the first mode was encouraged to produce uniform modal drift across all stories, while the second mode was shaped to provide uniform modal drift within each ES segment. This approach helps align the dynamic behavior of the structure with what the segmental ES is designed to do, allowing the inerters to work in tandem with the segmentation to

reduce demands and improve overall seismic performance. In MATLAB, this was achieved by defining an objective function that evaluates how well a given set of inerter values produces the desired drift distributions. The optimization algorithm searches for the set of inerter values that minimizes this objective function. **Figure 6-11** shows that how changing in inertance can affect the modal frequencies when equally distributed. Based on this trend, the range of inertance was selected between 0 and 3×10^6 kg, where the most significant influence on modal frequencies is observed.

The objective function for 5-story structure with segmental ES with pin at second floor is considered to be:

$$\begin{aligned}\text{Objective} = {} & \underset{\text{Multiplier}}{\text{A}} * \underbrace{\text{abs}\left(\text{abs}\left(\text{drift1}(3)\right)\text{-abs}\left(\text{drift1}(2)\right)\right)}_{\text{Pushing 1st mode to have equal drifts around the pin}} + \ldots \\ & \underset{\text{Multiplier}}{\text{B}} * \underbrace{\text{abs}\left(\text{abs}\left(\text{drift2}(3)\right)\text{-abs}\left(\text{drift2}(2)\right)\right)}_{\text{Pushing 2nd mode to have equal drifts around the pin}} + \ldots \\ & \underbrace{\text{max}(\text{abs}(\text{drift1}(4)\text{-drift1}(3)) + \text{abs}(\text{drift1}(2)\text{-drift1}(1)) + \text{abs}(\text{drift1}(5)\text{-drift1}(4)))}_{\text{Pushing 1st mode to have equal drifts in segments}} + \ldots \\ & \underbrace{\text{max}(\text{abs}(\text{drift2}(4)\text{-drift2}(3)) + \text{abs}(\text{drift2}(2)\text{-drift2}(1)) + \text{abs}(\text{drift2}(5)\text{-drift2}(4)))}_{\text{Pushing 2nd mode to have equal drifts in segments}}\end{aligned} \tag{6-12}$$

In this function, A and B are weighting multipliers used to emphasize desired performance objectives. In this study, A is set to 3 and B to 1. This process produced a non-zero inertance value for each story. The optimized inertance values, b_i, for the 1st through 5th stories, based on this structural configuration and EI = 6.406e11 N.m^2 and objective function, are: 1,593,608.22 kg, 1,353,262.36 kg, 2,497,457.73 kg, 1,641,522.90 kg, and 1,420,885.07 kg, respectively. The optimal non-equal values of b_i were then incorporated into the mass matrix to reflect the inertial effects.

The optimization was performed separately for each structural configuration and pin arrangement in the segmental ES with an optimization function similar to that shown in **Equation (6-12)**, but modified for the number of stories and pin arrangement. In addition to these, configurations using equal inertance values were also examined, where a single inertance value was applied to all stories based on the mean of the optimal b_i values. To better understand the impact of inerters in ES systems, a range of structural configurations is considered. These

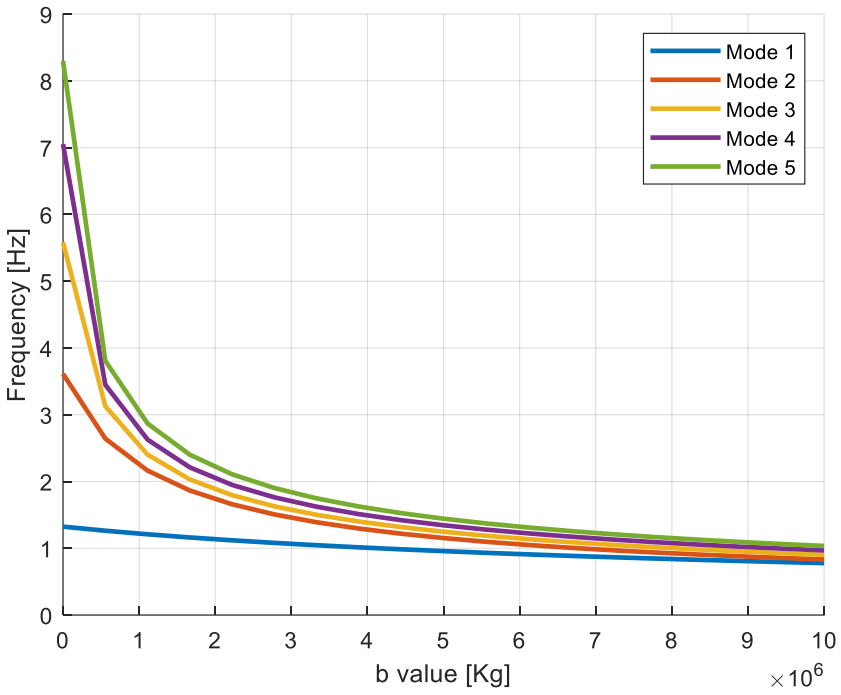


Figure 6-11: System natural frequencies over a range of inertance values, b, in the hybrid system with a unit ES and distributed inerters with equal inertance.

include cases with unit (continuous) ES and segmental ES. The ES stiffness is also varied over a wide range, from zero (representing no ES) to very high flexural rigidity (representing an ideally rigid ES), in order to capture the full spectrum of structural behavior. Furthermore, 4-, 5-, and 6-story structures were considered. For the segmental ES, pin locations are varied as follows: the 4-story structure with a segmental ES is only considered with a 2nd floor pin, the 5-story structure with a segmental ES is included with a 2nd or 3rd floor pin, and the 6-story structure with a segmental ES is considered with a 2nd, 3rd, or 4th floor pin.

For each structural configuration, three inerter arrangements are examined: (1) no inerters, serving as the baseline; (2) an optimized, non-uniform distribution of inertance values obtained through optimization; and (3) equal inertance values derived from the average of the optimized distribution. This parametric setup enables a systematic evaluation of how inerter placement and ES design interact to influence seismic performance.

The configurations are labeled as Unit ES and Seg ES to represent the unit ES and segmental ES systems, respectively. Each is considered with either equal inertance distribution (bEq), optimum non-equal inertance distribution (bOpt), or without inerters (b0). In addition to variation in inertance, three representative ES stiffness levels are considered for selected results and plots: EI0, EIdef, and EImax. These correspond to a system with no ES, a default spine stiffness, and a high spine stiffness, respectively. The maximum stiffness (EImax) represents the upper bound of the EI range explored in the parametric study. The default stiffness (EIdef) is chosen independently for each structural type. For the unit ES, EIdef was chosen for each structure such that it's second-mode natural frequency was 300% of the second mode natural frequency for the structure without an ES. This metric was chosen for determining EIdef in order to provide reasonable stiffness value for a realistic ES. For the segmental ES systems, an EIdef value approximately one-third of the corresponding unit spine EIdef was used, based on the observation that most significant changes in response occurred within this range. The values for EIdef for the different configurations are listed in **Table 6-3**.

6.2.3.2 Earthquake Suite

A total of 22 far-field ground motions, each recorded in two horizontal directions (44 records in total), were selected from the FEMA P695 (FEMA P695, 2009) ground motion set to serve as seismic input for this study. Each ground motion was first scaled using a normalization factor (NF) from Table A-4D of FEMA P695 to adjust its peak ground velocity (PGV) to match the median PGV of the full record set. In addition, the motions were scaled using the Seismic Design Category D scaling factor (SDC_D) from Table A-3 of FEMA P695 to anchor the normalized record set to the Maximum Considered Earthquake (MCE) spectral demand.

This two-step scaling ensures a consistent intensity level across all simulations and reflects design-level seismic hazard for structures in SDC D. The final scaled ground motion used in the analyses is computed as:

$$\ddot{U}_{g,scaled}(t) = SDC_D \times NF \times \ddot{U}_{g,recorded}(t) \tag{6-13}$$

Table 6-3: Default EI values used for unit and segmental ES; segmental EI is one-third of unit EI.

Number of stories	EIdef for unit ES ($N.m^2$)	EIdef for segmental ES ($N.m^2$)
4	3.265e11	1.088e11
5	6.406e11	2.135e11
6	9.796e11	3.265e11

The value of SDC_D is based on linear interpolation at the 5-story structure fundamental period of 0.7552 seconds. All ground motion records were resampled to a uniform sampling rate of 400 Hz to ensure consistency in numerical integration.

6.2.3.3 Performance Metrics

To evaluate the seismic performance of the structural systems under investigation, three key parameters are considered:

Maximum Absolute Floor Acceleration: The peak absolute acceleration is selected for each floor throughout the ground motion duration. This measure reflects the potential for damage to nonstructural components.

Maximum Inter-Story Drift: The absolute maximum relative lateral displacement between adjacent floors, is computed for each story and then the overall maximum is identified. This parameter is used to assess deformation demands and potential structural damage.

Maximum Bending Moment in the Elastic Spine: The moment developed in the ES element(s) is tracked over the ground motion duration and the maximum absolute value of the bending moment is identified. This maximum bending moment as an indicator of internal demand in the ES, and will influence the size of the members of the ES and its cost to produce.

For each configuration and demand parameter, the median of the maximum response values across all 44 ground motion records from FEMA P695 is considered to represent typical behavior while mitigating the effect of outliers.

6.2.4 Results and Discussion

This section presents the results of numerical simulations conducted to evaluate the seismic performance of various structural configurations, including systems with and without a unit ES, segmental ES, and distributed inerters. The findings are discussed in terms of key response measures such as story drift, floor acceleration, and moment demand in the ES. Emphasis is placed on how these parameters are influenced by different combinations of ES configurations and inerter distributions, providing insight into the effectiveness of the proposed hybrid control strategies.

To illustrate overall trends, 5-story structures with a segmental ES pinned at the second and at the third floor are selected for detailed presentation of results in **Section 6.2.4.1** through **Section 6.2.4.3**. Comparisons to the 5-story structure with unit ES are made for both. The response measures for these structures are assessed across a large range of ES stiffnesses and different inerter configurations. In addition to the detailed results for the 5-story structure, the response measures are assessed for 4-story, 5-story, and 6-story structures and different pin configurations. This broader comparison highlights the influence of structural height and ES segmentation on overall system performance with inerter configurations which will be discussed in **Section 6.2.4.4**.

To provide a reference for evaluating the impact of elastic spine and inerter systems, **Figure 6-12** presents all mode shapes of the 5-story structure without an ES and without distributed inerters. These baseline mode shapes illustrate how the structure naturally deforms under dynamic excitation. The first mode is characterized by a nearly linear shape, while the second mode exhibits a curvature reversal around the second floor. This reversal point becomes especially important when evaluating the effect of segmental ES placement and pin locations, as it directly influences how the control system interacts with the structure’s natural vibration modes.

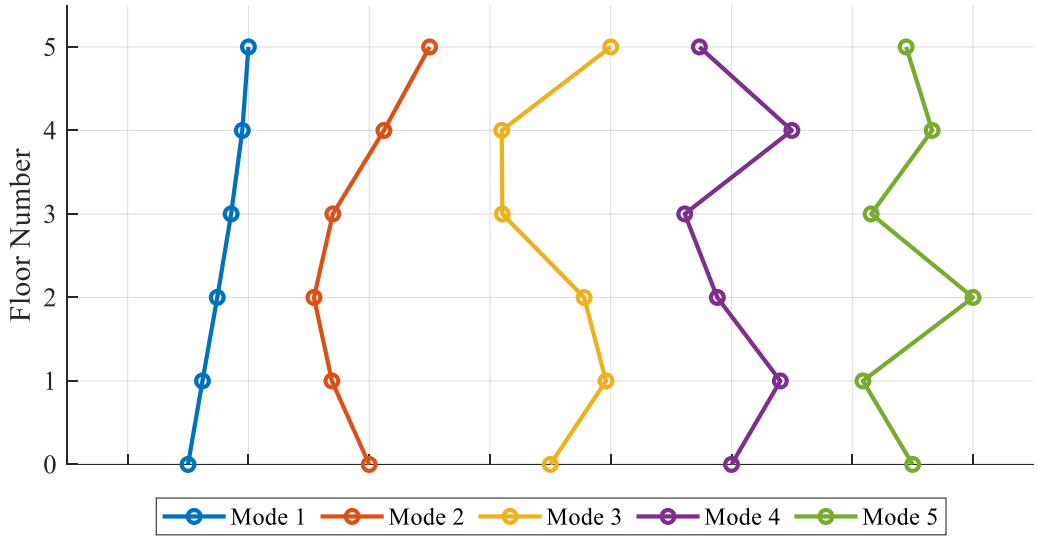


Figure 6-12: Natural mode shapes of the 5-story structure without ES and inerter

6.2.4.1 Inter-Story Drift of 5-Story Structure

6.2.4.1.1 When pin is at 2nd floor:

For the five-story structure with the segmental ES pinned at the second floor, using ES systems generally led to a reduction in median maximum story drift (MMSD) which can be seen in **Figure 6-13**. An exception was observed in the segmental ES without any inerter (b0), which resulted in a slight increase in MMSD. In the absence of ES, using equally distributed inerters (bEq) maintained MMSD at a level similar to the no-inerter (b0) case, whereas the optimally distributed inertance (bOpt) significantly increased the MMSD. This increase occurs because the bOpt configuration is optimized to enforce uniform interstory drift in ES each segment, which can amplify portions of the mode shapes and lead to higher maximum interstory drift when no ES is present.

Adding distributed inerters helped reduce MMSD across all configurations. In the unit ES, both equal (bEq) and optimal (bOpt) inertance distributions performed nearly the same. However, in the segmental ES, bEq was more effective than bOpt in reducing MMSD. In the optimal case, the b values are tuned to make story drifts more uniform across all floors. However, this can lead to a higher maximum drift in top segment specifically. For unit ES, MMSD values plateaued once spine stiffness exceeded approximately 3e+9 kN·m², while for segmental ES, this plateau

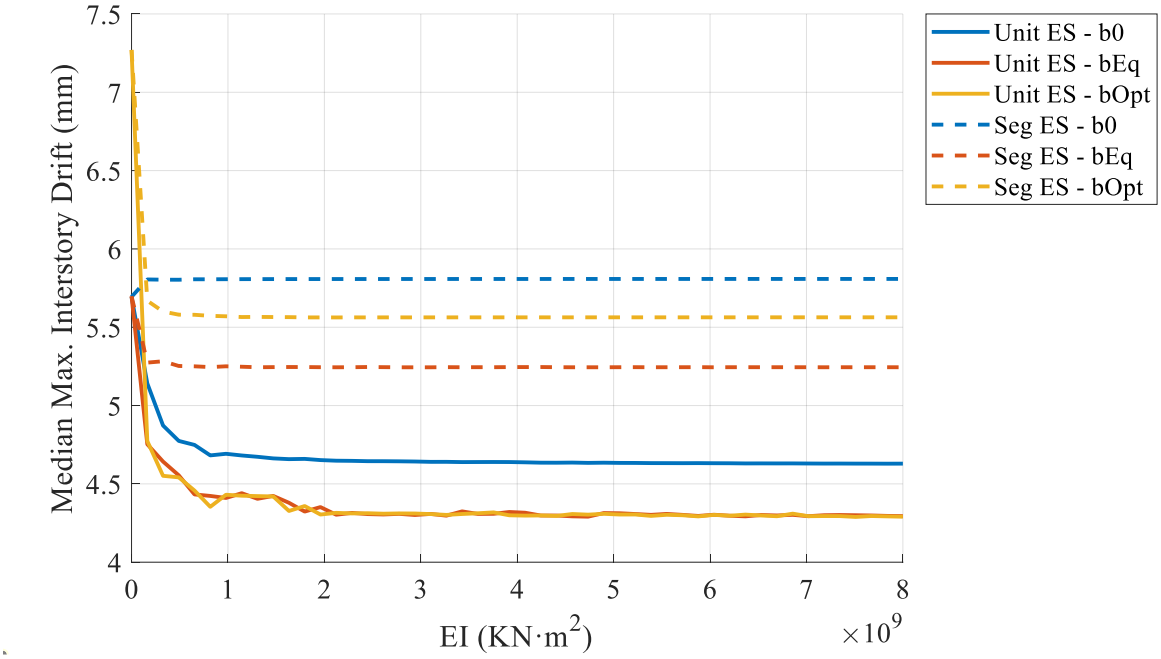


Figure 6-13: Median of maximum inter-story drift in mm for 5-story structure with unit and the segmental ES pinned at the second floor across a range of spine stiffness values (EI). Each point represents the median of suite of ground motions' maximum inter-story drift for a specific EI. Configurations include b0 (no inerter), bEq (equal distribution), and bOpt (optimized distribution) in both unit and segmental ES systems.

occurs at roughly about one-third of that spine stiffness value and further increases in EI offered little to no additional benefit in drift reduction.

It is important to note that the unit ES requires a higher flexural stiffness (EI) to reach a stiffness plateau because it spans the full height of the structure as a continuous element. In contrast, the segmental ES is interrupted by a pin connection, effectively reducing its active length. Since flexural stiffness is inversely related to the length of the element, the shorter segments in the segmental configuration become sufficiently stiff at lower EI values, leading to an earlier plateau in drift and it is true for following performance measures in this study.

6.2.4.1.2 When pin is at 3rd floor:

Include in **Figure 6-14** are the MMSD for the 5-story structure with a pin in the ES at the 3rd floor. **Figure 6-14** shows a similar trend as earlier results in **Figure 6-13**: the inclusion of ES systems reduces the median maximum story drift (MMSD), with the unit ES consistently outperforming the segmental configuration. However, contrasting these figures shows that the behavior of the segmental ES varies with pin location. When the pin is placed near the floor where the direction of the second mode shape naturally changes, like 2nd floor, it aligns more closely with the structure's vibration pattern. Since each segment can then achieve a nearly uniform drift distribution, the maximum story drift slightly increases as explained previously, and can be seen in the blue dashed line in **Figure 6-13**. In contrast, placing the pin farther from this transition point, such as at the 3rd floor, introduces more resistance to the structure's natural mode shape and reduces maximum story drift.

6.2.4.2 Moment Demand in Elastic Spine of 5-Story Structure

6.2.4.2.1 When pin is at 2nd floor:

Figure 6-15 shows median maximum moment (MMM) in the ES in the five-story structure with a segmental ES pinned at the second floor. The results indicate that the inclusion of distributed inerters effectively reduced MMM compared to the case without inerters. Interestingly, in the unit ES configuration, adding distributed inerters led to a noticeable increase in MMM, particularly at lower EI levels.

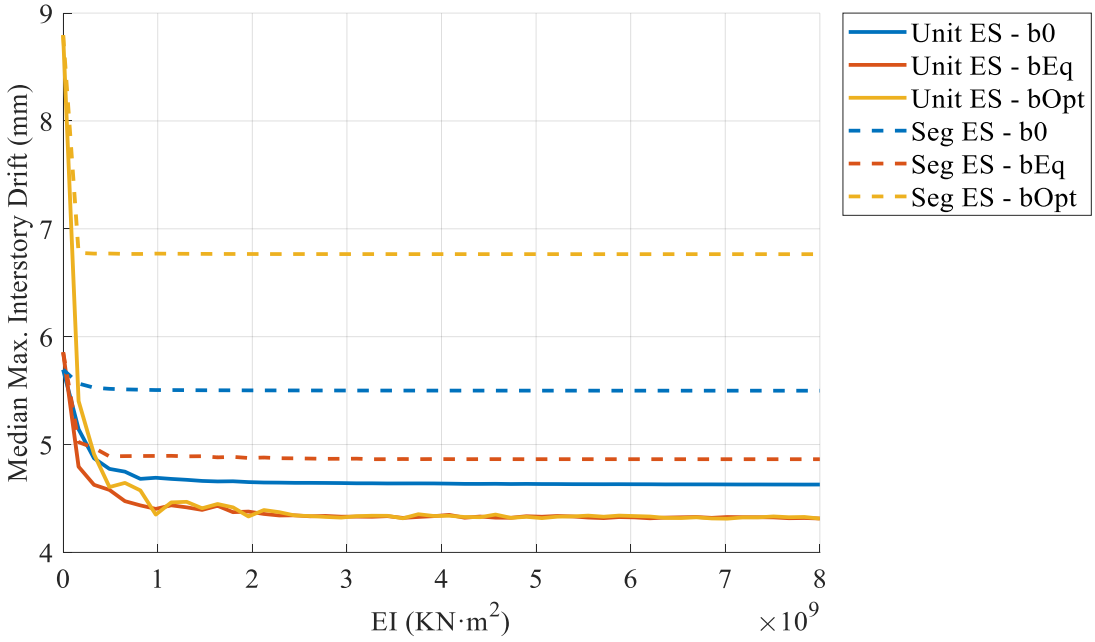


Figure 6-14: Median of maximum inter-story drift in mm for 5-story structure with unit and the segmental ES pinned at the third floor across a range of spine stiffness values (EI). Each point represents the median of suite of ground motions' maximum inter-story drift for a specific EI. Configurations include b0 (no inerter), bEq (equal distribution), and bOpt (optimized distribution) in both unit and segmental ES systems.

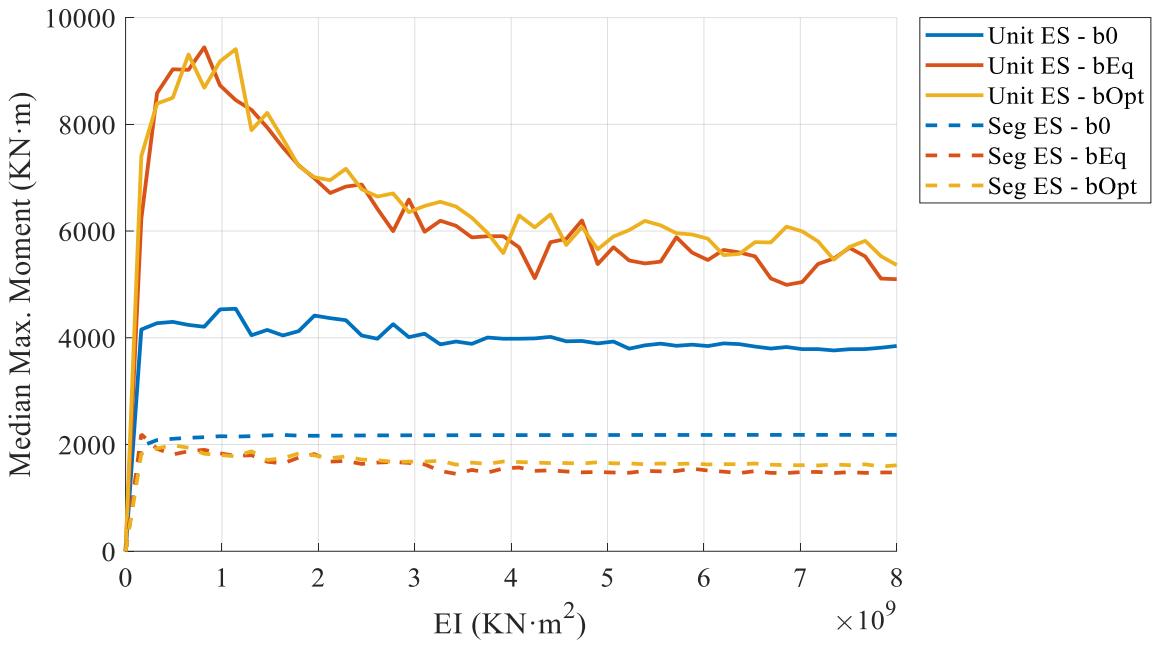


Figure 6-15: Median of maximum moment demand (KN.m) in the ES for 5-story structure with unit and the segmental ES pinned at the second floor across a range of spine stiffness values (EI). Each point represents the median of suite of ground motions' maximum moment for a specific spine stiffness. Configurations include b0 (no inerter), bEq (equal distribution), and bOpt (optimized distribution) in both unit and segmental ES systems.

Although MMM eventually decreased with a stiffer spine, it remained higher than in the no-inerter scenario. In contrast, within the segmental configuration, both equal and optimal inertance distributions performed similarly, and MMM remained relatively unchanged with increasing EI.

6.2.4.2.2 When pin is at 3rd floor:

When pin is located at the third floor, segmenting the ES proved beneficial by reducing MMM compared to the unit ES setup (**Figure 6-16**). MMM values in the unit ES and in the segmental configuration with b0 remained largely unaffected by increases in ES stiffness, suggesting limited sensitivity to EI. This insensitivity is even more evident in the segmental ES with inerters when the pin is located at the 2nd floor, compared to the 3rd floor pin case. However, the addition of distributed inerters initially increased the response, followed by a decrease that stabilized into a plateau once a stiffness threshold was exceeded. Notably, the addition of distributed inerters—whether equally or optimally distributed—consistently worsened MMM respect to b0 cases across all ES configurations, highlighting a potential tradeoff between moment control and the benefits of inerter-enhanced systems in this setup.

The difference in moment response with different pin locations can be attributed to how the ES interacts with the structure's dynamic behavior. When the pin is placed near the natural transition point of the second mode shape—as is the case with the second-floor pin—it better aligns with the structure's natural deformation patterns (**Figure 6-12**). This alignment reduces the fight between the mode shapes of the structure and the imposed constraints of the ES. In this condition, the inertial forces introduced by the distributed inerters are more effectively balanced across the spine. As a result, their net contribution to moment demand can partially cancel out, leading to a reduction in MMM, as observed in the second-floor pin case. However, if this cancellation does not occur, especially in cases where the segmentation misaligns with the structure's dynamic tendencies, then the inertial forces instead contribute to increased moment demands—an effect visible in the third-floor pin case in **Figure 6-16**. This behavior is also seen in the unit ES results. Although the optimization function was developed based on the segmental configuration, the same optimized inertance values were applied to the unit ES. When these values align with the natural dynamic behavior of the structure—such as when they are derived

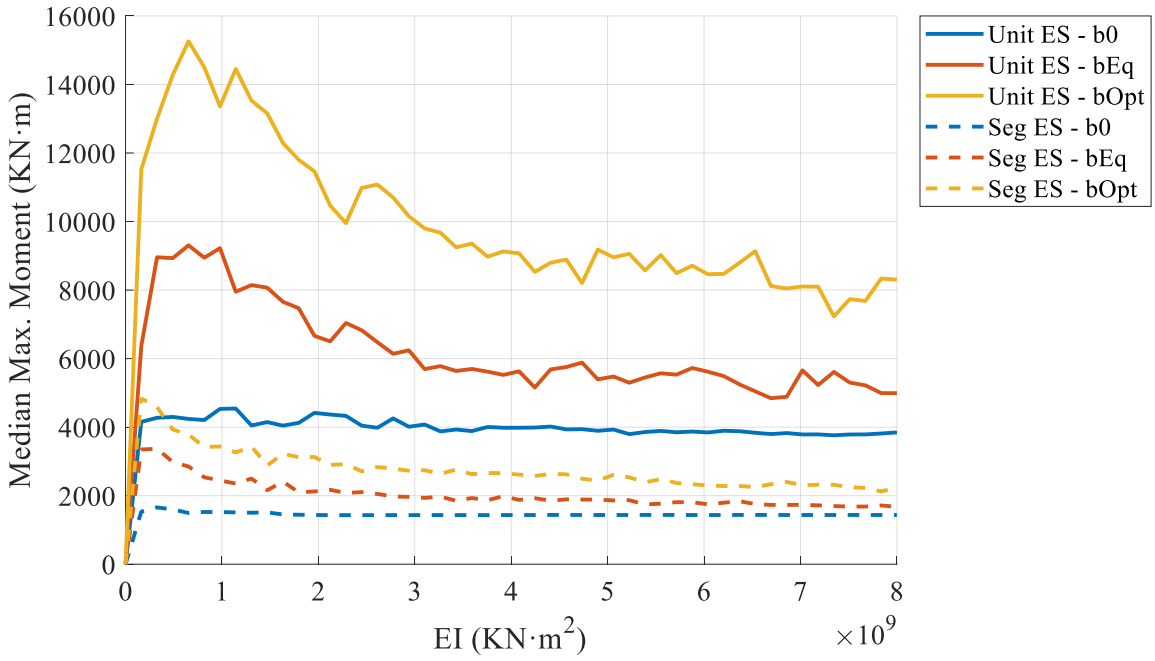


Figure 6-16: Median of maximum moment demand (KN.m) in the ES for 5-story structure with unit and the segmental ES pinned at the third floor across a range of spine stiffness values (EI). Each point represents the median of suite of ground motions' maximum moment for a specific spine stiffness. Configurations include b0 (no inerter), bEq (equal distribution), and bOpt (optimized distribution) in both unit and segmental ES systems.

from the second-floor pin configuration—the unit ES experiences less resistance against the natural mode shapes, resulting in lower moment demand. Conversely, using optimized values that are based on misaligned segmentation, such as those from the third-floor pin case, forces the structure away from its natural behavior and results in elevated moment demand in the spine.

6.2.4.3 Floor Acceleration in 5-Story Structure

6.2.4.3.1 When pin is at 2th floor:

Figure 6-17 shows median maximum floor acceleration (MMFA) in the five-story structure with the ES pinned at the second floor. Results indicate that both equal (bEq) and optimal (bOpt) inertance distributions significantly reduced MMFA in the absence of a ES system. This reduction in MMFA is thought to largely be due to the reduction in the frequencies of higher modes with inerters, as demonstrated in **Figure 6-11**. When a ES was introduced, MMFA generally increased; however, the effect varied by configuration. Notably, the unit ES cases reduced MMFA when the spine stiffness exceeded approximately 1×10^9 kN·m². Including distributed inerters slightly raised MMFA in both unit and segmental ES—by less than 8%—but the increase was smaller for the segmental configuration. With higher EI values, MMFA in the unit ES decreased and, with the inerters, eventually aligned with the segmental ES response. However, in the segmental ES system, adding and increasing EI showed no significant variation in MMFA. Within each ES type (unit or segmental), the trends were similar for both bEq and bOpt configurations.

6.2.4.3.2 When pin at 3rd floor:

In **Figure 6-18**, distributed inerters effectively reduced MMFA when no ES was present. However, the addition of ES systems led to increased MMFA in all configurations except for the unit ES with no inerter (b0), which initially caused a rise but then reduced MMFA when the spine stiffness exceeded approximately 2×10^9 kN·m². When distributed inerters were included, both bEq and bOpt configurations outperformed the no-inerter case across ES systems, showing similar results within each configuration. In the segmental ES, MMFA was less affected by increases in EI, indicating a more consistent acceleration response regardless of stiffness variation.

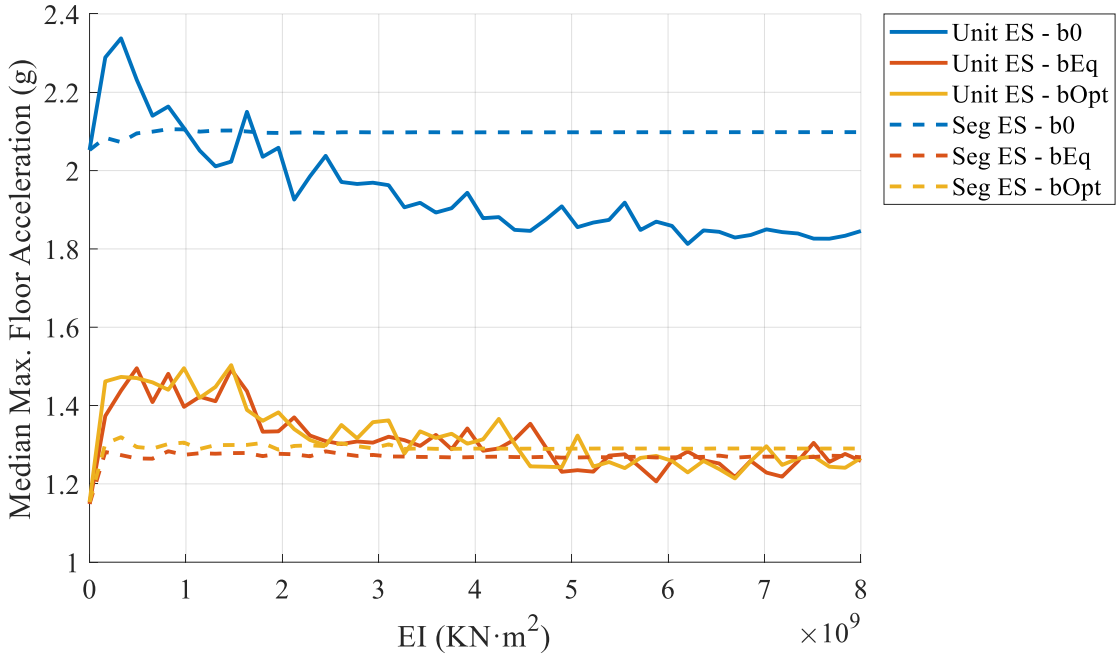


Figure 6-17: Median of maximum absolute floor acceleration (g) for the 5-story structure with unit and segmental ES pinned at the second floor, evaluated over a range of spine stiffness values (EI). Each point reflects the median of maximum floor accelerations recorded across a suite of ground motions for a given EI. Configurations include b0 (no inerter), bEq (equal distribution), and bOpt (optimized distribution) applied to both unit and segmental ES systems.

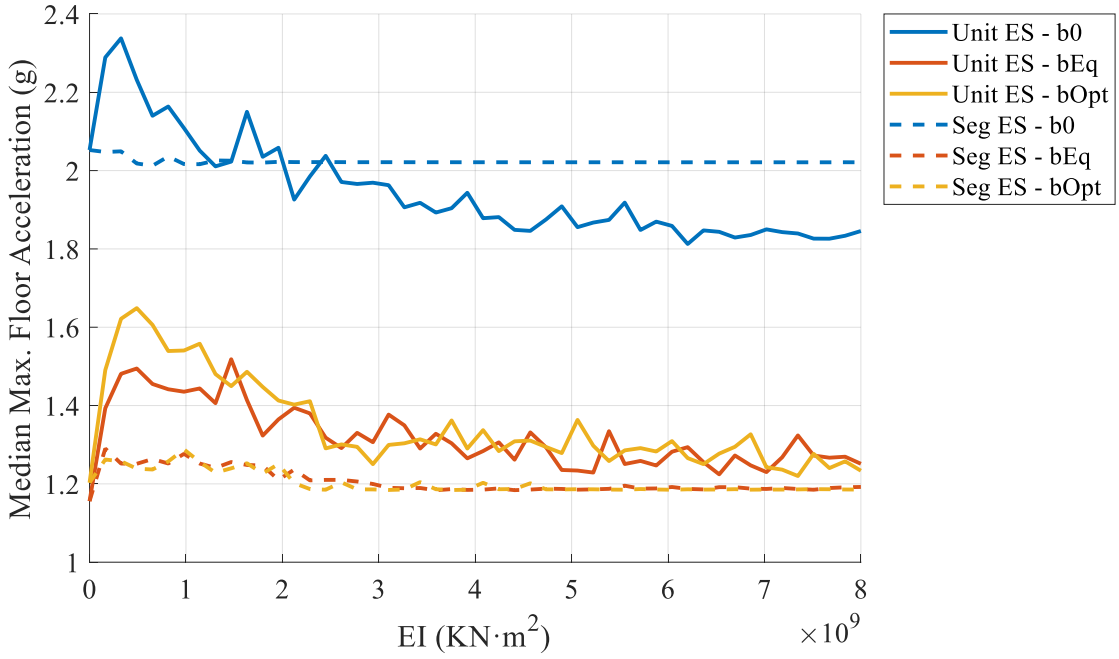


Figure 6-18: Median of maximum absolute floor acceleration (g) for the 5-story structure with unit and segmental ES pinned at the third floor, evaluated over a range of spine stiffness values (EI). Each point reflects the median of maximum floor accelerations recorded across a suite of ground motions for a given EI. Configurations include b0 (no inerter), bEq (equal distribution), and bOpt (optimized distribution) applied to both unit and segmental ES systems.

6.2.4.4 Measures Comparison Across All Structural Configurations

This section expands the discussion by presenting a broader comparison of the response measures across multiple structural types and configurations. It includes 4-story, 5-story, and 6-story structures with and without ES systems—both unit and segmental—paired with three inertance configurations: no inerter (b0), equal distribution (bEq), and optimized distribution (bOpt). Results are presented through plots of median maximum moment demand in the ES, as well as normalized median maximum story drift and floor acceleration. These plots facilitate direct comparison of overall trends, highlighting the relative effectiveness inerter distribution strategies across different building heights and ES configurations.

Figure 6-19 and **Figure 6-20** present the normalized median of the maximum floor acceleration and interstory drift, respectively, for each structural type and configuration, based on responses to a suite of ground motion records. Normalization is performed with respect to a baseline structure without a ES and with no inerters, allowing for a consistent comparison of relative performance improvements. In contrast, **Figure 6-21** reports the median of the maximum moment demand in the spine. Since moment only develops when a ES is present, normalization in the same way as the other measures is not applicable, and values are shown directly for each configuration. Details and observations from each figure are discussed in the following paragraphs.

The results in **Figure 6-19** indicate that the addition of a ES system, even without distributed inerters, consistently reduces the median maximum interstory drift across all structural types. In the absence of a ES, however, incorporating distributed inerters generally increases interstory drift—particularly when using an optimum non-equal inertance distribution—with the exception of the 4-story structure, where a modest reduction of approximately 10 percent is observed. When ES are combined with equally distributed inerters, the interstory drift is reduced most effectively compared to cases with optimum inertance values. This improvement is more pronounced in shorter structures, with the 4-story frame experiencing the most significant reduction. In contrast, the 6-story case benefit less from the same configurations, suggesting that drift reduction effectiveness decreases with building height.

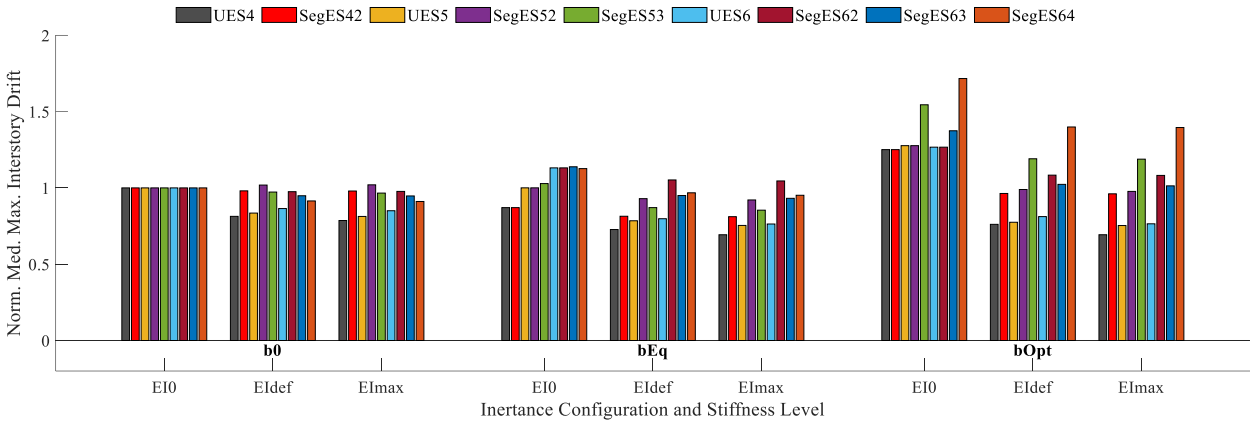


Figure 6-19: Normalized median of maximum interstory drift for various configurations with and without unit or segmental ES, considering different pin locations and distributed inerters in a 4-,5-, and 6-story structure. Values are normalized with respect to no ES and no distributed inerter. Each bar represents the median of maximum interstory drift responses across suite of ground motion records.

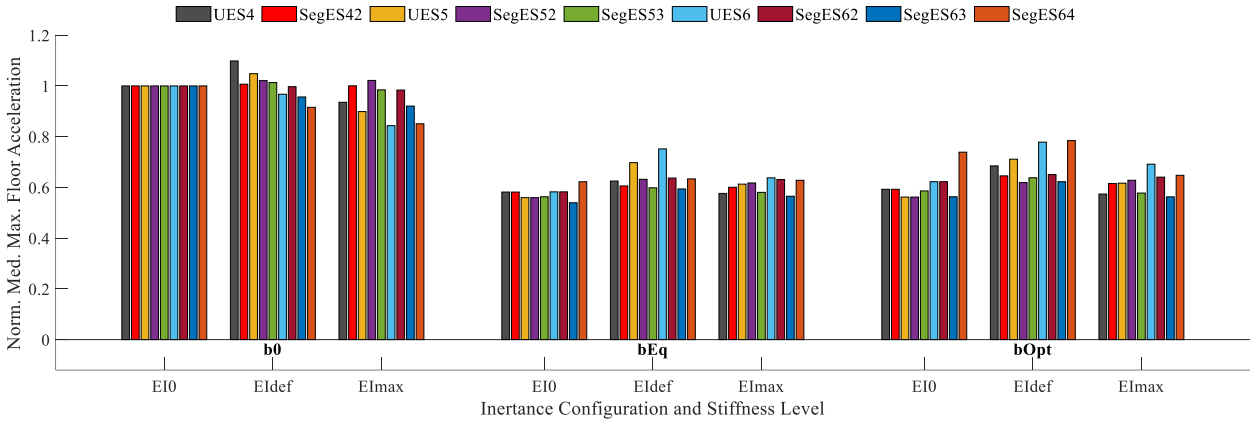


Figure 6-20: Normalized median of maximum absolute floor acceleration for various configurations with and without unit or segmental ES, considering different pin locations and distributed inerters in a 4-,5-, and 6-story structure. Values are normalized with respect to no ES and no distributed inerter. Each bar represents the median of maximum absolute floor acceleration responses across suite of ground motion records.

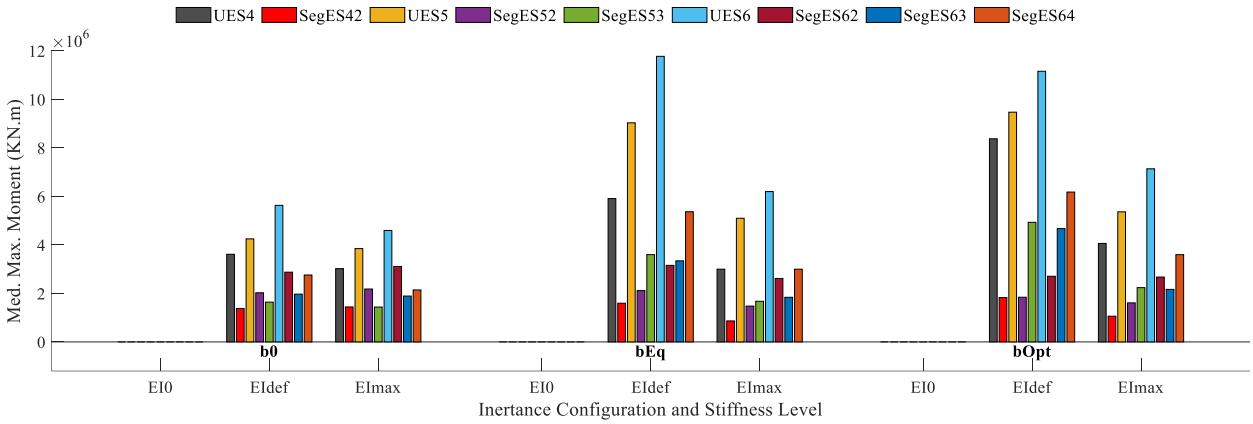


Figure 6-21: Median of the maximum moment demand (kN·m) in the spine for systems with and without unit or segmental ES, considering different pin locations and distributed inerter configurations in a 4-,5-, and 6-story structures. Each bar represents the median of the peak moment values across suite of ground motion records for a given structural configuration. Only configurations with a spine are shown, as moment is not generated without an ES.

Figure 6-20 indicates that incorporating a unit ES can initially lead to a moderate increase in the median maximum floor acceleration. However, as the spine becomes stiffer, this effect transitions into a reduction, reaching up to approximately 20%. In contrast, the segmental ES shows a more variable response depending on structural height: for shorter structures like the 4-story case, the addition of a segmental ES results in little to no change, while for taller structures such as the 6-story configuration, it leads to a reduction of up to 10%. This acceleration reduction becomes more pronounced as the segmental ES stiffness increases. Regardless of the ES type, introducing distributed inerters consistently yields a much more significant reduction—around 40%—in floor acceleration. This benefit appears largely unaffected by the ES configuration or the choice between equally distributed and optimally tuned inertance values, with only minimal and negligible differences observed between bEq and bOpt cases. However, a closer look at the segmental configurations, such as ES64 versus ES63, suggests that the pin location can influence floor acceleration trends.

Figure 6-21 presents the median maximum moment demands in the ES for each configuration. In unit ES systems, the inclusion of distributed inerters notably increases moment demands compared to the no-inerter cases. This increase is more moderate in segmental ES, where the pinned joint helps limit moment amplification. The relative performance of equally distributed (bEq) and optimally tuned (bOpt) inerter configurations varies depending on structural height

and ES configuration and the location of the pin in segmental ES systems. In some cases, such as SegES52, UES6, and SegES62, bOpt slightly outperformed bEq, while in others, bEq showed marginally better results. This variation also extends to their performance relative to the no-inerter (b0) case, suggesting that the effectiveness of distributed inerters in segmental configurations is highly dependent on both structural height and pin placement rather than the tuning strategy alone.

6.2.5 Conclusion

This study investigated the effectiveness of combining distributed inerters with both unit and segmental elastic spine (ES) systems to improve seismic performance in multi-story structures. The main objective was to explore how different configurations of inerter distributions and ES stiffness levels influence structural responses such as story drift, moment demands in the spine, and floor acceleration. A series of numerical analysis was conducted across various spine stiffness values and pin locations in 4-, 5-, and 6-story structures using ground motion records. The goal was to determine whether distributed inerters could enhance the performance of ES systems and whether their effects differed between unit and segmental implementations. Key findings of this study are as follow:

- Story Drift Reduction
    - ES systems without inerters already provided effective reduction in median maximum story drift (MMSD), particularly for unit configurations.
    - Equally distributed inerters (bEq) consistently outperformed optimally distributed ones (bOpt) in drift reduction, especially when paired with unit ES.
    - In segmental ES, distributed inerters were less effective; in some cases, the no-inerter (b0) configuration resulted in lower MMSD than bOpt.
    - Without ES, bOpt often increased drift, especially in taller structures.
    - Across all cases, MMSD values plateaued after reaching a certain stiffness threshold, indicating that further EI increases had minimal additional benefit.
- Moment Demands in the Elastic Spine

- Segmental ES generally resulted in lower median maximum moment (MMM) than unit configurations, particularly at low and moderate stiffness levels.
- Distributed inerters increased MMM most noticeably in unit ES, with the effect being more significant at lower EI values.
- In segmental configurations, the increase in MMM from distributed inerters was more moderate, and moment demands were largely unaffected by additional increases in EI beyond a certain threshold.
- The relative performance of bEq and bOpt in segmental configurations varied depending on structural height and pin location. In some cases, bOpt slightly outperformed bEq, while in others, bEq showed marginally better results. Their performance relative to the no-inerter case was also dependent on these parameters, suggesting that the effectiveness of distributed inerters in segmental systems is sensitive to both geometry and pin placement.
- Moment responses showed minimal sensitivity to increasing spine stiffness beyond a certain threshold in both segmental and unit ES systems, indicating that further increases in stiffness had limited impact on reducing moment demands.

- Floor Acceleration
  - Distributed inerters reduced median maximum floor acceleration by approximately 40% in most configurations, even in the absence of ES.
  - bEq and bOpt yielded nearly identical acceleration results in all configurations, making bEq a practical and simpler choice.
  - Adding ES alone had mixed effects on MMA: unit ES showed a reduction only after a specific stiffness threshold, indicating that unit ES was more sensitive to changes in EI, while segmental ES provided more stable and gradual improvements.

The findings underscore that integrating distributed inerters into ES systems can effectively reduce story drift and acceleration demands, with the best performance generally observed when inertance is equally distributed. However, distributed inerters lead to increased moment demands

in unit ES while they can either increase or decrease moment in segmental ES depending on the structural height and pin configuration. Segmental ES offer a more balanced solution by limiting moment amplification while still contributing to drift and acceleration mitigation.

Future research should expand to include a broader range of structural types, particularly taller buildings, to assess the scalability and applicability of ES–inerter systems in more complex configurations. As the performance of ES systems is inherently tied to mode shapes, the choice of optimization objective significantly influences their effectiveness. Different optimization goals—such as targeting uniform drift distribution, minimizing internal moments, or reducing accelerations—can alter the overall structural response. In addition, future work should explore more advanced optimization techniques, conduct nonlinear time-history analyses, and pursue experimental validation to bridge the gap between simulation-based insights and real-world applications. These steps are essential to refining ES–inerter systems and establishing practical design guidelines for enhanced seismic performance in mid- to high-rise structures.

Chapter 7 : CONCLUSION AND FUTURE WORKS

7.1 SUMMARY AND CONCLUSIONS

This dissertation investigated the behavior, effectiveness, and enhancement of strongback systems for improving the seismic performance of multi-story structures. Strongbacks have emerged as a promising strategy for mitigating soft-story mechanisms and promoting more uniform drift distributions by introducing vertical stiffness elements that influence lateral deformation patterns. Despite their potential, several aspects of strongback system behavior remain underexplored, particularly under different structural configurations and in combination with advanced control devices such as inerters.

To address these gaps, the research was structured around three main focus areas. Chapter 4 examined the effects of stiffness irregularity and damper arrangement on strongback behavior. Chapter 5 explored the role of a tunable joint in a segmental strongback system. Chapter 6 compared the dynamic performance of traditional strongbacks with systems that incorporate distributed inerters. Each chapter included detailed numerical or experimental analysis, and the findings contribute to a more comprehensive understanding of how strongback systems can be optimized for improved seismic resilience.

Chapter 4 experimentally investigated the influence of damper arrangement and the location of vertical stiffness irregularities—specifically soft-story conditions—on the seismic performance of structures with and without a strongback. The study was motivated by the practical challenge that many real-world buildings do not exhibit uniform stiffness along their height and that damper placement is often constrained by architectural or design limitations. Experimental testing was conducted on a small-scale four-story structure subjected to shake table ground motions, with different configurations of column stiffness and damper distributions. The structure was evaluated both with and without an attached elastic spine.

The results demonstrated that the inclusion of the strongback significantly enhanced structural performance, leading to more uniform drift distributions and reduced sensitivity to the location of stiffness irregularities. While the structure without the strongback exhibited large changes in natural frequency and drift concentration depending on the location of the irregularity, the strongback-stiffened system maintained a more stable first-mode frequency and more consistent drift behavior. Additionally, the strongback enabled flexibility in damper placement—similar

levels of performance were observed whether dampers were distributed across multiple stories or concentrated at a single level.

These findings highlight the strongback's capacity to mitigate the effects of vertical stiffness irregularities and improve structural consistency under a range of configurations. The results suggest that strongbacks offer new opportunities for seismic design, retrofit strategies, integration with concentrated energy dissipation devices, and potential control device contribution.

Chapter 5 explored the impact of joint behavior on the performance of segmented strongback systems, with a particular focus on how linear and nonlinear joint mechanisms influence dynamic response. The chapter combined experimental and numerical studies to evaluate whether tuning the joint—either through mechanical stiffness or inertial effects—can enhance drift control and overall structural performance.

The first study experimentally investigated the use of a nonlinear rotational inertial mechanism placed at the joint between two strongback segments. Various inertance configurations were tested using shaped white noise excitation at multiple amplitude levels. The results demonstrated that certain inertial configurations—particularly the Low to High Inertance case—significantly improved performance by reducing story drift, acceleration, and link force. Importantly, these benefits were achieved without compromising the segmented nature of the strongback, suggesting that rotational inertial devices can suppress or modify the second mode without making the spine behave like a unit spine.

The second study experimentally examined the effects of introducing linear rotational stiffness at the joint. Increased joint stiffness led to a consistent decrease in maximum story drift and an increase in link force demand. Although the first mode remained relatively unaffected, the second mode frequency shifted higher with increased stiffness. However, scatter in the data and variability in ground motion response limited the ability to draw firm conclusions. The findings suggested that the structural response was heavily influenced by the interaction between joint stiffness and ground motion characteristics.

To supplement the experimental findings, the third study involved a numerical investigation of linear joint stiffness. The analysis focused on evaluating interstory drift, moment demand, and

acceleration. These findings emphasize the trade-off between drift control and moment amplification. Results confirmed that increasing joint stiffness effectively reduced interstory drift but also substantially increased moment demand in the spine. Floor acceleration, however, remained relatively insensitive to joint stiffness. While modest performance improvements were observed at low stiffness levels, no clear optimal stiffness value was identified, as each level of stiffness exhibited trade-offs across different performance metrics.

Together, the studies in Chapter 5 demonstrate that modifying joint behavior can critically impact the performance of systems with segmented strongbacks. While linear stiffness alone offers limited tuning potential, nonlinear rotational inertial mechanisms show promise for achieving better control over dynamic response without sacrificing the benefits of segmentation.

Chapter 6 investigated the integration of distributed inerters with strongback systems through both experimental and numerical studies to better understand their combined seismic performance. The experimental component focused on a four-story structure equipped with an elastic spine and various inerter configurations, including both concentrated and distributed arrangements. The results demonstrated that while inerters alone can reduce maximum story drift, their effectiveness is inconsistent and highly configuration-dependent. However, when combined with an elastic spine, the system exhibited more stable and uniform drift patterns across stories, and the different inerter configurations—whether concentrated at a single floor or distributed—performed similarly well. These findings suggest that the inclusion of a spine can help overcome practical limitations associated with inerter deployment and may enable the use of tuned-inerter devices in concentrated forms, which are typically less feasible without such a supporting system.

The numerical portion extended the experimental investigation by systematically evaluating the effectiveness of distributed inerters in both unit and segmental elastic spine systems under a variety of configurations. Three main inerter arrangements were considered: (1) no inerter, (2) equally distributed inertance across all stories, and (3) optimized (non-uniform) inertance designed to achieve uniform drift in the first two vibration modes. These configurations were analyzed both with and without strongbacks, enabling a comprehensive comparison across structural systems. For structures with elastic spine, the analysis included a wide range of stiffness values for elastic spine and various pin locations to assess performance trends. The

results showed that distributed inerters—especially in the equally distributed configuration—were effective in reducing story drift, particularly in unit strongback systems. However, the integration of inerters also led to substantial increases in moment demand, especially in unit strongbacks, while segmental strongbacks helped limit this amplification. For floor acceleration, distributed inerters significantly reduced the maximum acceleration across most configurations. In cases where a strongback was also present, small increases in acceleration were observed, but these were modest and based on spine stiffness and more stable in segmental systems.

Overall, this dissertation contributes to the growing body of knowledge on strongback systems, both unit and segmental, by investigating their integration with damping devices and inertial mechanisms through both experimental and numerical approaches. Across all studies, the strongback concept demonstrated consistent benefits in promoting more uniform drift distributions and improving overall performance under seismic loading. However, the results also revealed important trade-offs. For example, while combining strongbacks with control devices like inerters increased moment demands, segmenting the strongback reduced those demands but led to higher interstory drifts. By exploring variations in strongback segmentation, joint properties, and control device configurations, this work has laid the foundation for a more nuanced understanding of how these systems potentially behave. The findings highlight the need for continued investigation into adaptive and tunable strongback solutions, advanced optimization strategies, and practical design methodologies that account for complex structural behaviors. Together, these efforts can help unlock the full potential of strongback systems as a resilient and versatile seismic design approach for mid- to high-rise buildings.

7.2 FUTURE WORKS

This dissertation lays the groundwork for further investigations of strongback-based seismic control systems. Several potential directions remain open for future research.

- Numerically expand upon the variable inertance concept explored in chapter 5, using a nonlinear rotational mechanism at the joint of segmental strongback. While the experimental study demonstrated that inertance could vary with joint rotation through a custom-designed nonlinear lead screw, the scope was limited by the physical device range and the use of only

white noise excitation. Future numerical investigations could idealize and extend this concept by evaluating how broader or more precisely controlled variable inertance profiles affect system behavior under diverse seismic records. For instance, lower inertance at small joint rotations could preserve segmented behavior, while higher inertance at larger rotations could enhance energy dissipation and limit drift. Such studies could also assess whether adaptive inertance mechanisms are more effective at disrupting second-mode resonance compared to fixed inertance or linear joint stiffness designs. Numerical modeling would allow for a deeper understanding of these devices without the constraints of prototype fabrication and inertance range and excitation limitations.

- Building on the findings of Chapter 6, future research could explore the use of variable inertance inerters in both unit and segmental strongback systems through numerical and experimental analyses. In unit strongback configurations, variable inertance devices may provide the ability to dynamically shift the fundamental frequency and mitigate resonance formation during strong shaking. Also, they can be able to modify mode shapes to help reducing the high moment demand induced in the spine. Similarly, distributing variable inertance devices across the height of a structure—or concentrating them at specific floors—could be evaluated to identify configurations that offer optimal reductions in drift and acceleration, while minimizing moment amplification in the spine. Such adaptive systems may be particularly beneficial for structures experiencing shifts in modal behavior during nonlinear response.

- Another future suggestion based on Chapter 6 is investigating whether strongback systems can enable more effective integration of tuned vibration mitigation devices (TVMDs) or other tuned inerter-based systems. A central question is whether these devices—typically distributed across several floors—could be concentrated at a single level when used in conjunction with a strongback. Because strongbacks promote linear behavior and shape mode responses, they could create conditions under which a TVMD performs optimally: namely, acting on a predictable, low-drift, and mostly linear system.

- Building on Chapter 6, the second (numerical) study could be experimentally validated by investigating segmental strongback–inerter systems at larger scales. Such experiments would

help confirm the trends observed in the numerical analysis and assess the practicality of the suggested configurations, paving the way for real-world implementation.

- All structural models in this dissertation—both experimental and numerical—were developed under the assumption of elastic, linear behavior. Future work should explore the influence of nonlinear structural response, especially under strong ground motions that may induce yielding or damage. Additionally, incorporating parameters such as soil–structure interaction would provide a more comprehensive understanding of the system's performance and real-world applicability.

Extending this research to taller and irregular structures, using systems with more than two segments in the segmental strongback, as well as exploring alternative control and energy dissipation devices, will enhance understanding of the scalability and broader applicability of strongback–based systems. These efforts are essential for translating the conceptual advantages demonstrated in this work into practical, implementable strategies for advancing seismic resilience in modern structural engineering.

REFERENCES

Abolghasemi, S., Sarkar, A., Manson, C., Wierschem, N., Denavit, M., 2024a. EXPERIMENTAL STUDY ON THE IMPACT OF AN ELASTIC SPINE IN A STRUCTURE WITH INERTER-BASED DEVICES. 18th World Conference on Earthquake Engineering, Milan, Italy.

Abolghasemi, S., Wierschem, N.E., Denavit, M.D., 2024b. Impact of strongback on structure with varying damper and stiffness irregularity arrangements. Journal of Constructional Steel Research 213, 108333. https://doi.org/10.1016/j.jcsr.2023.108333

ACI, 2011. ACI Committee 318: Building Code Requirements for Reinforced Concrete. American Concrete Institute, Farmington Hills, Michigan.

AISC, 2018. Seismic Design Manual. American Institute of Steel Construction.

Alavi, B., Krawinkler, H., 2004. Strengthening of moment-resisting frame structures against near-fault ground motion effects. Earthquake Engineering & Structural Dynamics 33, 707–722. https://doi.org/10.1002/eqe.370

Alemdar, F., Al-Gaadi, F.M.A., 2022. Experimental Study of Earthquake Simulator for 3D Cold-Formed Steel Frame Structure. Lat. Am. j. solids struct. 19, e426. https://doi.org/10.1590/1679-78256812

Ancheta, T.D., Darragh, R.B., Stewart, J.P., Seyhan, E., Silva, W.J., Chiou, B.S.-J., Wooddell, K.E., Graves, R.W., Kottke, A.R., Boore, D.M., Kishida, T., Donahue, J.L., 2014. NGA-West2 Database. Earthquake Spectra 30, 989–1005. https://doi.org/10.1193/070913EQS197M

Balazadeh-Minouei, Y., Tremblay, R., Koboevic, S., 2018. Seismic Retrofit of an Existing 10-Story Chevron-Braced Steel-Frame. Journal of Structural Engineering 144, 04018180. https://doi.org/10.1061/(ASCE)ST.1943-541X.0002180

Barley, G., Wierschem, N., Denavit, M., Abolghasemi, S., 2024. Design and Static Testing of Elastic Spine Joints.

Beck, J.L., Skinner, R.I., 1973. The seismic response of a reinforced concrete bridge pier designed to step. Earthquake Engineering & Structural Dynamics 2, 343–358. https://doi.org/10.1002/eqe.4290020405

Beeby, S.P., Tudor, M.J., White, N.M., 2006. Energy harvesting vibration sources for microsystems applications. Meas. Sci. Technol. 17, R175. https://doi.org/10.1088/0957-0233/17/12/R01

Charney, F.A., Heausler, T.F., Marshall, J.D., 2020. Seismic Loads: Guide to the Seismic Load Provisions of ASCE 7-16. ASCE Press.

Chen, C.H., Tsai, I.J., Tang, Y., 2017. Drift Concentration of a Three-Story Special Concentrically Braced Frame with Strongback under Earthquake Loading. AMM 863, 287–292. https://doi.org/10.4028/www.scientific.net/AMM.863.287

Chen, L., Tremblay, R., Tirca, L., 2019a. Practical seismic design procedure for steel braced frames with segmental elastic spines. Journal of Constructional Steel Research 153, 395–415. https://doi.org/10.1016/j.jcsr.2018.10.010

Chen, L., Tremblay, R., Tirca, L., 2019b. Modular tied eccentrically braced frames for improved seismic response of tall buildings. Journal of Constructional Steel Research 155, 370–384. https://doi.org/10.1016/j.jcsr.2019.01.005

Chen, L., Tremblay, R., Tirca, L., 2012. Seismic Performance of Modular Braced Frames for Multi-Storey Building Applications, in: Proc., 15th World Conf. on Earthquake Engineering. Lisbon, Portugal: Sociedade Portuguesa de Engenharia Sismica. Presented at the 15th World Conf. on Earthquake Engineering.

Chen, X., Tagawa, H., 2023. Seismic performance of rocking-delayed spine frame system with base initial gaps. Earthquake Engineering and Resilience 2, 131–157. https://doi.org/10.1002/eer2.39

Chen, X., Tagawa, H., Mateus, J.A.S., 2022. Seismic performance of steel frame structure adopting parallel spine frames with elastic braces. Engineering Structures 267, 114640. https://doi.org/10.1016/j.engstruct.2022.114640

Chen, X., Takeuchi, T., Matsui, R., 2018. Seismic Performance and Evaluation of Controlled Spine Frames Applied in High-rise Buildings. Earthquake Spectra 34, 1431–1458. https://doi.org/10.1193/080817EQS157M

Deierlein, G., Krawinkler, H., Ma, X., Eatherton, M., Hajjar, J., Takeuchi, T., Kasai, K., Midorikawa, M., 2011. Earthquake resilient steel braced frames with controlled rocking and energy dissipating fuses. Steel Construction 4, 171–175. https://doi.org/10.1002/stco.201110023

Di Egidio, A., Pagliaro, S., Fabrizio, C., 2021a. Combined Use of Rocking Walls and Inerters to Improve the Seismic Response of Frame Structures. Journal of Engineering Mechanics 147, 04021016. https://doi.org/10.1061/(ASCE)EM.1943-7889.0001920

Di Egidio, A., Pagliaro, S., Fabrizio, C., 2021b. Combined Use of Rocking Walls and Inerters to Improve the Seismic Response of Frame Structures. J. Eng. Mech. 147, 04021016. https://doi.org/10.1061/(ASCE)EM.1943-7889.0001920

Djojo, G.S., Clifton, G.C., Henry, R.S., 2014. Rocking steel shear walls with energy dissipation devices. Presented at the 2014 NZSEE Annual Conference.

Eatherton, M., Hajjar, J.F., Deierlein, G.G., Ma, X., Billington, S., Krawinkler, H., 2012. Steel-Framed Rocking Structural Systems for Moderate Seismic Zones 1–9. https://doi.org/10.1061/41031(341)88

Eatherton, M.R., Ma, X., Krawinkler, H., Mar, D., Billington, S., Hajjar, J.F., Deierlein, G.G., 2014. Design Concepts for Controlled Rocking of Self-Centering Steel-Braced Frames. Journal of Structural Engineering 140, 04014082. https://doi.org/10.1061/(ASCE)ST.1943-541X.0001047

Fahnestock, L., Sause, R., Ricles, J., Simpson, B., Kurata, M., Okazaki, T., Kawamata, Y., Tao, Z., Duke, J., Rivera, D., Astudillo, B., Qie, Y., 2021. U.S.-JAPAN COLLABORATION FOR SHAKE TABLE TESTING OF A FRAME-SPINE SYSTEM WITH FORCE-LIMITING CONNECTIONS, in: 17th World Conference on Earthquake Engineering, 17WCEE. Presented at the 17th World Conference on Earthquake Engineering, 17WCEE, Sendai, Japan - September 27th to October 2nd, 2021.

Faraj, R., Jankowski, Ł., Graczykowski, C., Holnicki-Szulc, J., 2019. Can the inerter be a successful shock-absorber? The case of a ball-screw inerter with a variable thread lead. Journal of the Franklin Institute, Special Issue on Inerter-based Systems 356, 7855–7872. https://doi.org/10.1016/j.jfranklin.2019.04.012

Faramarzi, M.S., Taghikhany, T., 2021. A comparative performance-based seismic assessment of strongback steel braced frames. Journal of Building Engineering 44, 102983. https://doi.org/10.1016/j.jobe.2021.102983

FEMA P695, 2009. Federal Emergency Management Agency (FEMA) Recommended Methodology for Quantification of Building System Performance and Response Parameters. Project ATC-63, Prepared by the Applied Technology Council, Redwood City.

Giaralis, A., Petrini, F., 2017a. Wind-Induced Vibration Mitigation in Tall Buildings Using the Tuned Mass-Damper-Inerter. Journal of Structural Engineering 143, 04017127. https://doi.org/10.1061/(ASCE)ST.1943-541X.0001863

Giaralis, A., Petrini, F., 2017b. Wind-Induced Vibration Mitigation in Tall Buildings Using the Tuned Mass-Damper-Inerter. J. Struct. Eng. 143, 04017127. https://doi.org/10.1061/(ASCE)ST.1943-541X.0001863

GUYAN, R.J., 1965. Reduction of stiffness and mass matrices. AIAA Journal 3, 380–380. https://doi.org/10.2514/3.2874

Hu, S., Wang, W., Qu, B., 2021. Self-centering companion spines with friction spring dampers: Validation test and direct displacement-based design. Engineering Structures 238, 112191. https://doi.org/10.1016/j.engstruct.2021.112191

Hwang, J.-S., Kim, J., Kim, Y.-M., 2007a. Rotational inertia dampers with toggle bracing for vibration control of a building structure. Engineering Structures 29, 1201–1208. https://doi.org/10.1016/j.engstruct.2006.08.005

Hwang, J.-S., Kim, J., Kim, Y.-M., 2007b. Rotational inertia dampers with toggle bracing for vibration control of a building structure. Engineering Structures 29, 1201–1208. https://doi.org/10.1016/j.engstruct.2006.08.005

Javidialesaadi, A., Wierschem, N.E., 2019a. Energy transfer and passive control of single-degree-of-freedom structures using a one-directional rotational inertia viscous damper. Engineering Structures 196, 109339. https://doi.org/10.1016/j.engstruct.2019.109339

Javidialesaadi, A., Wierschem, N.E., 2019b. Energy transfer and passive control of single-degree-of-freedom structures using a one-directional rotational inertia viscous damper. Engineering Structures 196, 109339. https://doi.org/10.1016/j.engstruct.2019.109339

Jiang, J., Matamoros-Sanchez, A., Zolotash, A., Goodall, R., Smith, M., 2013. Passive suspensions for ride quality improvement of two-axle railway vehicles. Proceedings of the Institution of Mechanical Engineers, Part F: Journal of Rail and Rapid Transit. 229(3):315-329. doi:10.1177/0954409713511592.

Kelly, J.M., Tsztoo, D.F., 1977. Earthquake simulation testing of a stepping frame with energy-absorbing devices. Bulletin of the New Zealand Society for Earthquake Engineering 10, 196–207. https://doi.org/10.5459/bnzsee.10.4.196-207

Kramer, S.L., Stewart, J.P., 2024. Geotechnical Earthquake Engineering, 2nd ed. CRC Press, Boca Raton. https://doi.org/10.1201/9781003512011

Kushwaha, P., Ghoshal, S.K., Dasgupta, K., 2020. Dynamic analysis of a hydraulic motor drive with variable inertia flywheel. Proceedings of the Institution of Mechanical Engineers, Part I: Journal of Systems and Control Engineering 234, 734–747. https://doi.org/10.1177/0959651819875914

Lai, J.-W., Mahin, S.A., 2015. Strongback System: A Way to Reduce Damage Concentration in Steel-Braced Frames. Journal of Structural Engineering 141, 04014223. https://doi.org/10.1061/(ASCE)ST.1943-541X.0001198

Li, C.S., Lam, S.S., Zhang, M.Z., Wong, Y.L., 2006. Shaking Table Test of a 1:20 Scale High-Rise Building with a Transfer Plate System. Journal of Structural Engineering 132, 1732–1744. https://doi.org/10.1061/(ASCE)0733-9445(2006)132:11(1732)

Lifsey, P., Drake, C., Wierschem, N., Abolghasemi, S., Denavit, M., 2023. Structural Design Drawings. https://doi.org/10.17603/ds2-r5wm-6b46

Lignos, D., 2008. Sidesway collapse of deteriorating structural systems under seismic excitations (Ph.D.). Stanford University, United States -- California.

Lin, J.-L., Kek, M.-K., Tsai, K.-C., 2019. Stiffness configuration of strongbacks to mitigate inter-story drift concentration in buildings. Engineering Structures 199, 109615. https://doi.org/10.1016/j.engstruct.2019.109615

Lu, X., Chen, Y., Mao, Y., 2012. Shaking table model test and numerical analysis of a supertall building with high-level transfer storey. https://doi.org/10.1002/tal.632

Lu, X., Zhou, Y., Yan, F., 2008. Shaking Table Test and Numerical Analysis of RC Frames with Viscous Wall Dampers. Journal of Structural Engineering 134, 64–76. https://doi.org/10.1061/(ASCE)0733-9445(2008)134:1(64)

Ma, R., Bi, K., Hao, H., 2021a. Inerter-based structural vibration control: A state-of-the-art review. Engineering Structures 243, 112655. https://doi.org/10.1016/j.engstruct.2021.112655

Ma, R., Bi, K., Hao, H., 2021b. Inerter-based structural vibration control: A state-of-the-art review. Engineering Structures 243, 112655. https://doi.org/10.1016/j.engstruct.2021.112655

Ma, X., Krawinkler, H., Deierlein, G.G., 2013. Seismic Design and Behavior of Self-Centering Braced Frame with Controlled Rocking and Energy Dissipating Fuses, John A. Blume Earthquake Engineering Center, Technical Report 174.

MacRae, G.A., Kimura, Y., Roeder, C., 2004. Effect of Column Stiffness on Braced Frame Seismic Behavior. Journal of Structural Engineering 130, 381–391. https://doi.org/10.1061/(ASCE)0733-9445(2004)130:3(381)

Mahato, A.C., Ghoshal, S.K., Samantaray, A.K., 2019. Influence of variable inertia flywheel and soft switching on a power hydraulic system. SN Appl. Sci. 1, 605. https://doi.org/10.1007/s42452-019-0623-0

Mahin, S.A., Bertero, V.V., Chopra, A.K., Collins, R.G., 1976. RESPONSE OF THE OLIVE VIEW HOSPITAL MAIN BUILDING DURING THE SAN FERNANDO EARTHQUAKE (No. EERC-76-22). National Science Foundation, Washington, D.C.

Maree, A., Nielsen, T., Dangol, S., Parks, J., Sanders, D., Ibarra, L., Pantelides, C., 2015. Shaking Table Experiments of Dry Storage Casks.

Martin, A., Deierlein, G.G., 2021. Generalized modified modal superposition procedure for seismic design of rocking and pivoting steel spine systems. Journal of Constructional Steel Research 183, 106745. https://doi.org/10.1016/j.jcsr.2021.106745

Mashhadiali, N., Saadati, S., Mohajerani, S.A.M., Ebadi, P., 2021. Hybrid braced frame with buckling-restrained and strong braces to mitigate soft story. Journal of Constructional Steel Research 181, 106610. https://doi.org/10.1016/j.jcsr.2021.106610

Montuori, R., Nastri, E., Piluso, V., 2022. Theory of plastic mechanism control: A new approach for the optimization of seismic resistant steel frames. Earthquake Engineering & Structural Dynamics 51, 3598–3619. https://doi.org/10.1002/eqe.3737

Moraes, F. de H., Silveira, M., Gonçalves, P.J.P., 2018. On the dynamics of a vibration isolator with geometrically nonlinear inerter. Nonlinear Dyn 93, 1325–1340. https://doi.org/10.1007/s11071-018-4262-6

Nakamura, Y., Fukukita, A., Tamura, K., Yamazaki, I., Matsuoka, T., Hiramoto, K., Sunakoda, K., 2014a. Seismic response control using electromagnetic inertial mass dampers. Earthquake Engineering & Structural Dynamics 43, 507–527. https://doi.org/10.1002/eqe.2355

Nakamura, Y., Fukukita, A., Tamura, K., Yamazaki, I., Matsuoka, T., Hiramoto, K., Sunakoda, K., 2014b. Seismic response control using electromagnetic inertial mass dampers: Seismic response control using EIMD. Earthquake Engng Struct. Dyn. 43, 507–527. https://doi.org/10.1002/eqe.2355

Palermo, M., Laghi, V., Gasparini, G., Silvestri, S., Trombetti, T., 2021a. Seismic Design and Performances of Frame Structures Connected to a Strongback System and Equipped with

Different Configurations of Supplemental Viscous Dampers. Frontiers in Built Environment 7.

Palermo, M., Laghi, V., Gasparini, G., Silvestri, S., Trombetti, T., 2021b. Seismic Design and Performances of Frame Structures Connected to a Strongback System and Equipped with Different Configurations of Supplemental Viscous Dampers. Frontiers in Built Environment 7. https://doi.org/10.3389/fbuil.2021.748087

Panian, L., Bucci, N., Janhunen, B., 2015. BRBM Frames: An Improved Approach to Seismic-Resistant Design Using Buckling-Restrained Braces 632–643. https://doi.org/10.1061/9780784479728.052

Qu, Z., Wada, A., Motoyui, S., Sakata, H., Kishiki, S., 2012. Pin-supported walls for enhancing the seismic performance of building structures. Earthquake Engineering & Structural Dynamics 41, 2075–2091. https://doi.org/10.1002/eqe.2175

Roke, D., Sause, R., Ricles, J., Gonner, N., 2008. Design Concepts for Damage-Free Seismic-Resistant Self-Centering Steel Concentrically-Braced Frames. https://doi.org/10.1201/9780203861592.ch1

Sabelli, R., 2001. Research on improving the design and analysis of earthquake-resistant steel braced frames.

Sarkar, A.T., Wierschem, N.E., 2024a. Dynamic analysis and response attenuation of a two-degree-of-freedom structure with a variable inertia rotational mechanism subjected to ground excitation. Engineering Structures 316, 118586. https://doi.org/10.1016/j.engstruct.2024.118586

Sarkar, A.T., Wierschem, N.E., 2024b. Dynamic analysis and response attenuation of a two-degree-of-freedom structure with a variable inertia rotational mechanism subjected to ground excitation. Engineering Structures 316, 118586. https://doi.org/10.1016/j.engstruct.2024.118586

Shokrgozar-Yatimdar, E., Yaghmaei-Sabegh, S., Shoaeifar, P., Chen, P., 2024. Smoothing-Based Aftershock Probabilistic Seismic Hazard Assessment Using the Spatiotemporal ETAS

Model. Bulletin of the Seismological Society of America 115, 349–365. https://doi.org/10.1785/0120240172

Siami, A., Karimi, H.R., Cigada, A., Zappa, E., Sabbioni, E., 2018. Parameter optimization of an inerter-based isolator for passive vibration control of Michelangelo's Rondanini Pietà. Mechanical Systems and Signal Processing 98, 667–683. https://doi.org/10.1016/j.ymssp.2017.05.030

Siar Mahmood Shah, A., Moradi, S., 2020. Cyclic response sensitivity of energy dissipating steel plate fuses. Structures 23, 799–811. https://doi.org/10.1016/j.istruc.2019.12.026

Simpson, B., Mahin, S., 2017. ANALYTICAL INVESTIGATION OF OFFSET GEOMETRIES IN STEEL STRONGBACK BRACED FRAMES, in: Eleventh U.S. National Conference on Earthquake Engineering. Presented at the Eleventh U.S. National Conference on Earthquake Engineering, Los Angeles, California, June 25-29, 2018.

Simpson, B.G., Mahin, S.A., 2018. Experimental and Numerical Investigation of Strongback Braced Frame System to Mitigate Weak Story Behavior. Journal of Structural Engineering 144, 04017211. https://doi.org/10.1061/(ASCE)ST.1943-541X.0001960

Simpson, B.G., Rivera Torres, D., 2021. Simplified Modal Pushover Analysis to Estimate First- and Higher-Mode Force Demands for Design of Strongback-Braced Frames. Journal of Structural Engineering 147, 04021196. https://doi.org/10.1061/(ASCE)ST.1943-541X.0003163

Slovenec, D., Sarebanha, A., Pollino, M., Mosqueda, G., Qu, B., 2017. Hybrid Testing of the Stiff Rocking Core Seismic Rehabilitation Technique. Journal of Structural Engineering 143, 04017083. https://doi.org/10.1061/(ASCE)ST.1943-541X.0001814

Smith, M.C., 2012. Force-Controlling Hydraulic Device. US 2021/0199428 A1.

Smith, M.C., 2002a. Synthesis of mechanical networks: the inerter. IEEE Transactions on Automatic Control 47, 1648–1662. https://doi.org/10.1109/TAC.2002.803532

Smith, M.C., 2002b. Synthesis of mechanical networks: the inerter. IEEE Trans. Automat. Contr. 47, 1648–1662. https://doi.org/10.1109/TAC.2002.803532

Smith, M.C., Houghton, N.E., Long, P.J.G., Glover, A.R., 2012. Force-Controlling Hydraulic Device. US20120199428A1.

Sugimura, Y., Goto, W., Saito, K., Nimomiya, T., Tanizawa, H., 2012a. Sugimura, Y., Goto, W., Tanizawa, H., Saito, K. and Nimomiya, T., 2012, September. Response control effect of steel building structure using tuned viscous mass damper. In Proceedings of the 15th world conference on earthquake engineering (Vol. 9, pp. 24-28). pp. 24–28.

Sugimura, Y., Goto, W., Tanizawa, H., Saito, K., Ninomiya, T., Nagasaku, T., 2012b. Response Control Effect of Steel Building Structure Using Tuned Viscous Mass Damper, in: Proceedings of the 15th World Conference on Earthquake Engineering. Presented at the 15WCEE, p. (Vol. 9, pp. 24-28).

Swain, S.S., Patro, S.K., 2015. Seismic Protection of Soft Storey Buildings Using Energy Dissipation Device, in: Matsagar, V. (Ed.), Advances in Structural Engineering. Springer India, New Delhi, pp. 1311–1338. https://doi.org/10.1007/978-81-322-2193-7_102

Swift, S.J., Smith, M.C., Glover, A.R., Papageorgiou, C., Gartner, B., Houghton, N.E., 2013a. Design and modelling of a fluid inerter. International Journal of Control 86, 2035–2051. https://doi.org/10.1080/00207179.2013.842263

Swift, S.J., Smith, M.C., Glover, A.R., Papageorgiou, C., Gartner, B., Houghton, N.E., 2013b. Design and modelling of a fluid inerter. International Journal of Control 86, 2035–2051. https://doi.org/10.1080/00207179.2013.842263

Takeuchi, T., Chen, X., Matsui, R., 2015. Seismic performance of controlled spine frames with energy-dissipating members. Journal of Constructional Steel Research 114, 51–65. https://doi.org/10.1016/j.jcsr.2015.07.002

Talley, P.C., Denavit, M.D., Wierschem, N.E., 2024. Evaluation of Methods of Design for Strongback Braced Frames. Journal of Structural Engineering 150, 04024160. https://doi.org/10.1061/JSENDH.STENG-13403

Teh, A.B.K., Venkatratnam, C., 2015. Design and development of a seismic shaking table for evaluation and analysis of the performance of elastomeric bearing, in: 2015 IEEE Student Conference on Research and Development (SCOReD). Presented at the 2015 IEEE

Student Conference on Research and Development (SCOReD), pp. 111–116. https://doi.org/10.1109/SCORED.2015.7449306

The MathWorks Inc, 2020a. MATLAB version: 9.9 (R2020b).

The MathWorks Inc, 2020b. System Identification Toolbox version: 9.13 (R2020b).

Tremblay, R., Chen, L., Tirca, L., 2014. Enhancing the Seismic Performance of Multi-storey Buildings with a Modular Tied Braced Frame System with Added Energy Dissipating Devices. International journal of High-Rise Buildings 3, 21–33.

Tremblay, R., Poirier, L.-P., Bouaanani, N., Leclerc, M., Rene, V., Fronteddu, L., Rivest, S., 2008. Innovative viscously damped rocking braced steel frames.

Wang, F., Hong, M., Chen, C., 2010. Building suspensions with inerters. Part C: Journal of Mechanical Engineering Science, 224(8), pp.1605-1616.

Wang, X., Qu, Z., Gong, T., 2023. Role of dampers on the seismic performance of pin-supported wall-frame structures. Earthq. Eng. Eng. Vib. 22, 453–467. https://doi.org/10.1007/s11803-022-2092-5

Wiebe, L., Christopoulos, C., Leclerc, R.T.& M., 2012. Shake table testing of a rocking steel frame designed to mitigate higher mode effects, in: Behaviour of Steel Structures in Seismic Areas. CRC Press.

Yang, J., Jiang, J.Z., Neild, S.A., 2020. Dynamic analysis and performance evaluation of nonlinear inerter-based vibration isolators. Nonlinear Dyn 99, 1823–1839. https://doi.org/10.1007/s11071-019-05391-x

Yu, Y., Naganathan, N.G., Dukkipati, R.V., 2001. A literature review of automotive vehicle engine mounting systems. Mechanism and Machine Theory 36, 123–142. https://doi.org/10.1016/S0094-114X(00)00023-9

Zhang, R., Zhang, L., Pan, C., De Domenico, D., Chen, Q., 2021. Targeted modal response control of structures using inerter systems based on master oscillator principle. International Journal of Mechanical Sciences 206, 106636. https://doi.org/10.1016/j.ijmecsci.2021.106636

VITA

Sima Abolghasemi was born in Rasht, Iran. She received her Bachelor of Science (2013) and Master of Science (2016) degrees in Civil Engineering from the University of Guilan, specializing in Structural Engineering. Her master's thesis was titled “Semi-active Control of Structures on Elastic Foundation with Regulated Damping Force.” Driven by a passion for advanced research in structural dynamics, she began her doctoral studies in 2020 at the University of Tennessee, Knoxville, where she served as a research and teaching assistant in the Department of Civil and Environmental Engineering. Her Ph.D. research focused on the dynamic performance and seismic control of strongback structures, combining both experimental and numerical investigations. During her doctoral studies, she contributed to multiple projects funded by NASA and the National Science Foundation (NSF). The outcomes of her research have been published in peer-reviewed journals and conference proceedings, and she has presented her work at several national conferences. She also collaborated with researchers from the University of Sydney, resulting in two journal articles—one published and one currently under submission. Following her Ph.D., she will begin a new role as a structural engineer with Keller, a global construction company.